Optimised Localisation in Wireless Sensor Networks

by

Muhammad Waqas Khan

Submitted in accordance with the requirements for the degree of

Doctor of Philosophy

University of Leeds

School of Electronic and Electrical Engineering

January 2016

The candidate confirms that the work submitted is his own, except where work which has formed part of jointly authored publications has been included. The contribution of the candidate and the other authors to this work has been explicitly indicated below. The candidate confirms that appropriate credit has been given within the thesis where reference has been made to the work of others.

Chapters 2 & 3: M. W. Khan derived the algorithms and performed the simulations. N. Salman and A. H. Kemp were involved in the theoretical development of the solutions, in editing and structuring the thesis. All authors were involved in discussing potential solutions, the results and determining the test scenarios to be used and performance validation.

Chapters 4 & 5 : M. W. Khan, N. Salman and A. H. Kemp derived the algorithms. Simulations were performed by M. W. Khan. L. Mihaylova and A. H. Kemp were involved in editing and structuring the manuscript. A.Ali and A.M Khan were involved in discussing potential solutions and the results.

This copy has been supplied on the understanding that it is copyright material and that no quotation from the thesis may be published without proper acknowledgement.

©2016 The University of Leeds and Muhammad Waqas Khan

Research is what I'm doing when I don't know what I'm doing.

Wernher von Braun

Acknowledgments

I am most grateful to my supervisor, Dr Andrew Kemp, for his continuous encouragement and guidance. Working with Dr. Kemp was a pleasure, we had countless meetings and he always kept me motivated through ups and downs. I have learned a lot from Dr. Kemp and he played a key role in my professional and personal development over the past three years.

I am also grateful to Dr. Lyudmila Mihaylova, University of Sheffield. We had many fruitful meetings during which new ideas were discussed and my work was reviewed.

I also thank my colleague and friend Dr Naveed Salman for his continuous support and encouragement throughout the three years of my Ph.D.

Finally, above all, I thank my parents, my father Prof. Abdul Mutalib and my loving mother Naheeda Yasmin for their support. I know it must have been difficult for them to live away from me over these years as it was for me. But whatever I am now is because of them. Thank you.

Abstract

Wireless sensor networks (WSNs) comprise of tens, hundreds or thousands of low powered, low cost wireless nodes, capable of sensing environmental data such as humidity and temperature. Other than these sensing abilities, these nodes are also able to locate themselves. Different techniques can be found in literature to localise wireless nodes in WSNs. These localisation algorithms are based on the distance estimates between the nodes, the angle estimates between the nodes or hybrid schemes. In the context of range based algorithms, two prime techniques based on the time of arrival (ToA) and the received signal strength (RSS) are commonly used. On the other hand, angle based approach is based on the angle of arrival (AoA) of the signal. A hybrid approach is sometimes used to localise wireless nodes. Hybrid algorithms are more accurate than range and angle based algorithms because of additional observations.

Modern WSNs consist of a small group of highly resourced wireless nodes with known locations called anchor nodes (ANs) and a large group of low resourced wireless nodes known as the target nodes (TNs). The ANs can locate themselves through GPS or they may have a predetermined location given to them during network deployment. Based on these known locations and the range/angle estimates, the TNs are localised.

Since hybrid algorithms (a combination of RSS, ToA and AoA) are more ac-

curate than other algorithms, a major portion of this thesis will focus on these approaches. Two prime hybrid signal models are discussed: *i*) The AoA-RSS hybrid model and *ii*) the AoA-ToA hybrid signal model. A hybrid AoA-ToA model is first studied and is further improved by making the model unbiased and by developing a new weighted linear least squares algorithm for AoA-ToA signal (WLLS-AoA-ToA) that capitalise on the covariance matrix of the incoming signal. A similar approach is taken in deriving a WLLS algorithm for AoA-RSS signal (WLLS-AoA-RSS). Moreover expressions of theoretical mean square error (MSE) of the location estimate for both signal models are derived. Performances of both signal models are further improved by designing an optimum anchor selection (OAS) criterion for AoA-ToA signal model and a two step optimum anchor selection (TSOAS) criterion for AoA-RSS signal model. To bound the performance of WLLS algorithms linear Cramer Rao bounds (LCRB) are derived for both models, which will be referred to as LCRB-AoA-ToA and LCRB-AoA-RSS, for AoA-ToA and AoA-RSS signal models, respectively.

These hybrid localisation schemes are taken one step further and a cooperative version of these algorithms (LLS-Coop) is designed. The cooperation between the TNs significantly improves the accuracy of final estimates. However this comes at a cost that not only the ANs but the TNs must also be able to estimate AoA and ToA/RSS simultaneously. Thus another version of the same cooperative model is designed (LLS-Coop-X) which eliminates the necessity of simultaneous angle-range estimation by TNs. A third version of cooperative model is also proposed (LLS-Opt-Coop) that capitalises the covariance matrix of incoming signal for performance improvement. Moreover complexity analysis is done for all three versions of the cooperative schemes and is compared with its non cooperative counterparts.

In order to extract the distance estimate from the RSS the correct knowledge

of path-loss exponent (PLE) is required. In most of the studies this PLE is assumed to be accurately known, also the same and fixed PLE value is used for all communication links. This is an oversimplification of real conditions. Thus error analysis of location estimates with incorrect PLE assumptions for LLS technique is done in their respective chapters. Moreover a mobile TN and an unknown PLE vector is considered which is changing continuously due to the motion of TN. Thus the PLE vector is first estimated using the generalized pattern search (GenPS) followed by the tracking of TN via the Kalman filter (KF) and the particle filter (PF). The performance comparison in terms of root mean square error (RMSE) is also done for KF, extended Kalman filter (EKF) and PF.

Contents

List of Figures

List of Tables

Nomenclature

ACK	Acknowledge
AN	Anchor node
AoA	Angle of Arrival
AoA-RSS	Angle of arrival-received signal strength
AoA-ToA	Angle of arrival-time of arrival
API	Aircraft positioning system
Avg. RMSE	Average root mean square error
AWGN	Additive white Gaussian noise
BS	Base station
CRB	Cramer-Rao bound
CW	Continuous waves
dB	Decibel
DoD	Department of defense
EKF	Extended Kalman filter

ESPRIT	Estimation of signal parameters via rotational invariance technique
FIM	Fisher information matrix
GDoP	Geometric dilution of precision
GenPS	Generalized pattern search
GHz	GigaHertz
GLONASS	Global navigation satellite system
GPS	Global positioning system
IR	Infra red
KF	Kalman filter
kHz	kilo Hertz
LCRB	Linear Cramer Rao bound
LLS	Linear least squares
LLS-NoCoop	Linear least square with no cooperation
LORAN	Long range navigation
LoS	Line of sight
LPS	Local positioning service
MDS	Multidimensional scaling
MHz	MegaHertz

MIT	Massachussets institute of technology
ML	Maximum likelihood
MSE	Mean square error
MUSIC	Multiple signal classification
NLoS	Non line of sight
NLS	Nonlinear least square
OW-ToA	One way time of arrival
PDF	Probility density function
PF	Particle filter
PLE	Path loss exponent
PTN	Pseudo target node
RF	Radio frequency
RMSE	Root mean square error
RSS	Received signal strength
SNR	Signal-to-Noise Ratio
TDoA	Time difference of arrival
TN	Target Node
ToA	Time of arrival
TW-ToA	Two way time of arrival

WLLS Weighted linear least squares

WLLS-AoA-RSS Weighted linear least squares-AoA-RSS

WLLS-AoA-ToA Weighted linear least square-AoA-ToA

WLS Weighted least squares

WSN Wireless sensor networks

List of Symbols

$\mathbf{A}^{\dagger}$ Moore–Penrose pseudoinverse

d Euclidean distance

d_0 Reference distance

d_T Distance estimated via ToA

d_R Distance estimated via RSS

θ_{ij} Angle between i^{th}AN and j^{th}TN

Φ_{jk} Angle between j^{th} and k^{th}TN

δ Unbiasing constant

δ_T Unbiasing constant for AoA-ToA signal model

δ_R Unbiasing constant for AoA-RSS signal model

E Expectation operator

G_t Transmitter antenna gain

G_r Receiver antenna gain

$\mathbf{I}$ Fisher information matrix

$\mathbf{J}$ Jacobian matrix

ℓ Number of iterations

$\mathscr{L}$ Path-loss

$\mathcal{N}$ Normal distribution

$\mathcal{U}$ Uniform distribution

n Guassian noise in range estimated via ToA

$\check{w}$ Shadowing noise in range estimated via RSS

m Guassian noise in estimated angle.

$p\,(.)$ Probability density function

P_t Transmit power

$\mathbb{R}^n$ Set of n dimensional real numbers

Tr Trace of matrix

ϕ Phase

μ Mean

σ^2 Variance

$\mathbf{C}_{\mathrm{AR}}$ Covariance for AoA-RSS signal

$\mathbf{C}_{\mathrm{AT}}$ Covariance for AoA-ToA signal

$\mathbf{u}$ Unknown parameters (to be estimated)

α PLE

$\Delta\alpha$ PLE error

$\check{\alpha}$ Incorrect PLE

α_0 True PLE

ε Cost function

N Total number of ANs

M Total number of TNs

N_s Number of particles

ℓ Number of independent simulations

η Number of Monte Carlo runs

$\triangle_0$ Initial step size for GenPS

τ Stopping value for GenPS

ξ Step increment/decrement size for GenPS

List of publications

Part of this thesis was published in the following papers.

Journal Publications

1. **M. W. Khan**, Naveed Salman, A. H. Kemp, L. Mihaylova "Optimised Hybrid Localisation with Cooperation in Wireless Sensor Networks," *IET Signal Processing*, (Accepted awaiting publication).
2. **M. W. Khan**, N. Salman, A. H. Kemp, L. Mihaylova "Positioning with Hybrid Measurements in Wireless Sensor Networks," (Submitted to MDPI Sensor journal).
3. **M. W. Khan**, Naveed Salman, A. H. Kemp, L. Mihaylova "Optimised Localisation Using Angle of Arrival-Time of Arrival Measurements in Wireless Networks," (Submitted to IEEE sensor journal).

Refereed Conferences

1. **M. W. Khan**, Naveed Salman, A. H. Kemp "Enhanced Hybrid Positioning in Wireless Networks I: AoA-ToA," *IEEE International Conference on Telecommunications and Multimedia* (TEMU), pp. 86-91, July 2014, (Heraklion, Greece).

2. Naveed Salman, **M. W. Khan**, A. H. Kemp "Enhanced Hybrid Positioning in Wireless Networks II: AoA-RSS," *IEEE International Conference on Telecommunications and Multimedia* (TEMU), pp. 92-97, July 2014, (Heraklion, Greece).

3. **M. W. Khan**, Naveed Salman, A. H. Kemp "Cooperative Positioning Using Angle of Arrival and Time of Arrival," *in Sensor Signal Processing for Defence (SSPD)*, pp.1-5, 8-9 Sept. 2014, (Edinburgh, Scotland).

4. **M. W. Khan**; A. H. Kemp; N. Salman; L. Mihaylova, "Tracking of wireless mobile nodes in he presence of unknown path-loss characteristics," *18th International Conference on Information Fusion (Fusion 2015)* , pp.104-111, 6-9 July 2015, (Washington DC, USA).

5. **M. W. Khan**; N. Salman; A. M. Khan; A.Ali; A. H. Kemp, "A Comparative Study of Target Tracking With Kalman Filter, Extended Kalman Filter and Particle Filter Using Received Signal Strength Measurements," *IEEE International Conference on Emerging Technologies (ICET), pp. 1-6, 2015* (Peshawar, Pakistan).

1 Introduction

Wireless communications is one of the greatest engineering achievements of the past few decades. From a market growth point of view to our daily lives, from social interaction to our professional progress, every aspect of our lives is influenced by advancement in wireless communications. With the advent of new technologies, the applications of wireless communication has increased significantly. Internet browsing, video telephony, electronic mails are some of the few achievements of wireless communication that play a vital role in our daily life. However, in the last two decades, new technologies such as global positioning system (GPS) and local positioning service (LPS) have become very popular and localisation in these systems promises many new applications.

Localisation systems have its roots in the military circles. During world war 2, two localisation systems, the Decca and the LORAN (Long Range Navigation) were developed, which were followed by the development of two more systems, the Omega and the GPS. Other positioning systems include, the Russian CHAYKA [2] and GLONASS [3], the British Gee, and GALILEO [4], a European navigation system named after the Italian astronomer Galileo Galilei.

1.1 Wireless Sensor Networks

A WSN comprises of inexpensive, low powered wireless nodes networked together via a communication channel [5]. The wireless nodes must have sensing capabilities such as sensing temperature, humidity and velocity, depending upon network's application [6], [7]. WSN will play a key role in many future applications.

A typical WSN consist of a number of wireless nodes. Each node must be equipped with a radio transceiver. The size, cost, power and number of these nodes are network and application dependent. The physical dimensions of these node may vary from grain sized nodes to the size of a football. The cost of a single wireless node is of vital importance as the number of nodes in the network can vary from a few nodes, as in robot tracking systems to several thousands, as in forest fire detection systems. Fig. 1.1 shows a typical WSN configuration which generally consists of one or more coordinators, tens, hundreds or thousands of sensor nodes and a server (laptop in this case).

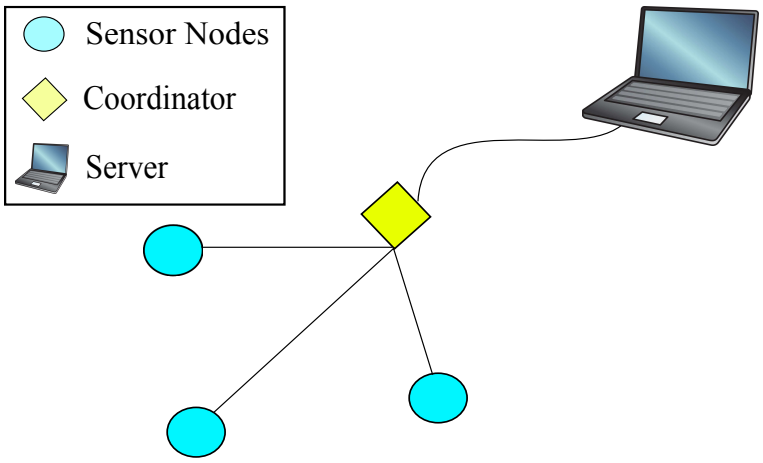

Figure 1.1: WSN configuration.

Localisation in wireless sensor networks: One of the most important feature of WSN is location aware WSN. In many applications, the data received by the base station will be useless if the location from where the data

is transmitted is not known. For example, if the sensors sense fire in a forest, the exact location of the transmission source is vital for the fire fighters to take control of the situation. Similarly, in avalanche rescue the exact location of the victims is required by the rescue team.

1.1.1 Range Based Localisation

Range based localisation [8], works on the principle of trilateration. Distance between two nodes can be estimated via RSS or ToA. For a two dimensional networks, atleast 3 ANs are required to determine the TN's location (4 ANs are required for 3-dimensional localisation). Each AN defines a circle (a sphere in 3-D case), where the center of the circle is the AN's location and the radius of the circle is the distance between AN and TN. The TN's location is the point of intersection of these circles. This is shown in Fig.1.2, where d_i represents the distance between i^{th} AN and the TN and is given by

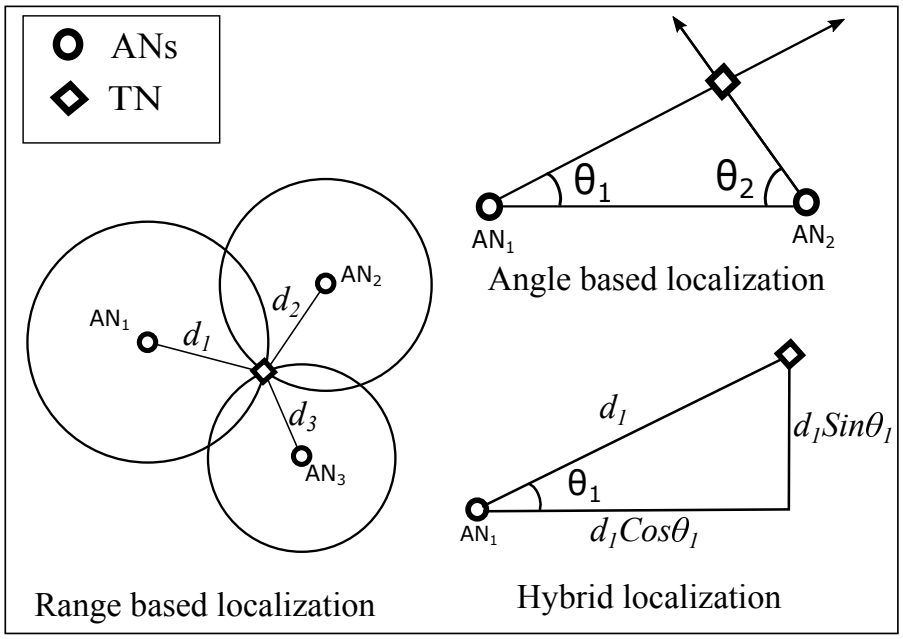

Figure 1.2: Range, angle and hybrid based approach for positioning assuming exact distances and angles.

$$d_i = \sqrt{(x - \bar{x}_i)^2 + (y - \bar{y}_i)^2}, \quad i = 1, 2, 3. \tag{1.1}$$

where $(\bar{x}_i, \bar{y}_i)$ are the coordinates of i^{th} AN and (x, y) are the TN's coordinates.

1.1.2 Angle Based Localisation

In angle based localisation [9], each AN defines a line rather then a circle. The point of intersection of two lines, points to the TN's location. Hence in angle based localisation, atleast two ANs are required for localisation. This is shown in fig.1.2 where θ_i represents the AoA at i^{th} AN and is given by

$$\theta_i = \arctan\left[\frac{(y - \bar{y}_i)}{(x - \bar{x}_i)}\right], \quad i = 1, 2. \tag{1.2}$$

1.1.3 Hybrid Localisation

In some scenarios both range and angle of arrival are available [10], [11]. In these hybrid cases, localisation requires only one AN. However to improve localisation accuracy more ANs can be added to the network. In this case, an AN defines a line of fixed length. One end of the line represents the AN's position, while the TN is situated on the other end for which the coordinates are to be estimated. If the slope (AoA) and the magnitude (ToA or RSS) of this line is available, then the TN's coordinates can be easily calculated using simple trigonometric equations. This scheme is represented in fig.1.2. The x and y coordinated of the TN are calculated using (1.3) and (1.4)

$$x = x_i + d_i \cos\theta_i \tag{1.3}$$

$$y = y_i + d_i \sin \theta_i \tag{1.4}$$

1.2 Applications of Localisation Systems

The applications of wireless location systems are widespread and are increasing rapidly. Localisation of wireless sensors will play a significant role in the internet of things paradigm in the coming years. The requirements of a localisation system depend on the applications. Previously, localisation systems were only used for military purposes e.g. aircraft detection\localisation. With the advent of new technologies, the applications of localisation systems grew significantly. Localisation of wireless nodes have a wide variety of applications now a days. From military point of view to environmental domain, these systems are now an integrated part of our daily life. Some applications are discussed briefly here.

1.2.1 Health and Safty

Patient monitoring is one of the most important application of wireless sensor networks. Traditional monitoring systems need the patients to be wired to the system, which limits the mobility of the patients. In [12], a system MEDiSN is proposed in which sensors, which records the vital signs are attached to the patient's body. In case of an emergency an alarm is raised which alerts the medical staff.

Wireless location systems can be used in avalanche rescue systems. The main problem in rescuing avalanche victims is the lack of precise knowledge of the position of the victim. In [13], numerous experiments are performed in which

vital sign are detected in an avalanche scenario.

1.2.2 Tracking

Tracking may be of wildlife, humans or robots. In case of wildlife tracking, animals are tagged with sensors. These sensors record data like the animal's movement. These nodes will record the data for a very long period of time, thus a power hungry device like GPS chip fail to perform in this case. A system is developed for this purpose known as ZebraNet [14]. In another case, smart robots are tagged with location sensors, through which they can localise themselves and avoid collisions.

1.2.3 Security

Security of a restricted area can be improved by WSN. For example individuals in a building are tagged with a specialised sensors. The sensor alerts and send the location of the trespasser to the security when he/she enters a restricted/hazardous area.

1.2.4 Military

WSN has a high number applications in military domain. Soldiers in the battlefield are tagged with sensors which send health/physical conditions and location to the base. Another military application can be localisation of acoustic objects like moving vehicles, and snipers [15].

1.2.5 Logistics

An important application of WSN is in logistics. Boxes in a factory, a grocery store or a warehouse are tagged with sensors. These sensors monitor the temperature, humidity and pressure etc and notifies the staff about the location of a box with abnormal condition. Thus boxes with abnormal or expired content are removed before further damage is done to other boxes.

1.2.6 Other Domains

WSN localisation has various other applications. For example, it can be used in interactive gaming in which a users wears ornaments like gloves with sensors while the gaming console can read data from the sensor and locate its position, thus creating a wireless interface between user and console. A perfect example is PlayStation eye. It is also used in movie industry where animation of a human being are duplicated to fine resolution. In this case sensors are attached to key points of human body which records the movements of human body parts which can be reproduced as computer graphics. Similarly, WSNs can be used in agriculture monitoring [16], cattle herding [17], industrial process monitoring etc.

1.3 Classification of Localisation Systems

Classification of localisation systems can be based on a number of parameters. Following [18] and [19], some of these classifications are as follows

1.3.1 Classification based on signal type

Different types of signals can be utilised for localisation, some of which are mentioned here.

1.3.1.1 Radio signals

One of the most widely used signal for localisation is the radio signal [20], [21]. High localisation accuracy is achieved in the presence of LOS signals. Radio waves can travel longer distances and are thus ideal for large networks. Localisation using radio waves are highly affected by electromagnetic phenomenon like reflection, diffraction and scattering and is also dependent on the centre frequency of the signal. However numerous techniques are developed to counter the effects of these electromagnetic phenomenons. Since radio waves travel with the speed of light, the transceivers used for location estimation must be equipped with high frequency clocks.

1.3.1.2 Ultrasound Waves

With relatively low propagation speed compared to radio waves, ultrasound waves eliminate the requirement of high frequency clocks on the transceivers. This however comes at a cost, as ultrasound waves are not suitable for long range propagation. Thus localisation systems based on ultrasound waves [22], [23] will fail at large transmitter-receiver separation. Consequently, a powerful transmitter is required for transmission of ultrasound waves at larger distances.

1.3.1.3 Infrared signals

Infrared signals (IR) require very low power transmitters. However the requirement of LOS signal makes infrared signal an unsuitable candidate for indoor localisation [24], [25]. On the other hand, these signals are affected by sunlight, hence are not suitable for outdoor localisation either, even in the case of a perfect LOS signal. Due to these reasons IR signals are rarely used for localisation.

1.3.2 Classification based on Range and Angle

Localisation systems can be classified based on the type of estimated parameter. These parameters can be range based like time of arrival (ToA) and received signal strength (RSS) or angle based i.e., angle of arrival (AoA) or it can be a hybrid between any of these.

1.3.2.1 Time of Arrival

Localisation via ToA [26], [27] is based on the time, the signal takes to propagate from transmitter to receiver. Hence propagation speed of the signal plays a vital role in these systems. ToA shows better accuracy than RSS at the cost of system complexity and cost of synchronized clocks on all transceivers. If the speed of signal, c and time of flight, T_{ToF} is known, then distance, d can be calculated by using the formula

$$d = cT_{ToF}. \tag{1.5}$$

ToA is further classified into two type

- One way time of arrival (OW-ToA)

- Two way time of arrival (TW-ToA)

OW-ToA **:** OW-ToA is the simplest form of ToA, however it requires highly synchronized clocks on all nodes, as a small off-set in clocks can decreases the accuracy of the system significantly. Fig. 1.3 shows the line diagram of OW-ToA. In Fig. 1.3, t_1 is the transmit time and t_2 is the receive time of the signal. T_{ToF} is the time the signal takes to propagate from node A to node B. T_{ToF} in this case is given by [8]

$$T_{ToF} = t_2 - t_1. \tag{1.6}$$

Putting values in (1.5), we obtain the distance as

$$d = c\left(t_2 - t_1\right). \tag{1.7}$$

TW-ToA **:** Fig. 1.4 shows the mechanism of TW-ToA [28]. Let t_1 be the transmit time at node A and t_2, the receive time at node B. An acknowledge (ACK) is sent by node B at t_3 which is received by node A at t_4. In TW-ToA the signal covers twice the distance between the two transceivers. The distance equation is given by

$$d = \frac{(cToF)}{2}, \tag{1.8}$$

where

$$ToF = t_4 - T_{\text{Reply}} - t_1, \tag{1.9}$$

and T_{Reply} is the processing time node B takes to send the ACK signal. Putting (1.9) in (1.8) [29], we obtain

$$d = c\left(t_4 - T_{\text{Reply}} - t_1\right)/2. \tag{1.10}$$

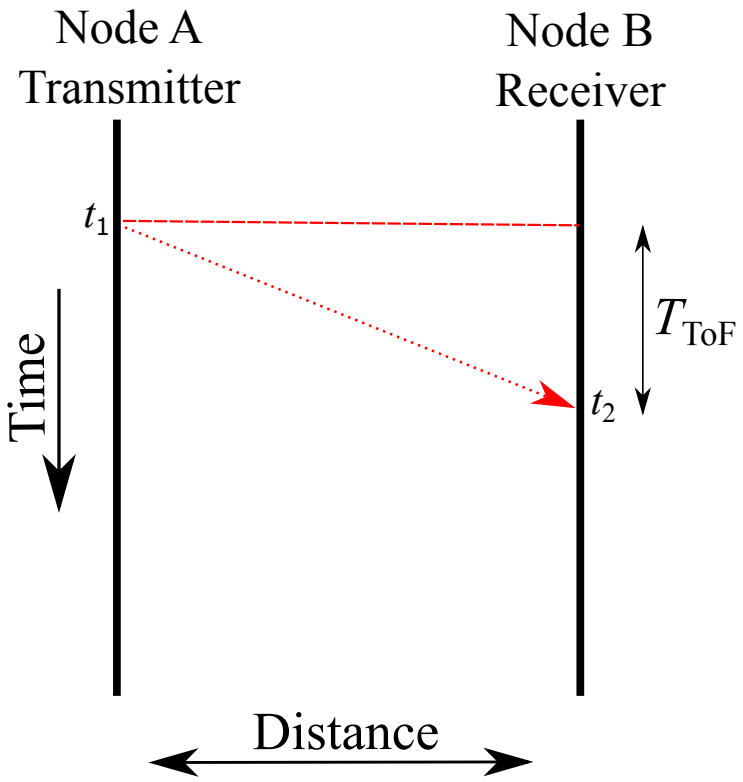

Figure 1.3: Time-line diagram of OW-ToA.

1.3.2.2 Received Signal Strength

Localisation based on RSS acts on the principle of signal attenuation as it propagates through the channel [30], [31]. This attenuation is directly proportional to distance between transmitter and receiver. RSS based localisation eliminates the necessity of synchronized high frequency clocks on the transceivers. This makes it one of the most attractive method for localisation in wireless sensor networks (WSNs).

In RSS based techniques, the transmitter transmits a signal with a fixed reference power, P_t which is known to the receiver. The receiver measure the power of the received signal and based on the attenuation in signal power, estimates the distance between transmitter and receiver. For free space propagation, the Friis formula gives the relation between the attenuation and distance between

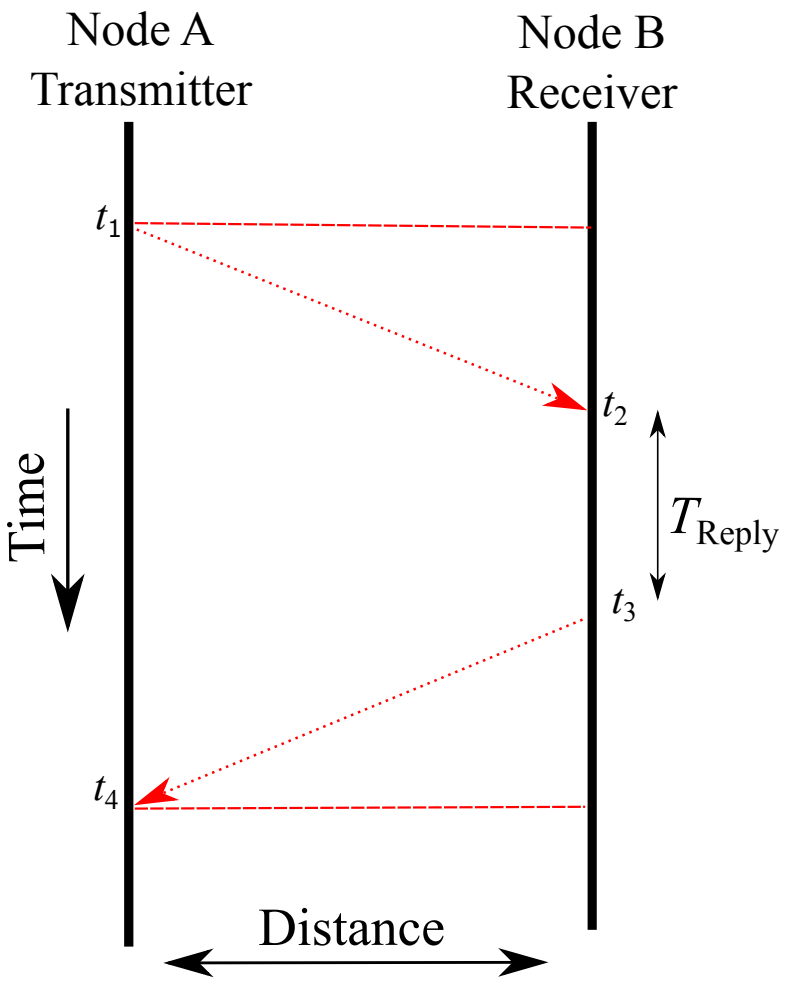

Figure 1.4: Time-line diagram of TW-ToA.

transmitter and receiver [32]. The measured power P_r is given by

$$P_r = \frac{P_t G_t G_r \lambda^2}{(4\pi d)^2} \tag{1.11}$$

where G_t and G_r are the transmitter and the receiver gains, respectively and λ is the signal's wavelength. An inverse relation between distance and received power is seen from (1.11). This is shown using real data in Fig. 1.5 using the NXP Jennic evaluation kit [33]. The relation between P_r and P_t as shown in (1.11) is valid only for free space propagation. In real world the received power is corrupted by

multipath and shadowing. Multipath occurs as a result of non line of sight (NLoS) propagation of the signal. As a result the receiver receives multiple copies of the same signal that may interfere constructively or destructively. Shadowing occurs due to the hindrance of the signal by trees, walls etc. This multipath effect can be mitigated by taking the average of the received power over a sufficient window. The average power is given by [34]

$$P_{avg} = P_0 - 10\alpha \log\left(\frac{d}{d_0}\right) \tag{1.12}$$

where P_{avg} is the average power in deciBells (dBs), P_0 is the power received at reference distance d_0, which is usually taken as 1m for indoor scenarios and it depends on the antenna's characteristics. α is the path loss exponent (PLE) associated with the communication link and is environment dependent. The shadowing effect is generally modelled as a random process. The average power is log-normally distributed or Gaussianly distributed if the power is taken in dBs i.e $p_{avg} \sim \mathcal{N}\left(P_{avg}, \sigma^2_{shadowing}\right)$.

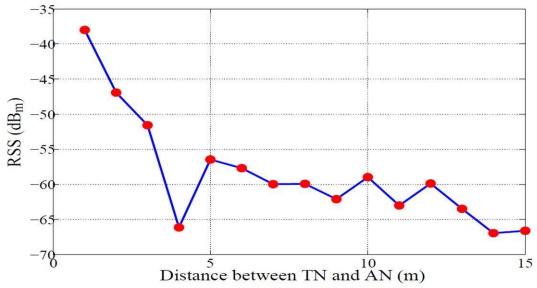

Figure 1.5: Relation between distance and RSS [1].

1.3.2.3 Angle of Arrival

Localisation based on the arrival angle [35], [36] of the signal requires additional hardware. This hardware can be a multiple element array of antennas [37] or an antenna with high directivity capable of physical rotation [35]. In the former case, the angle of arrival is estimated based on the phase difference of the signal at each element of the array and by using techniques like Multiple Signal Classification (MUSIC) [38] or estimation of signal parameters via rotational invariance techniques (ESPRIT) [39]. Equ. (1.13) shows the the relationship between phase difference and angle of arrival of the signal for two element array [40].

$$\phi_1 - \phi_2 = \frac{2\pi \vec{d} \sin\theta}{\lambda} \tag{1.13}$$

where $\phi_1 - \phi_2$ represents the phase difference of the signals received by each element of the antenna array. $\vec{d}$ is the distance between elements, λ represents the wavelength of the signal and θ is the angle of arrival of the signal. In the later case, the angle is estimated based on the rotation of a directed beam of radiation. Thus when the antenna is facing in the direction of the incoming signal, maximum power is received.

1.3.2.4 Hybrid Models

Localisation based on the utilisation of range and angle simultaneously is referred to as hybrid localisation [41], [42], [43]. High accuracy is achieved with these models as the number of measurements per sensor increases as compared to non-hybrid case.

1.3.3 Cooperative and non-cooperative localisation systems

This classification of localisation systems is based on the cooperation between the target nodes (TNs) [44], [45]. In cooperative localisation TNs can communicate with each other while this communication link is not available in non-cooperative localisation systems [18], [34].

1.3.4 Centralized and distributed localisation systems

In centralized localisation systems, the data is transferred to a base station (BS) before processing [46], while in distributed localisation systems, the data processing is done at the node level [47].

1.3.5 Single-hop and multi-hop localisation systems

Single-hop localisation system [48] are based on the data transmission directly from transmitter to receiver while in a multi-hop system [49], data is received by receiver via a number of hops.

1.3.6 Range based and Range free localisation systems

In range based localisation the absolute distance between the nodes is estimated [50]. This makes the system more accurate but the TN must have a long communication range to reach the anchor nodes (ANs). On the other hand, in range free localisation, the absolute distance is not estimated, but is based on the number of hops for communication between two nodes [51]. This makes the system less complex but it requires a highly dense network. Range free localisation shows poor performance in case of less dense networks.

1.4 Factors Affecting WSN Localisation

1.4.1 Cost

One of the most important factor in localisation systems is the cost of the network. Since the network can be composed of hundreds of nodes, the cost of individual node is of primary concern.

1.4.2 Computational complexity

Another factor of key importance is the computational complexity of localisation systems. Nodes in WSNs are often low on resources, which makes them unable to perform tasks that require a high computational power.

1.4.3 Robustness

Nodes used in a localisation system may be placed in harsh environments. These nodes must overcome heat, humidity and other extreme weather conditions. In some scenarios these nodes may be dropped from an aircraft, hence they must be shock resistant. Thus, these wireless nodes must be robust to survive in extreme conditions.

1.4.4 Size and weight

The size and weight of a wireless node varies from system to system. In a weather station usually bulky nodes are installed [52]. However a small and light node is an appealing feature of a good localisation system. Specially in situations where the node has to be attached to the body of a human, an animal or a small robot [53].

1.4.5 System deployment

System deployment may be pre-determined or it may be random [54]. Whatever the case is, installation of nodes should be simple. System maintenance also effects the systems performance. Maintenance should be easy and should not require high level of expertise. In an ideal case, the the system should be maintenance free.

1.4.6 Accuracy of location estimates

Accuracy of the location estimates is another prime performance metric of a localisation system. It is measured as the difference between actual node's location and estimated node's location.

1.5 Major Contributions

The main contributions in this thesis are as follows:

- Unbiased linear least squares (LLS) estimators for positioning are proposed based on hybrid AoA-ToA and hybrid AoA-RSS signals.
- Analytical expressions for the mean square error (MSE) for both unbiased hybrid estimators.
- Weighted linear least squares (WLLS) algorithms are proposed that enhances the performance of the proposed unbiased LLS estimators.
- An optimal ANs selection criteria is designed for AoA-ToA signal model and a two step optimal ANs selection criteria is designed for AoA-RSS signal model to further enhance the performance.

- Linear Cramer-Rao Bound (LCRB), a benchmark, for the WLLS is derived for both hybrid signal models.
- Cooperative LLS algorithm is developed using hybrid AoA-ToA and AoA-RSS signal models.
- Performance of cooperative LLS algorithm is enhanced by proposing an optimized cooperative LLS using both hybrid signals.
- Complexity analysis is done for cooperative LLS, optimized cooperative LLS, non-cooperative LLS using hybrid signal models.
- Analytical expression for the MSE of location estimate using incorrect PLEs is derived for LLS algorithm using AoA-RSS signal model.
- A joint PLE-coordinate estimator is proposed using hybrid AoA-RSS signal model using generalized pattern search technique (GenPS) and tracking of a wireless node is performed using the Kalman filter (KF) and particle filter (PF).
- A Comparative study of target tracking with KF, extended Kalman filter (EKF) and PF using RSS measurements is presented.

1.6 Thesis Outline

Following the introduction, classification of positioning systems, some performance metrics and some applications were discussed, the rest of the thesis is organized as follows:

Chapter 2 A hybrid AoA-ToA signal model for localisation is presented. An unbiased LLS solution and a WLLS solution (WLLS-AoA-ToA), based on the noise covariance is proposed. To analyse the performance of LLS algorithm, a

theoretical MSE expression is derived. Further optimisation to LLS is achieved by designing an optimal ANs selection criteria (OAS). Finally in order to lower bound the performance of WLLS-AoA-ToA, a LCRB is derived (LCRB-AoA-ToA).

Chapter 3 An unbiased LLS solution is presented for hybrid AoA-RSS signal model for localisation. Followed by the proposal of WLLS solution (WLLS-AoA-RSS) that is based on the noise covariance matrix of AoA-RSS signal. Moreover a two step optimal ANs selection (TSOAS) is designed to further enhance the performance of LLS. A novel PLE vector estimator based on GenPS is also proposed. Finally, to lower bound WLLS-AoA-RSS, a LCRB is derived (LCRB-AoA-RSS).

Chapter 4 In this chapter, a cooperative version of hybrid AoA-ToA and hybrid AoA-RSS signal model for localisation is presented. A LLS solution is presented (LLS-Coop) which is modified in resource constraint networks (LLS-Coop-X). An enhanced version of the algorithm (LLS-Opt-Coop) is also proposed. Analysis of the system in terms of partial connectivity is done followed by the complexity analysis of the algorithms.

Chapter 5 Chapter 5 deals with the localisation and tracking of a mobile TN using the RSS and the AoA-RSS signal model. In order to examine the effect of erroneous PLE vector on localisation accuracy, a theoretical MSE expression for incorrect PLE is derived for the AoA-RSS signal model. After the estimation of PLE vector with GenPS, an extensive performance comparison of tracking of mobile TN with KF and PF is presented. Finally, the performance evaluation of tracking using the RSS observation is also presented using KF, EKF and PF.

Chapter 6 Chapter 6 presents the conclusion and future aspects of the research presented in this thesis.

Appendices All mathematical derivations are presented in appendices section. These include the derivation of covariance matrix and Fisher Information matrix (FIM) of the unbiased AoA-ToA signal model, the covariance matrix and FIM of the unbiased AoA-RSS signal model, the covariance matrix of the AoA-RSS signal model with incorrect PLE values and all the expectation taken in this thesis which are given in table. 2.1.

2 Enhanced Positioning Using Angle of Arrival and Time of Arrival Measurements

The material of this chapter is presented in

i) M. W. Khan, Naveed Salman, A. H. Kemp "Enhanced Hybrid Positioning in Wireless Networks I: AoA-ToA," *IEEE International Conference on Telecommunications and Multimedia* (TEMU), pp. 86-91, July 2014.

ii) M. W. Khan, Naveed Salman, A. H. Kemp, L. Mihaylova "Optimised Localisation Using Angle of Arrival-Time of Arrival Measurements in Wireless Networks," (Submitted to IEEE sensor journal).

2.1 Overview

Localisation of wireless nodes introduce many new applications and present new challenges for scientists and engineers in the field of wireless communication. Scientists are working on new methods to improve the accuracy of localisation. Some of these methods are based on the utilisation of hybrid signals. In this chapter, a new unbiased hybrid AoA-ToA signal model is presented for static

nodes. The mathematical expression for overall bias is derived and is verified via Monte Carlo simulation. In order to analyse the performance of the LLS solution for the proposed model, the analytical MSE expression is derived. To improve the performance of LLS, weights are given to individual communication links. These weights are based on the noise covariance of the signal, thus the noise covariance matrix is first derived and a new unbiased WLLS algorithm (WLLS-AoA-ToA) is proposed. Further improvement is achieved via an optimal AN selection algorithm (OAS), which selects only those ANs for positioning that guarantees to improve the accuracy of localisation. In order to lower bound the performance of WLLS-AoA-ToA, the LCRB is derived (LCRB-AoA-ToA). Finally, the notion of critical distance in hybrid localisation systems is introduced. Through simulation, it is shown that the theoretical MSE accurately predicts the system performance. Furthermore, the improved performance of WLLS-AoA-ToA methods over the LLS is also demonstrated via Monte Carlo simulation.

The rest of the chapter is organized as follows: Section II presents the LLS solution to previously developed ToA, RSS, AoA and hybrid signal models. In section III, the new unbiased hybrid AoA-ToA signal model is presented, mathematical verification of unbiasness is done and the theoretical MSE and the noise covariance matrix are derived. Optimisation techniques are presented in section IV, by first proposing a WLLS-AoA-ToA solution and then by OAS design. To lower bound the performance of WLLS-AoA-ToA, the LCRB-AoA-ToA is derived in section V followed by the introduction of critical distance in section VI. All proposed algorithm, derivations and estimators are verified via extensive Monte Carlo simulation in section VII. A summary of the chapter is presented in section VIII.

$E_\tau[\tau] = 0$
$E_\tau[\tau^2] = \sigma_\tau^2$
$E_\tau(\cos\tau) = \exp\left(-\frac{\sigma_\tau^2}{2}\right)$
$E_\tau[\cos 2\tau] = \exp(-2\sigma_\tau^2)$
$E_\tau[\sin\tau] = 0$
$E_\tau[\sin 2\tau] = 0$
$E_\tau\left[\exp\left(\frac{\tau}{ab}\right)\right] = \exp\left(\frac{\sigma_\tau^2}{2(ab)^2}\right)$
$E_\tau\left[\exp\left(\frac{2\tau}{ab}\right)\right] = \exp\left(\frac{2\sigma_\tau^2}{(ab)^2}\right)$

Table 2.1: Expectation used in this thesis.

2.2 System Models

For ease of understanding some terms and equations already explained in chapter 1 are re written in this chapter. We also specify the following notation for future use: $\mathbb{R}^n$ is a set of n dimensional real number, $(.)^T$ is the transpose operator, $Tr(M)$ is the trace of matrix M, $E(.)$ refers to the expectation operator. For later use we also define the expectations given in table 1, by considering τ as a Gaussian random variable with zero mean and σ_τ^2 variance, i.e., $\tau \sim \mathcal{N}(0, \sigma_\tau^2)$, also a and b are assumed to be constants. The proof of all the expectations taken in this thesis is given in appendix I.

Some commonly used range and angle based localisation techniques based on LLS are first reviewed. We consider a 2-D network (extension to its 3-D form is straight forward) composed of a TN with unknown coordinates $\mathbf{u}=[x\,y]^T \in \mathbb{R}^2$ and N ANs where $[\bar{x}_i\,\bar{y}_i]^T \in \mathbb{R}^2$ are the coordinates of i^{th} AN.

2.2.1 Linear Least Squares Solution for ToA Based System.

If only range estimates are available as in ToA and RSS based system, the minimum AN requirement is 3 for 2-D localisation and 4 for 3-D localisation. The range, $\hat{d}_{T,i}$ estimated via ToA, between i^{th} AN and the TN is given by [55]

$$\hat{d}_{T,i} = d_i + n_i, \tag{2.1}$$

where $d_i = \sqrt{(x - \bar{x}_i)^2 + (y - \bar{y}_i)^2}$ is the true distance and n_i is the noise which is a modeled as zero mean Gaussian random variable with variance $\sigma^2_{n_i}$, i.e., $n_i \sim \mathcal{N}\left(0, \sigma^2_{n_i}\right)$. Clearly (2.1) is not linear in terms of x and y and can be solved for x and y by high complexity methods like maximum likelihood and Gause Newton that are based on individual readings from the sensor. An alternative solution is the LLS technique for which (2.1) needs to be linearised first. This linearisation technique was first presented in [56]. Let $\hat{d}^2_{T,i}$ be the 2-D noisy distance estimated via ToA, i.e.,

$$\hat{d}^2_{T,i} \approx (x - \bar{x}_i)^2 + (y - \bar{y}_i)^2, \tag{2.2}$$

To linearize (2.2), a reference AN is selected with estimated distance, $\hat{d}^2_{T,r}$ from TN.

$$\hat{d}^2_{T,r} \approx (x - \bar{x}_r)^2 + (y - \bar{y}_r)^2, \tag{2.3}$$

where $(\bar{x}_r, \bar{y}_r)$ are the coordinates of reference AN. Each distance equation (2.2) for $i = 1, ..., N$ $(i \neq r)$ is now subtracted from the reference distance (2.3). Thus we have

$$\left[(x - \bar{x}_r)^2 + (y - \bar{y}_r)^2\right] - \left[(x - \bar{x}_i)^2 + (y - \bar{y}_i)^2\right] = \hat{d}^2_{T,r} - \hat{d}^2_{T,i} \quad \text{for}\, i = 1, ..., N\,(i \neq r)\,. \tag{2.4}$$

This reference AN can be randomly chosen or a special criteria can be developed to select it as in [57]. (2.4) can be written as

$$\left[x^2+\bar{x}_r^2-2x\bar{x}_r+y^2+\bar{y}_r^2-2y\bar{y}_r\right]-\left[x^2+\bar{x}_i^2-2x\bar{x}_i+y^2+\bar{y}_i^2-2y\bar{y}_i\right]=\hat{d}_{T,r}^2-\hat{d}_{T,i}^2, \tag{2.5}$$

which can be simplified to

$$(\bar{x}_i-\bar{x}_r)\,x+(\bar{y}_i-\bar{y}_r)\,y=0.5\left[\left(\bar{x}_i^2+\bar{y}_i^2\right)-\left(\bar{x}_r^2+\bar{y}_r^2\right)+\hat{d}_r^2-\hat{d}_i^2\right]. \tag{2.6}$$

Equ. (2.6) is linear in terms of x and y. In matrix form (2.6) can be written as

$$\mathbf{A}_{\mathrm{ToA}}\mathbf{u}=0.5\hat{\mathbf{b}}_{\mathrm{ToA}}, \tag{2.7}$$

where

$$\mathbf{A}_{\mathrm{ToA}}=\begin{bmatrix}\bar{x}_1-\bar{x}_r & \bar{y}_1-\bar{y}_r\\ \bar{x}_2-\bar{x}_r & \bar{y}_2-\bar{y}_r\\ \vdots & \vdots\\ \bar{x}_{(N-1)}-\bar{x}_r & \bar{y}_{(N-1)}-\bar{y}_r\end{bmatrix}\in\mathbb{R}^{(N-1)\times 2},\qquad \mathbf{u}=\begin{bmatrix}x\\ y\end{bmatrix}\in\mathbb{R}^{2\times 1},$$

$$\hat{\mathbf{b}}_{\mathrm{ToA}}=\begin{bmatrix}(\bar{x}_1^2+\bar{y}_1^2)-(\bar{x}_r^2+\bar{y}_r^2)+\hat{d}_r^2-\hat{d}_1^2\\ (\bar{x}_2^2+\bar{y}_2^2)-(\bar{x}_r^2+\bar{y}_r^2)+\hat{d}_r^2-\hat{d}_2^2\\ \vdots\\ (\bar{x}_{(N-1)}^2+\bar{y}_{(N-1)}^2)-(\bar{x}_r^2+\bar{y}_r^2)+\hat{d}_r^2-\hat{d}_{(N-1)}^2\end{bmatrix}\in\mathbb{R}^{(N-1)\times 1}. \tag{2.8}$$

The LLS solution to (2.7) can be obtained as

$$\hat{\mathbf{u}}=0.5\left(\mathbf{A}_{\mathrm{ToA}}^{\dagger}\hat{\mathbf{b}}_{\mathrm{ToA}}\right), \tag{2.9}$$

where $\mathbf{A}_{\mathrm{ToA}}^{\dagger}$ is the Moore Penrose pseudo inverse of matrix $\mathbf{A}_{\mathrm{ToA}}$, i.e., $\mathbf{A}_{\mathrm{ToA}}^{\dagger}=\left(\mathbf{A}_{\mathrm{ToA}}^T\mathbf{A}_{\mathrm{ToA}}\right)^{-1}\mathbf{A}_{\mathrm{ToA}}^T$.

2.2.2 Linear Least Squares Solution for RSS Based System.

RSS based localisation systems [58], are of low complexity compared to ToA based system as no additional hardware is required for its implementation. However this comes at a cost of low estimation accuracy as the performance of RSS based system is inferior to the performance of a ToA based system. This is because noise in range estimate, calculated from the received power is distance dependant. Another drawback of RSS based systems is the knowledge of the value of the path loss exponent (PLE) for each communication link. Joint PLE and coordinates estimation will be presented in chapter 3 and chapter 5. For now, we assume that the PLE vector is known. Furthermore we assume a same PLE value for all communication links.

The RSS based ranging works on the principle of signal strength attenuation as it propagates through the channel. The i^{th} range estimates via RSS will be represented by $d_{R,i}$ and can be extracted from the received path loss as [59]

$$\mathcal{L}_i = \mathcal{L}_0 + 10\alpha_i \log_{10} \frac{d_i}{d_0} + \breve{w}_i, \tag{2.10}$$

where $\mathcal{L}_i$ is the received path loss at the i^{th} AN, $\mathcal{L}_0$ is the path loss at a reference distance d_0 usually taken as 1m, α_i is the PLE associated with i^{th} AN, d_i is the true distance between i^{th} AN and TN and $\breve{w}_i$ represents the log normal shadowing which is modeled as a Gaussian random variable with mean zero and variance $\sigma^2_{\breve{w}_i}$, i.e., $\breve{w}_i \sim \mathcal{N}\left(0, \sigma^2_{\breve{w}_i}\right)$. The path loss is the difference between the observed power at the AN and transmit power at the TN and can be represented as

$$\mathcal{L}_i = 10 \log_{10} P - 10 \log_{10} P_i, \tag{2.11}$$

where P is the transmit power of the TN which is known to all ANs and P_i is the received power at i^{th} AN. The path loss z_i from d_0 to d_i, observed at i^{th} AN can be represented as

$$\hat{z}_i = \gamma\alpha_i \ln d_i + \check{w}_i, \tag{2.12}$$

where $\gamma = \frac{10}{\ln 10}$. RSS based range estimate from (2.12) can be obtained as

$$\hat{d}_{R,i} \approx \exp\left(\frac{\hat{z}_i}{\gamma\alpha_i}\right). \tag{2.13}$$

Equ. (2.13) represents the biased distance estimate via RSS. To make the model unbiased we introduce an unbiasing constant β_i. The idea of unbiasing constant in RSS based localisation systems was first coined in [60]. Taking the unbiasing constant in (2.13), and then taking the expectation operator with respect to $\check{w}_i$, results in the true distance estimate, i.e.,

$$E_{\check{w}_i}\left[\beta_i \exp\left(\frac{\hat{z}_i}{\gamma\alpha_i}\right)\right] = d_i, \tag{2.14}$$

where d_i is the true distance between AN and TN and $\beta_i = \exp\left(-\frac{\sigma^2_{\check{w}_i}}{2(\gamma\alpha_i)^2}\right)$. Thus the unbiased range, estimated via RSS is given as

$$\hat{d}_{R,i} = \beta_i d_i \exp\left(\frac{\check{w}_i}{\gamma\alpha_i}\right). \tag{2.15}$$

Equ. (2.15) can be written in vector form as $\hat{\mathbf{d}}_R = \boldsymbol{\beta} \odot \mathbf{d} \odot \left[\exp\left(\frac{1}{\gamma\boldsymbol{\alpha}}(\mathbf{w})\right)\right]$, where $\hat{\mathbf{d}}_R$ is the erroneous observation vector given by $\hat{\mathbf{d}}_R = \left[\hat{d}_{R,1}, \ldots, \hat{d}_{R,N}\right]^T$, $\boldsymbol{\alpha}$ is the PLE vector given as $\boldsymbol{\alpha} = [\alpha_1, \ldots, \alpha_N]^T$, $\mathbf{d}$ is the true distance vector given as $\mathbf{d} = [d_1, \ldots, d_N]^T$, $\mathbf{w}$ is the noise vector representing shadowing, given as $\mathbf{w} = [\check{w}_1, \ldots, \check{w}_N]^T$ and $\odot$represents the Schur product. Clearly, (2.15) is non linear in terms of x and y. Thus we linearise it using a similar approach as was used for ToA based system, i.e., we subtract the square of a selected reference distance from square of all other distances. Thus we obtain

$$\left[(x-\bar{x}_r)^2+(y-\bar{y}_r)^2\right]-\left[(x-\bar{x}_i)^2+(y-\bar{y}_i)^2\right]=\beta_r^2\exp\left(\frac{2\hat{z}_r}{\gamma\alpha_r}\right)-\beta_i^2\exp\left(\frac{2\hat{z}_i}{\gamma\alpha_i}\right), \tag{2.16}$$

which can be simplified to

$$(\bar{x}_i-\bar{x}_r)\,x+(\bar{y}_i-\bar{y}_r)\,y=0.5\left[\left(\bar{x}_i^2+\bar{y}_i^2\right)-\left(\bar{x}_r^2+\bar{y}_r^2\right)+\beta_r^2\exp\left(\frac{2\hat{z}_r}{\gamma\alpha_r}\right)-\beta_i^2\exp\left(\frac{2\hat{z}_i}{\gamma\alpha_i}\right)\right]. \tag{2.17}$$

Equ. (2.17) can be written in matrix form as

$$\mathbf{A}_{\mathrm{RSS}}\mathbf{u}=0.5\mathbf{b}_{\mathrm{RSS}}, \tag{2.18}$$

where

$$\mathbf{A}_{\mathrm{RSS}}=\begin{bmatrix}\bar{x}_1-\bar{x}_r & \bar{y}_1-\bar{y}_r\\ \bar{x}_2-\bar{x}_r & \bar{y}_2-\bar{y}_r\\ \vdots & \vdots\\ \bar{x}_{N-1}-\bar{x}_r & \bar{y}_{N-1}-\bar{y}_r\end{bmatrix}\in\mathbb{R}^{(N-1)\times 2},\qquad \mathbf{u}=\begin{bmatrix}x\\ y\end{bmatrix}\in\mathbb{R}^{2\times 1}, \tag{2.19}$$

$$\mathbf{b}_{\mathrm{RSS}}=\begin{bmatrix}\beta_r^2\exp\left(\frac{2\hat{z}_r}{\gamma\alpha_r}\right)-\beta_1^2\exp\left(\frac{2\hat{z}_{1,t}}{\gamma\alpha_1}\right)-\varepsilon_r+(\bar{x}_1^2+\bar{y}_1^2)\\ \beta_r^2\exp\left(\frac{2\hat{z}_r}{\gamma\alpha_r}\right)-\beta_2^2\exp\left(\frac{2\hat{z}_2}{\gamma\alpha_2}\right)-\varepsilon_r+(\bar{x}_2^2+\bar{y}_2^2)\\ \vdots\\ \beta_r^2\exp\left(\frac{2\hat{z}_r}{\gamma\alpha_r}\right)-\beta_{N-1}^2\exp\left(\frac{2\hat{z}_{N-1}}{\gamma\alpha_{N-1}}\right)-\varepsilon_r+(\bar{x}_{N-1}^2+\bar{y}_{N-1}^2)_{N-1}\end{bmatrix}\in\mathbb{R}^{(N-1)\times 1}, \tag{2.20}$$

where $\varepsilon_r=(\bar{x}_r^2+\bar{y}_r^2)$. The LLS solution to (2.18) is obtained as

$$\hat{\mathbf{u}}=0.5\left(\mathbf{A}_{\mathrm{RSS}}^{\dagger}\hat{\mathbf{b}}_{\mathrm{RSS}}\right), \tag{2.21}$$

where $\mathbf{A}_{\mathrm{RSS}}^{\dagger}$ is Moore Penrose pseudo inverse of matrix $\mathbf{A}_{\mathrm{RSS}}$.

2.2.3 Linear Least Squares Solution for AoA Based System.

The AoA impinging at i^{th} AN, transmitted from TN is given as [37]

$$\hat{\theta}_i = \arctan\left[\frac{(y-\bar{y}_i)}{(x-\bar{x}_i)}\right] + m_i, \tag{2.22}$$

where m_i is the noise in angle estimate which is modelled as zero mean Gaussian random variable with variance $\sigma^2_{m_i}$, i.e., $m_i \sim \mathcal{N}\left(0, \sigma^2_{m_i}\right)$. (2.22) can be represented as

$$x\tan\theta_i - y = \bar{x}_i\tan\theta_i - \bar{y}_i, \tag{2.23}$$

which can be written in matrix form as

$$\hat{\mathbf{A}}_{\text{AoA}}\mathbf{u} = \hat{\mathbf{b}}_{\text{AoA}}, \tag{2.24}$$

where

$$\hat{\mathbf{A}}_{\text{AoA}} = \begin{bmatrix} \tan\hat{\theta}_1 & -1 \\ \tan\hat{\theta}_2 & -1 \\ \vdots & \vdots \\ \tan\hat{\theta}_N & -1 \end{bmatrix} \in \mathbb{R}^{N\times 2}, \qquad \mathbf{u} = \begin{bmatrix} x \\ y \end{bmatrix} \in \mathbb{R}^{2\times 1}, \tag{2.25}$$

$$\hat{\mathbf{b}}_{\text{AoA}} = \begin{bmatrix} \bar{x}_1\tan\hat{\theta}_1 - \bar{y}_1 \\ \bar{x}_2\tan\hat{\theta}_2 - \bar{y}_2 \\ \vdots \\ \bar{x}_N\tan\hat{\theta}_N - \bar{y}_N \end{bmatrix} \in \mathbb{R}^{N\times 1}. \tag{2.26}$$

The LLS solution to (2.24) is obtained as

$$\hat{\mathbf{u}} = \hat{\mathbf{A}}^{\dagger}_{\text{AoA}}\hat{\mathbf{b}}_{\text{AoA}}, \tag{2.27}$$

where $\hat{\mathbf{A}}^{\dagger}_{\text{AoA}}$ is the Moore Penrose inverse of $\hat{\mathbf{A}}_{\text{AoA}}$.

2.2.4 LLS solution for Hybrid AoA-ToA Based Systems

When both range and bearing are available, global location of a TN can be estimated with one AN only. Indeed, to improve accuracy, more ANs can be introduced. The requirement of only a single AN for localisation makes hybrid signal models an attractive feature in localisation schemes. In this subsection, we explain one the most commonly used hybrid model that is based on the AoA-ToA signal model.

Let $\hat{d}_{T,i}$ be the noisy range, estimated via ToA of the signal given by (2.1). In matrix form, (2.1) can be written as $\hat{\mathbf{d}}_T = \mathbf{d} + \mathbf{n}$, where $\hat{\mathbf{d}}_T = \left[\hat{d}_{T,1}, \ldots, \hat{d}_{T,N}\right]^T$ and $\mathbf{d} = [d_1, \ldots, d_N]^T$ while $\mathbf{n} = [n_1, \ldots, n_N]^T$ is the noise vector. Similarly for angle estimate (2.22) can be written in vector form as $\hat{\boldsymbol{\theta}} = \mathbf{f} + \mathbf{m}$, where $\hat{\boldsymbol{\theta}} = \left[\hat{\theta}_1, \ldots, \hat{\theta}_N\right]^T$ and $\mathbf{f} = \left[\arctan\left[(y-\bar{y}_1)/(x-\bar{x}_1)\right], \ldots, \arctan\left[(y-\bar{y}_N)/(x-\bar{x}_N)\right]\right]^T$ and $\mathbf{m} = [m_1, \ldots, m_N]^T$is the noise vector. With both range and angle estimates available, the x and y coordinates of the TN can be calculated using simple trigonometric equations [41].

$$x = \bar{x}_i + \hat{d}_{T,i} \cos\hat{\theta}_i \tag{2.28}$$

$$y = \bar{y}_i + \hat{d}_{T,i} \sin\hat{\theta}_i \tag{2.29}$$

As can be seen, (2.28) and (2.29) are linear in terms of x and y. Thus the linearising steps involved in ToA and RSS based localisation systems are not required. Equ. (2.28) and (2.29) can be written in matrix form for N ANs as

$$\mathbf{A}\mathbf{u} = \hat{\mathbf{t}}_u,$$

where

$$\mathbf{A} = \begin{bmatrix} 1_1 & 0 \\ \vdots & \vdots \\ 1_N & 0 \\ 0 & 1_1 \\ \vdots & \vdots \\ 0 & 1_N \end{bmatrix} \in \mathbb{R}^{2N\times 2},\ \mathbf{u} = \begin{bmatrix} x \\ y \end{bmatrix} \in \mathbb{R}^{2\times 1},\ \hat{\mathbf{t}}_u = \begin{bmatrix} \hat{\mathbf{m}}_x \\ \hat{\mathbf{m}}_y \end{bmatrix} \in \mathbb{R}^{2N\times 1} \quad (2.30)$$

$$\hat{\mathbf{m}}_x = \begin{bmatrix} \bar{x}_1 + \hat{d}_{T,1}\cos\hat{\theta}_1 \\ \vdots \\ \bar{x}_N + \hat{d}_{T,N}\cos\hat{\theta}_N \end{bmatrix}, \quad \hat{\mathbf{m}}_y = \begin{bmatrix} \bar{y}_1 + \hat{d}_{T,1}\sin\hat{\theta}_1 \\ \vdots \\ \bar{y}_N + \hat{d}_{T,N}\sin\hat{\theta}_N \end{bmatrix}. \quad (2.31)$$

The standard LLS solution is then given by

$$\hat{\mathbf{u}} = \mathbf{A}^{\dagger}\hat{\mathbf{t}}_u, \quad (2.32)$$

where $\mathbf{A}^{\dagger}$ is the Moore Penrose inverse of matrix $\mathbf{A}$.

2.2.4.1 Bias Calculation

For the LLS estimator explained in previous section, the bias can be calculated as [61]

$$\text{Bias} = E_{\mathbf{m},\mathbf{n}}\left(\hat{\mathbf{u}}\right) - \mathbf{u}, \quad (2.33)$$

where $\hat{\mathbf{u}}$ is the noisy estimate, $\mathbf{u}$ is the noise free estimate and the expectation is taken w.r.t noise vector $\mathbf{m}$ and $\mathbf{n}$. Equ. (2.33) can be written as

$$\text{Bias} = E_{\mathbf{m},\mathbf{n}}\left(\mathbf{A}^{\dagger}\hat{\mathbf{t}}_u\right) - \mathbf{A}^{\dagger}\mathbf{t}. \quad (2.34)$$

Where $\mathbf{t}$ represents the noise free observation matrix. Equ. (2.34) is further simplified to

$$\text{Bias} = \mathbf{A}^{\dagger} E_{\mathbf{m},\mathbf{n}} \left(\hat{\mathbf{t}}_u \right) - \mathbf{t} \tag{2.35}$$

$$\text{Bias} = \mathbf{A}^{\dagger} \left[\kappa \left(x \right) \ \kappa \left(y \right) \right]^T, \tag{2.36}$$

where $\boldsymbol{\kappa}\left(x\right) = E_{\mathbf{m},\mathbf{n}}\left(\hat{\mathbf{m}}_x\right) - \mathbf{m}_x$ and $\boldsymbol{\kappa}\left(y\right) = E_{\mathbf{m},\mathbf{n}}\left(\hat{\mathbf{m}}_y\right) - \mathbf{m}_y$. Then the i^{th} term of $\boldsymbol{\kappa}\left(x\right)$ is given by

$$\begin{aligned}
\boldsymbol{\kappa}\left(x\right)_i &= E_{m_i,n_i}\left[\bar{x}_i + \left(d_{T,i} + n_i\right)\cos\left(\theta_i + m_i\right) - \bar{x}_i - d_{T,i}\cos\theta_i\right] \\
&= E_{m_i,n_i}\left[d_{T,i}\cos\left(\theta_i + m_i\right) + n_i\cos\left(\theta_i + m_i\right) - d_{T,i}\cos\theta_i\right] \\
&= \left[d_{T,i}\cos\theta_i E_{m_i}\left(\cos m_i\right) + d_{T,i}\sin\theta_i E_{m_i}\left(\sin m_i\right) + E_{n_i}\left(n_i\right)\cos\theta_i\right. \\
&\quad \left. \times\ E_{m_i}\left(\cos m_i\right) + \ E_{n_i}\left(n_i\right)\sin\theta_i E_{m_i}\left(\sin m_i\right) - d_{T,i}\cos\theta_i\right] \qquad (2.37) \\
&= d_{T,i}\cos\theta_i\left[\exp\left(-\sigma^2_{m_i}/2\right) - 1\right] \qquad \text{for } i = 1, ..., N. \qquad (2.38)
\end{aligned}$$

Similarly the i^{th} term of $\boldsymbol{\kappa}\left(y\right)$ is given by

$$\boldsymbol{\kappa}\left(y\right)_i = d_{T,i}\sin\theta_i\left[\exp\left(-\sigma^2_{m_i}/2\right) - 1\right] \text{ for } i = 1, ..., N.$$

Equ. (2.38) is obtained from (2.37) by using the expectations which are given in table. 2.1

According to (2.38), the estimator presented in (2.32) is biased. In order to render (2.32) unbiased, we introduce an unbiasing constant, δ, in (2.28) and (2.29) which reduces (2.33) to zero. The new unbiased LLS estimator is explained next.

2.3 The New unbiased Hybrid AoA-ToA Estimator

In this section, we present an unbiased version of hybrid AoA-ToA estimator presented in the previous section. We mathematically verify that the estimator

is unbiased. Furthermore, to analyse the performance of LLS solution we derive the theoretical MSE expression for the estimator.

2.3.1 Hybrid AoA-ToA Signal Model

The formulation for the LLS technique presented in section 2.2.4, produces biased estimates of the unknown vector $\mathbf{u}$. The formulation of unbiased hybrid LLS estimator is similar to that in section 2.2.4, other than the fact that we introduce an unbiasing constant to (2.28) and (2.29). In order to counter the effect of the bias, for known variances, the modified LLS formulation for static nodes, is proposed below.

$$x = \bar{x}_i + \hat{d}_{T,i} \cos\hat{\theta}_i \delta_{T,i} \tag{2.39}$$

$$y = \bar{y}_i + \hat{d}_{T,i} \sin\hat{\theta}_i \delta_{T,i} \tag{2.40}$$

where $\delta_{T,i}$ is the unbiasing constant associated with i^{th} link for AoA-ToA signal model and is given by

$$\delta_{T,i} = \exp\left(\frac{\sigma^2_{m_i}}{2}\right). \tag{2.41}$$

By the introduction of (2.41) in (2.39) and (2.40), the estimator produces unbiased estimates of the unknown vector $\mathbf{u}$, i.e., (2.34) reduces to zero. Equ. (2.39) and (2.40) can be written in matrix form as $\mathbf{Au} = \hat{\mathbf{t}}$ where $\mathbf{A}$ and $\mathbf{u}$ are given by (2.30) and $\hat{\mathbf{t}} = \left[\hat{\mathbf{t}}_x, \hat{\mathbf{t}}_y\right]^T$ for

$$\hat{\mathbf{t}}_x = \begin{bmatrix} \bar{x}_1 + \hat{d}_{T,1}\cos\hat{\theta}_1\delta_{T,1} \\ \vdots \\ \bar{x}_N + \hat{d}_{T,N}\cos\hat{\theta}_N\delta_{T,N} \end{bmatrix}, \quad \hat{\mathbf{t}}_y = \begin{bmatrix} \bar{y}_1 + \hat{d}_{T,1}\sin\hat{\theta}_1\delta_{T,1} \\ \vdots \\ \bar{y}_N + \hat{d}_{T,N}\sin\hat{\theta}_N\delta_{T,1} \end{bmatrix}. \tag{2.42}$$

The LLS solution for the unbiased AoA-ToA signal model is given by

$$\hat{\mathbf{u}} = \mathbf{A}^{\dagger}\hat{\mathbf{t}}, \tag{2.43}$$

where $\mathbf{A}^{\dagger}$ is the Moore Penrose pseudo inverse of $\mathbf{A}$.

2.3.1.1 Bias Calculation

In this subsection, we show that the new unbiased AoA-ToA LLS estimator produces unbiased estimates of the unknown vector $\mathbf{u}$. Following similar formulation as in 2.2.4.1 we calculate the bias as

$$\text{Bias} = E_{\mathbf{m},\mathbf{n}}\left(\mathbf{A}^{\dagger}\hat{\mathbf{t}}\right) - \mathbf{A}^{\dagger}\mathbf{t}, \tag{2.44}$$

which after some mathematical manipulation can be written as

$$\text{Bias} = \mathbf{A}^{\dagger}\left[\boldsymbol{\kappa}\left(x\right)\ \boldsymbol{\kappa}\left(y\right)\right]^{T}, \tag{2.45}$$

for $\boldsymbol{\kappa}\left(x\right) = E_{\mathbf{m},\mathbf{n}}\left(\hat{\mathbf{t}}_x\right) - \mathbf{t}_x$ and $\boldsymbol{\kappa}\left(y\right) = E_{\mathbf{m},\mathbf{n}}\left(\hat{\mathbf{t}}_y\right) - \mathbf{t}_y$ .Then the i^{th} term of $\boldsymbol{\kappa}\left(x\right)$ is given by

$$\begin{aligned}
\boldsymbol{\kappa}\left(x\right)_i =& E_{m_i,n_i}\left[\bar{x}_i + \left(d_{T,i} + n_i\right)\cos\left(\theta_i + m_i\right)\delta_{T,i} - \bar{x}_i - d_{T,i}\cos\theta_i\right] \\
=& E_{m_i,n_i}\left[d_{T,i}\cos\left(\theta_i + m_i\right)\delta_{T,i} + n_i\cos\left(\theta_i + m_i\right)\delta_{T,i} - d_{T,i}\cos\theta_i\right] \\
=& \left[d_{T,i}\cos\theta_i E_{m_i}\left(\cos m_i\right)\delta_{T,i} + d_{T,i}\sin\theta_i E_{m_i}\left(\sin m_i\right)\delta_{T,i} + E_{n_i}\left(n_i\right)\cos\theta_i\right. \\
& \left.\times E_{m_i}\left(\cos m_i\right)\delta_{T,i} + E_{n_i}\left(n_i\right)\sin\theta_i E_{m_i}\left(\sin m_i\right)\delta_{T,i} - d_{T,i}\cos\theta_i\right].
\end{aligned} \tag{2.46}$$

After taking the expectations in (2.46) and plugging the value of $\delta_{T,i}$, (2.46) reduces to

$$\boldsymbol{\kappa}\left(x\right)_i = d_{T,i}\cos\theta_i\exp\left(-\frac{\sigma_{m_i}^2}{2} + \frac{\sigma_{m_i}^2}{2}\right) - d_{T,i}\cos\theta_i$$

$$\boldsymbol{\kappa}\left(x\right)_i = 0,$$

which proves that the estimated vector $\mathbf{u}$ is unbiased. Similarly by replacing the cos function in (2.46) with a sin function it can be shown that $\boldsymbol{\kappa}\left(y\right)_i$ is 0 for all $i = 1, ..., N$.

2.3.2 Theoretical MSE for AoA-ToA based LLS

In order to analyse the performance of the unbiased AoA-ToA signal based estimator, the theoretical MSE is derived. For a LLS estimator the theoretical MSE is given by.

$$\mathrm{MSE}(\mathbf{u}) = Tr\left\{E_{\mathbf{m},\mathbf{n}}\left[(\hat{\mathbf{u}}-\mathbf{u})(\hat{\mathbf{u}}-\mathbf{u})^T\right]\right\}, \tag{2.47}$$

which can be simplified to

$$\begin{aligned}
\mathrm{MSE}(\mathbf{u}) &= Tr\left\{E_{\mathbf{m},\mathbf{n}}\left[\left(\mathbf{A}^\dagger\hat{\mathbf{t}}-\mathbf{A}^\dagger\mathbf{t}\right)\left(\mathbf{A}^\dagger\hat{\mathbf{t}}-\mathbf{A}^\dagger\mathbf{t}\right)^T\right]\right\} \\
&= Tr\left\{E_{\mathbf{m},\mathbf{n}}\left[\left(\mathbf{A}^\dagger\hat{\mathbf{t}}-\mathbf{A}^\dagger\mathbf{t}\right)\left(\hat{\mathbf{t}}\left(\mathbf{A}^\dagger\right)^T-\mathbf{t}\left(\mathbf{A}^\dagger\right)^T\right)\right]\right\} \\
&= Tr\left\{\mathbf{A}^\dagger E_{\mathbf{m},\mathbf{n}}\left[\left(\hat{\mathbf{t}}-\mathbf{t}\right)\left(\hat{\mathbf{t}}-\mathbf{t}\right)\right]\left(\mathbf{A}^\dagger\right)^T\right\} \\
&= Tr\left\{\mathbf{A}^\dagger\mathbf{C}_{\mathrm{AT}}(\mathbf{u})\left(\mathbf{A}^\dagger\right)^T\right\},
\end{aligned}$$

where $\mathbf{C}_{\mathrm{AT}}(\mathbf{u})$ is the noise covariance for AoA-ToA signal model, i.e.,

$$\mathbf{C}_{\mathrm{AT}}(\mathbf{u}) = E_{\mathbf{m},\mathbf{n}}\left[\left(\hat{\mathbf{t}}-\mathbf{t}\right)\left(\hat{\mathbf{t}}-\mathbf{t}\right)\right]. \tag{2.48}$$

The matrix $\mathbf{C}_{\mathrm{AT}}(\mathbf{u})$ can be partitioned into separate submatrices as

$$\mathbf{C}_{\mathrm{AT}}(\mathbf{u}) = \begin{bmatrix} \mathbf{C}_{\mathrm{AT}}^{x} & \mathbf{C}_{\mathrm{AT}}^{xy} \\ \mathbf{C}_{\mathrm{AT}}^{xy} & \mathbf{C}_{\mathrm{AT}}^{y} \end{bmatrix} \in \mathbb{R}^{2N\times 2N}, \tag{2.49}$$

where

$$\begin{aligned}
\mathbf{C}_{\mathrm{AT}}^{x} &= E\left[\left(\hat{\mathbf{t}}_x-\mathbf{t}_x\right)\left(\hat{\mathbf{t}}_x-\mathbf{t}_x\right)^T\right]\in\mathbb{R}^{N\times N} \quad \mathbf{C}_{\mathrm{AT}}^{xy} = E\left[\left(\hat{\mathbf{t}}_x-\mathbf{t}_x\right)\left(\hat{\mathbf{t}}_y-\mathbf{t}_y\right)^T\right]\in\mathbb{R}^{N\times N} \\
\mathbf{C}_{\mathrm{AT}}^{xy} &= E\left[\left(\hat{\mathbf{t}}_x-\mathbf{t}_x\right)\left(\hat{\mathbf{t}}_y-\mathbf{t}_y\right)^T\right]\in\mathbb{R}^{N\times N} \quad \mathbf{C}_{\mathrm{AT}}^{y} = E\left[\left(\hat{\mathbf{t}}_y-\mathbf{t}_y\right)\left(\hat{\mathbf{t}}_y-\mathbf{t}_y\right)^T\right]\in\mathbb{R}^{N\times N}
\end{aligned} \tag{2.50}$$

For $i=j$, $\mathbf{C}_{\mathrm{AT}}^{x}$, $\mathbf{C}_{\mathrm{AT}}^{y}$ and $\mathbf{C}_{\mathrm{AT}}^{xy}$ are given as follows

$$\mathbf{C}^{x}_{\mathrm{AT}_{ii}} = \left(\frac{d^2_{T,i}}{2} + \frac{\sigma^2_{n_i}}{2}\right)\exp\left(\sigma^2_{m_i}\right) + \left(\frac{d^2_{T,i}}{2}\cos\left(2\theta_i\right) + \frac{\sigma^2_{n_i}}{2}\cos\left(2\theta_i\right)\right)\exp\left(-\sigma^2_{m_i}\right) - \left(d_{T,i}\cos\theta_i\right)^2 \quad (2.51)$$

$$\mathbf{C}^{y}_{\mathrm{AT}_{ii}} = \left(\frac{d^2_{T,i}}{2} + \frac{\sigma^2_{n_i}}{2}\right)\exp\left(\sigma^2_{m_i}\right) - \left(\frac{d^2_{T,i}}{2}\cos\left(2\theta_i\right) + \frac{\sigma^2_{n_i}}{2}\cos 2\theta_i\right)\exp\left(-\sigma^2_{m_i}\right) - \left(d_{T,i}\sin\theta_i\right)^2 \quad (2.52)$$

$$\mathbf{C}^{xy}_{\mathrm{AT}_{ii}} = \left(d^2_{T,i} + \sigma^2_{n_i}\right)\cos\theta_i\sin\theta_i\exp\left(-\sigma^2_{m_i}\right) - d^2_{T,i}\cos\theta_i\sin\theta_i. \quad (2.53)$$

For $i \neq j$, i.e., $\mathbf{C}^{x}_{\mathrm{AT}_{ij}} = \mathbf{C}^{y}_{\mathrm{AT}_{ij}} = \mathbf{C}^{xy}_{\mathrm{AT}ij} = 0$. The derivation of these equations is provided in appendix II A.

2.4 Performance Enhancements

In order to improve positioning accuracy we propose two enhancements to LLS approach: *i*) WLLS-AoA-ToA and *ii*) OAS algorithm.

2.4.1 WLLS-AoA-ToA

In order to achieve a higher accuracy of localisation a WLLS-AoA-ToA algorithm is presented in this section that utilize the noise covariance matrix. The noise covariance matrix stores all the information about the link quality, thus a noisy link is given less weight than a less noisy link. The WLLS-AoA-ToA solution is obtained by minimising the cost function.

$$\varepsilon_{\mathrm{w}} = \left(\hat{\mathbf{t}} - \mathbf{A}\mathbf{u}\right)^{T}\mathbf{C}^{-1}_{\mathrm{AT}}\left(\mathbf{u}\right)\left(\hat{\mathbf{t}} - \mathbf{A}\mathbf{u}\right), \quad (2.54)$$

where $\mathbf{C}^{-1}_{\mathrm{AT}}$ is the inverse of the covariance matrix given by (2.49). The minimum of (2.54) can be obtained by taking its derivative with respect to $\mathbf{u}$, equating it

to zero and then solving it for $\mathbf{u}$, i.e.,

$$\begin{aligned}
0 =& \frac{\delta}{\delta \mathbf{u}} \left(\hat{\mathbf{t}} - \mathbf{A}\mathbf{u}\right)^T \mathbf{C}_{\mathrm{AT}}^{-1}(\mathbf{u}) \left(\hat{\mathbf{t}} - \mathbf{A}\mathbf{u}\right) \\
0 =& \frac{\delta}{\delta \mathbf{u}} \left(\hat{\mathbf{t}}^T - \mathbf{u}^T\mathbf{A}^T\right) \left(\mathbf{C}_{\mathrm{AT}}^{-1}(\mathbf{u})\,\hat{\mathbf{t}} - \mathbf{C}_{\mathrm{AT}}^{-1}(\mathbf{u})\,\mathbf{A}\mathbf{u}\right) \\
0 =& \frac{\delta}{\delta \mathbf{u}} \left(\hat{\mathbf{t}}^T\mathbf{C}_{\mathrm{AT}}^{-1}(\mathbf{u})\,\hat{\mathbf{t}} - \hat{\mathbf{t}}^T\mathbf{C}_{\mathrm{AT}}^{-1}(\mathbf{u})\,\hat{\mathbf{t}}\mathbf{A}\mathbf{u} - \mathbf{u}^T\mathbf{A}^T\mathbf{C}_{\mathrm{AT}}^{-1}(\mathbf{u})\,\hat{\mathbf{t}} + \mathbf{u}^T\mathbf{A}^T\mathbf{C}_{\mathrm{AT}}^{-1}(\mathbf{u})\,\mathbf{A}\mathbf{u}\right)
\end{aligned} \tag{2.55}$$

After taking the derivative, we obtain

$$\begin{aligned}
0 &= -\hat{\mathbf{t}}^T\mathbf{C}_{\mathrm{AT}}^{-1}(\mathbf{u})\,\hat{\mathbf{t}}\mathbf{A} - \mathbf{A}^T\mathbf{C}_{\mathrm{AT}}^{-1}(\mathbf{u})\,\hat{\mathbf{t}} + 2\mathbf{A}^T\mathbf{C}_{\mathrm{AT}}^{-1}(\mathbf{u})\,\mathbf{A}\mathbf{u} \\
0 &= -2\mathbf{A}^T\mathbf{C}_{\mathrm{AT}}^{-1}(\mathbf{u})\,\hat{\mathbf{t}} + 2\mathbf{A}^T\mathbf{C}_{\mathrm{AT}}^{-1}(\mathbf{u})\,\mathbf{A}\mathbf{u} \\
\mathbf{A}^T\mathbf{C}_{\mathrm{AT}}^{-1}(\mathbf{u})\,\mathbf{A}\mathbf{u} &= \mathbf{A}^T\mathbf{C}_{\mathrm{AT}}^{-1}(\mathbf{u})\,\hat{\mathbf{t}} \\
\mathbf{u} &= \left(\mathbf{A}^T\mathbf{C}_{\mathrm{AT}}^{-1}(\mathbf{u})\,\mathbf{A}\right)^{-1}\mathbf{A}^T\mathbf{C}_{\mathrm{AT}}^{-1}(\mathbf{u})\,\hat{\mathbf{t}}.
\end{aligned}$$

The covariance matrix depends on the real values of distances and angles, which are not available. Thus their estimated values are used in the covariance matrix. Hence the estimated covariance matrix, i.e., $\mathbf{C}_{\mathrm{AT}}^{-1}(\hat{\mathbf{u}})$ is used. Now the WLLS-AoA-ToA solution is obtained as

$$\hat{\mathbf{u}}_{WLLS} = \mathbf{A}^{\ddagger}\mathbf{t}^{\ddagger}, \tag{2.56}$$

where

$\mathbf{A}^{\ddagger} = \left[\mathbf{A}^T\mathbf{C}_{\mathrm{AT}}^{-1}(\hat{\mathbf{u}})\,\mathbf{A}\right]^{-1}\mathbf{A}^T$ and $\hat{\mathbf{t}}^{\ddagger} = \mathbf{C}_{\mathrm{AT}}^{-1}(\hat{\mathbf{u}})\,\hat{\mathbf{t}}$.

The OAS is a LLS based approach, so WLLS will be better than OAS. However, The WLLS requires the covariance matrix which is not easy to calculate for some signal models. In such scenarios OAS can be used.

2.4.2 OAS Algorithm

Conventionally with the addition of more ANs to the system, the accuracy of localisation is improved. However this is not always the case. Some ANs that are

situated at a longer distance from the TN and/or receives signal after multiple reflection actually deteriorate the overall performance of the system. Hence an optimal subset of ANs can achieve better accuracy than using all ANs. Thus in this section, an optimal AN selection algorithm is designed that guarantees enhanced accuracy. This optimum combination of ANs is based on the theoretical MSE of LLS. The optimum combination, $\mathrm{C_{opt}}$ is the one that minimizes the MSE on localisation. Let C be any combination of ANs, then $\mathrm{C_{opt}}$ is obtained as

$$\mathrm{C_{opt}} = \arg\min_{\mathrm{C}} \left\{ \mathrm{MSE}(\hat{\mathbf{u}}) \right\}. \tag{2.57}$$

Thus a small number of ANs (in some cases even one AN) can achieve superior performance than using all ANs.

2.5 LCRB-AoA-ToA

The LCRB characterizes the best possible accuracy that can be achieved by an unbiased estimator. In order to lower bound the performance of the WLLS-AoA-ToA, the LCRB-AoA-ToA is derived in this section. For a two dimensional system the MSE bound is given by [61]

$$\mathrm{MSE}\left(\mathbf{u}\right) \geq \frac{\left[\mathbf{I}\left(\mathbf{u}\right)\right]_{11} + \left[\mathbf{I}\left(\mathbf{u}\right)\right]_{22}}{\det\left[\mathbf{I}\left(\mathbf{u}\right)\right]}, \tag{2.58}$$

where $[\mathbf{I}(\mathbf{u})]$ is the Fisher information matrix (FIM) whose elements are given by

$$\begin{aligned}\left[\mathbf{I}\left(\mathbf{u}\right)\right]_{kl} = &\left[\frac{\partial \boldsymbol{\mu}_t\left(\mathbf{u}\right)}{\partial \mathbf{u}_k}\right] \mathbf{C}_{\mathrm{AT}}^{-1}\left(\mathbf{u}\right) \left[\frac{\partial \boldsymbol{\mu}_t\left(\mathbf{u}\right)}{\partial \mathbf{u}_l}\right] \\ &+ \frac{1}{2} Tr\left[\left(\mathbf{C}_{\mathrm{AT}}^{-1}\left(\mathbf{u}\right) \frac{\partial \mathbf{C}_{\mathrm{AT}}\left(\mathbf{u}\right)}{\partial \mathbf{u}_k} \mathbf{C}_{\mathrm{AT}}^{-1}\left(\mathbf{u}\right) \frac{\partial \mathbf{C}_{\mathrm{AT}}\left(\mathbf{u}\right)}{\partial \mathbf{u}_l}\right)\right], \text{ for } k,l = 1,2.\end{aligned} \tag{2.59}$$

where $\boldsymbol{\mu}_t$ is the mean of observation vector $\hat{\mathbf{t}}$, and $\frac{\partial \boldsymbol{\mu}_t(\mathbf{u})}{\partial \mathbf{u}_1}$ is the derivative w.r.t x, i.e.,

Function	**Derivative w.r.t** x	**Derivative w.r.t** y
$\frac{d_{T,i}^2}{2}$	$\Big(x-\bar{x}_i\Big)$	$\Big(y-\bar{y}_i\Big)$
$\Big(\frac{\sigma_{n_i}^2}{2}\Big)$	0	0
$\Big(\frac{d_{T,i}^2}{2}\cos 2\theta_i\Big)$	$\sin 2\theta_i\Big(y-\bar{y}_i\Big)+\cos 2\theta_i\Big(x-\bar{x}_i\Big)$	$\cos 2\theta_i\Big(y-\bar{y}_i\Big)-\sin 2\theta_i\Big(x-\bar{x}_i\Big)$
$\Big(\frac{\sigma_{n_i}^2}{2}\cos 2\theta_i\Big)$	$\sigma_{n_i}^2 \sin 2\theta_i \frac{(y-\bar{y}_i)}{d_{T,i}^2}$	$-\sigma_{n_i}^2 \sin 2\theta_i \frac{(x-\bar{x}_i)}{d_{T,i}^2}$
$\Big(d_{T,i}\cos\theta_i\Big)^2$	$2\Big(x-\bar{x}_i\Big)$	0
$d_{T,i}^2 \cos\theta_i \sin\theta_i$	$(y-\bar{y}_i)$	$(x-\bar{x}_i)$
$\cos\theta_i \sin\theta_i$	$\sin^2\theta_i \frac{\Big(y-\bar{y}_i\Big)}{d_{T,i}^2} - \cos^2\theta_i \frac{\Big(y-\bar{y}_i\Big)}{d_{T,i}^2}$	$\cos^2\theta_i \frac{(x-\bar{x}_i)}{d_{T,i}^2} - \sin^2\theta_i \frac{(x-\bar{x}_i)}{d_{T,i}^2}$

Table 2.2: Derivate of covariance matrix for AoA-ToA.

$$\frac{\partial \boldsymbol{\mu}_t(\mathbf{u})}{\partial x} = [1_1, 1_2, \cdots 1_N, 0_1, 0_2, \cdots 0_N]^T,$$

and $\frac{\partial \boldsymbol{\mu}_t(\mathbf{u})}{\partial \mathbf{u}_2}$ is the derivative of the mean of observation vector w.r.t y, i.e.,

$$\frac{\partial \boldsymbol{\mu}_t(\mathbf{u})}{\partial y} = [0_1, 0_2, \cdots 0_N, 1_1, 1_2, \cdots 1_N]^T.$$

Similarly $\partial \mathbf{C}_{\mathrm{AT}}(\mathbf{u})/\partial_{\mathbf{u}_1}$ is the derivative of the covariance matrix w.r.t x, i.e.,

$$\frac{\partial \mathbf{C}_{\mathrm{AT}}(\mathbf{u})}{\partial \mathbf{u}_1} = \frac{\partial}{\partial x}\begin{bmatrix} \mathbf{C}_{\mathrm{AT}}^{x} & \mathbf{C}_{\mathrm{AT}}^{xy} \\ \mathbf{C}_{\mathrm{AT}}^{xy} & \mathbf{C}_{\mathrm{AT}}^{y} \end{bmatrix}, \tag{2.60}$$

and $\partial \mathbf{C}_{\mathrm{AT}}(\mathbf{u})/\partial_{\mathbf{u}_2}$ is the derivative w.r.t y, i.e.,

$$\frac{\partial \mathbf{C}_{\mathrm{AT}}(\mathbf{u})}{\partial \mathbf{u}_2} = \frac{\partial}{\partial y}\begin{bmatrix} \mathbf{C}_{\mathrm{AT}}^{x} & \mathbf{C}_{\mathrm{AT}}^{xy} \\ \mathbf{C}_{\mathrm{AT}}^{xy} & \mathbf{C}_{\mathrm{AT}}^{y} \end{bmatrix}. \tag{2.61}$$

The derivatives involved in (2.60) and (2.61) are given in table. 2.2, the complete derivation of which is given in appendix II-B.

Putting the values of table. 2.2 in (2.60) and (2.61), we get

$$\frac{\partial}{\partial x}\mathbf{C}_{\mathrm{AT}}^{x} = (x-\bar{x}_i)\exp\left(\sigma_{m_i}^2\right) + \Bigg[\sin 2\theta_i\,(y-\bar{y}_i) + \cos 2\theta_i\,(x-\bar{x}_i) + \sigma_{n_i}^2 \sin(2\theta_i)\,\frac{(y-\bar{y}_i)}{d_{T,i}^2}\Bigg]\exp\left(-\sigma_{m_i}^2\right) - 2(x-\bar{x}_i). \quad (2.62)$$

$$\frac{\partial}{\partial y}\mathbf{C}_{\mathrm{AT}}^{x} = (y-\bar{y}_i)\exp\left(\sigma_{m_i}^2\right) + \Bigg[\cos 2\theta_i\,(y-\bar{y}_i) - \sin 2\theta_i(x-\bar{x}_i) - \sigma_{n_i}^2 \sin 2\theta_i\frac{(x-\bar{x}_i)}{d_{T,i}^2}\Bigg] \times \exp\left(-\sigma_{m_i}^2\right). \quad (2.63)$$

$$\frac{\partial}{\partial x}\mathbf{C}_{\mathrm{AT}}^{y} = (x-\bar{x}_i)\exp\left(\sigma_{m_i}^2\right) - \Bigg[\sin 2\theta_i\,(y-\bar{y}_i) + \cos 2\theta_i\,(x-\bar{x}_i) + \sigma_{n_i}^2 \sin 2\theta_i\frac{(y-\bar{y}_i)}{d_{T,i}^2}\Bigg] \times \exp\left(-\sigma_{m_i}^2\right). \quad (2.64)$$

$$\frac{\partial}{\partial y}\mathbf{C}_{\mathrm{AT}}^{y} = (y-y_i)\exp\left(\sigma_{m_i}^2\right) + \Bigg[\cos 2\theta_i\,(y-\bar{y}_i) - \sin 2\theta_i(x-\bar{x}_i) - \sigma_{n_i}^2 \sin 2\theta_i\frac{(x-\bar{x}_i)}{d_{T,i}^2}\Bigg]\exp\left(\sigma_{m_i}^2\right) - 2\,(y-\bar{y}_i). \quad (2.65)$$

$$\frac{\partial}{\partial x}\mathbf{C}_{\mathrm{AT}}^{xy} = (x-\bar{x}_i)\left[\exp\left(-\sigma_{m_i}^2\right) - 1\right] + \left[\cos^2\theta_i\frac{(y-\bar{y}_i)}{d_{T,i}^2} - \sin^2\theta_i\frac{(y-\bar{y}_i)}{d_{T,i}^2}\right] \times \left[\sigma_{n_i}^2\exp\left(-\sigma_{m_i}^2\right)\right]. \quad (2.66)$$

$$\frac{\partial}{\partial y}\mathbf{C}_{\mathrm{AT}}^{xy} = \left[(y-\bar{y}_i)\left[\exp\left(-\sigma_{m_i}^2\right) - 1\right] + \left[\cos^2\theta_i\frac{(x-\bar{x}_i)}{d_{T,i}^2} - \sin^2\theta_i\frac{(x-\bar{x}_i)}{d_{T,i}^2}\right] \times \left[\sigma_{n_i}^2\exp\left(-\sigma_{m_i}^2\right)\right]. \quad (2.67)$$

The derivation of (2.62) to (2.67) is given in appendix II-B.

2.6 Critical Distance Analysis

In this section, we introduce the idea of the critical distance for hybrid systems. The error in the angle estimates is distance dependent, however, distance estimates based on the delay follow an additive noise model [62], [63] and is independent of the true distance between the nodes. We refer to the critical distance, d_c as the distance at which the error in location estimates due to noise in angle measurement equates the error due to noise in delay estimates. We derive a critical distance expression for a given noise variance in angle and distance.

At the critical distance, the MSE of location estimate due to noise in angle measurement is equal to the MSE due to the noise in distance measurement. Thus, at the critical distance,

$$\mathrm{MSE}_n\left(\mathbf{u}\right) = \mathrm{MSE}_m\left(\mathbf{u}\right), \tag{2.68}$$

where $\mathrm{MSE}_n\left(\mathbf{u}\right)$ represents the MSE of AoA-ToA signal model due to noise in the distance measurement only and is given by[1]

$$\mathrm{MSE}_n\left(\mathbf{u}\right) = Tr\left(\mathbf{A}^{\dagger}\mathbf{C}_n(\mathbf{u})\mathbf{A}^{\dagger^T}\right), \tag{2.69}$$

where

$$\mathbf{C}_n\left(\mathbf{u}\right) = \begin{bmatrix} \sigma_n^2\cos^2\theta & \sigma_n^2\cos\theta\sin\theta \\ \sigma_n^2\cos\theta\sin\theta & \sigma_n^2\sin^2\theta \end{bmatrix}. \tag{2.70}$$

On the other hand, $\mathrm{MSE}_m\left(\mathbf{u}\right)$ represents the MSE of AoA-ToA signal model due to the noise in the angle measurements only and is given by

$$\mathrm{MSE}_m\left(\mathbf{u}\right) = Tr\left[\mathbf{A}^{\dagger}\mathbf{C}_m\left(\mathbf{u}\right)\mathbf{A}^{\dagger^T}\right], \tag{2.71}$$

where

$$\mathbf{C}_m\left(\mathbf{u}\right) = d_c^2\bar{\mathbf{C}}\left(\mathbf{u}\right),$$

[1] $\mathrm{MSE}_m\left(\mathbf{u}\right)$ and $\mathrm{MSE}_n\left(\mathbf{u}\right)$ are for one AN in this case.

and

$$\bar{\mathbf{C}}\left(\mathbf{u}\right) = \begin{bmatrix} 0.5\delta_T^2 + 0.5\cos\left(2\theta\right)\delta_T^{-2} - \cos^2\theta & \cos\theta\sin\theta\delta_T^2 - \cos\theta\sin\theta \\ \cos\theta\sin\theta\delta_T^2 - \cos\theta\sin\theta & 0.5\delta_T^2 - 0.5\cos\left(2\theta\right)\delta_T^{-2} - \sin^2\theta \end{bmatrix}. \tag{2.72}$$

Putting (2.69) and (2.71) in (2.68), we obtain

$$d_c^2 Tr\left[\mathbf{A}^\dagger \bar{\mathbf{C}}\left(\mathbf{u}\right)\mathbf{A}^{\dagger^T}\right] = Tr\left[\mathbf{A}^\dagger \mathbf{C}_n(\mathbf{u})\mathbf{A}^{\dagger^T}\right]. \tag{2.73}$$

For one AN, $\mathbf{A}^\dagger$ is a 2×2 identity matrix. Thus (2.73) leads to

$$d_c^2 Tr\left[\bar{\mathbf{C}}\left(\mathbf{u}\right)\right] = Tr\left[\mathbf{C}_n(\mathbf{u})\right]. \tag{2.74}$$

Putting elements of $\bar{\mathbf{C}}\left(\mathbf{u}\right)$ and $\mathbf{C}_n(\mathbf{u})$ in (2.74) and then taking the trace, results in

$$d_c = \sqrt{\sigma_n^2/\left(\delta_T^2 - 1\right)}. \tag{2.75}$$

Numerical Example We take $\sigma_n^2 = 7$ m^2 and $\sigma_m^2 = 0.07$ rad, then $\delta_T^2 = 1.0723$. Using these values in (2.75) we get

$$d_c = \sqrt{7/\left(1.0723 - 1\right)} = 9.8\,\text{m}. \tag{2.76}$$

This result will be verified by Monte Carlo simulation in the following section.

2.7 Simulation Results

Performance evaluation is done in this section via Monte Carlo simulation. The reason to use Monte Carlo simulation is to show that the derived close form solutions are correct. All simulations are run independently ℓ number of times and the noise variance of all communication links is considered same. We take a network of 300 m $\times$ 200 m dimension with subsets of 4 ANs at fixed and known

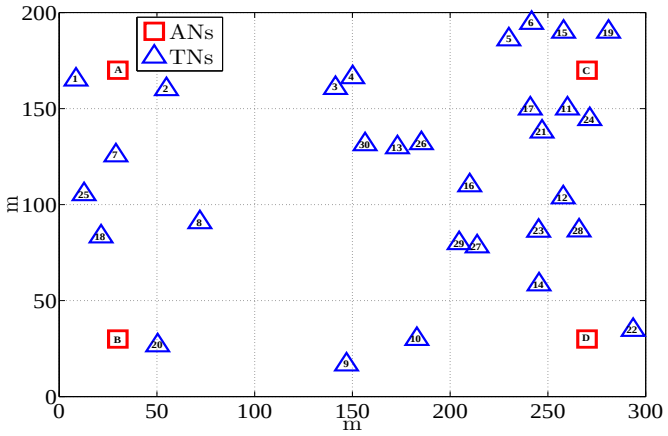

Figure 2.1: Network deployment.

locations and subsets of 30 TNs taken at random positions. A same network deployment, shown in Fig. 2.1 is considered for all simulation in each chapter. Though, the performance of the proposed algorithms will be different in different network scenarios, the proposed techniques will always outperform its previous counterparts. Though, the performance of the proposed algorithms will be different in different network scenarios, the proposed techniques will always outperform its previous versions.

Figure 2.2 demonstrates the performance of the hybrid signal model via theoretical MSE for LLS, Monte Carlo simulation for LLS and Monte Carlo simulation for WLLS-AoA-ToA. It is evident from the figure that the theoretical MSE accurately predicts the system performance for LLS and that the WLLS-AoA-ToA outperforms the LLS solution.

In Fig. 2.3 the performance is evaluated for different combinations of ANs. It is observed that the combination [A,C,D] of ANs given in Fig.2.1, gives us the better accuracy than using all ANs simultaneously as shown by the combination [A,B,C,D]. For clarity purpose the performance achieved by some combinations is not shown in the figure.

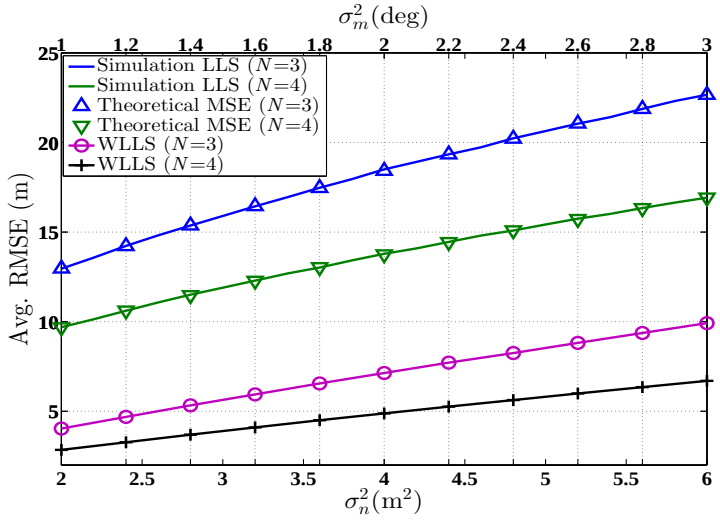

Figure 2.2: Performance comparison between LLS, WLLS-AoA-ToA and theoretical MSE for LLS. ANs = $[(\mathrm{A},\mathrm{B},\mathrm{C})\ ,(\mathrm{A},\mathrm{B},\mathrm{C},\mathrm{D})]$, TN = $[1-30]$, $\ell = 1500$.

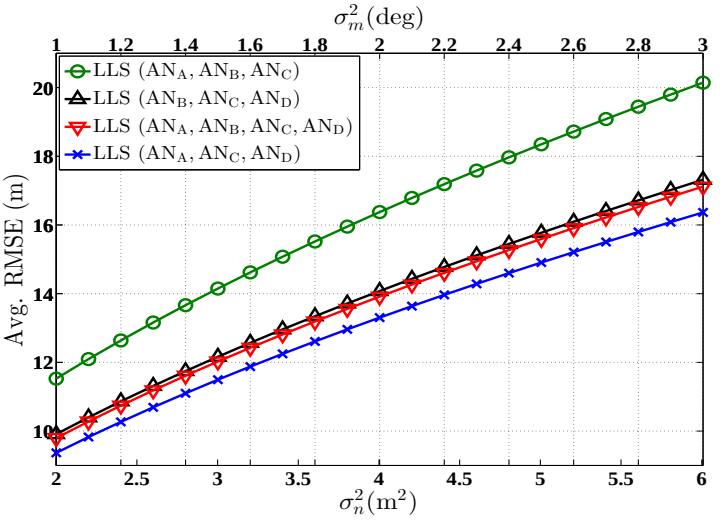

Figure 2.3: Performance evaluation for different combinations of ANs. ANs = $[(\mathrm{A},\mathrm{B},\mathrm{C})\ ,(\mathrm{B},\mathrm{C},\mathrm{D})\ ,(\mathrm{A},\mathrm{C},\mathrm{D})\ ,(\mathrm{A},\mathrm{B},\mathrm{C},\mathrm{D})]$, TNs = $[5, 11\ , 15, 16, 17, 21, 23, 24\ , 26]$, $\ell = 3000$.

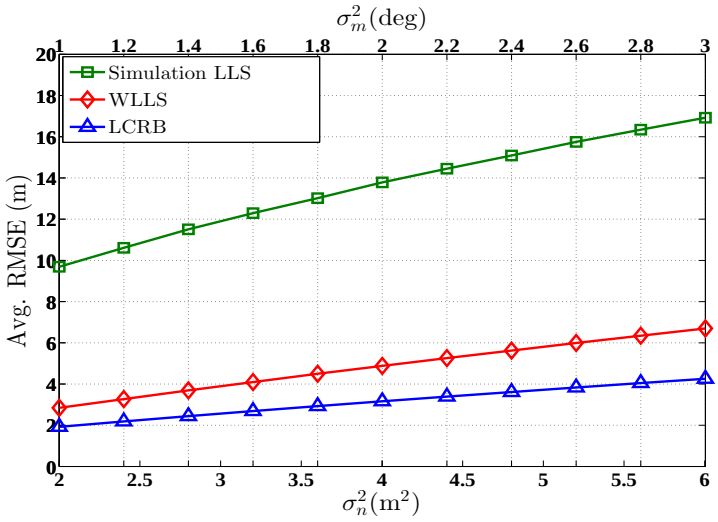

Figure 2.4: LCRB comparison with WLLS-AoA-ToA and LLS. ANs $= [\mathrm{A} - \mathrm{D}]$, TNs $= [1 - 30]$, $\ell = 3000$.

The LCRB is compared with WLLS-AoA-ToA solution in Fig. 2.4. It is demonstrated that the LCRB presented in section 5 tightly bounds the performance of the WLLS-AoA-ToA solution. For comparison the LLS solution is also presented in the figure.

The critical distance expression was derived in section 2.6 and a numerical example was presented. Via Monte Carlo simulation, the LLS solution is obtained for AoA-ToA signal model for different values of d, once with noise in angle estimates only and then with noise in distance estimates only which is represented by the bold and dashed curve in Fig 2.5, respectively. It is observed that both of these curves coincide when the distance between AN and TN is 9.8 m. Which agrees with the critical distance obtained numerically. Hence, verifying that our derivation for critical distance expression is correct.

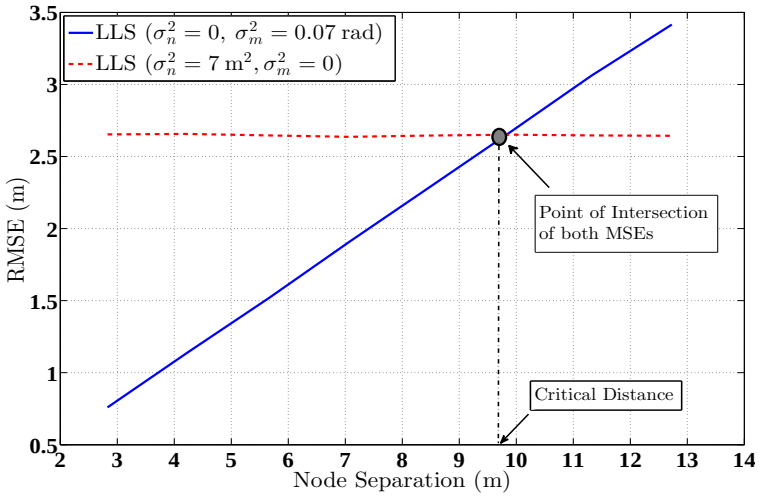

Figure 2.5: Critical distance verification.

2.8 Summary

In this chapter some of the most commonly used techniques and signal models used for localisation were reviewed. These include ToA based, RSS based, AoA based and hybrid signal models. A new unbiased LLS estimator based on the AoA-ToA signal model was presented and the theoretical MSE expression for LLS was derived. Furthermore, performance enhancement was achieved by proposing a weighting strategy based on the noise covariance matrix of the signal and a WLLS-AoA-ToA algorithm was presented. Also by designing an optimal AN selection criteria the accuracy of estimation is further improved, hence OAS algorithm is proposed. Moreover to lower bound the performance of the WLLS-AoA-ToA algorithm, the LCRB-AoA-ToA is derived which tightly bounds the performance of WLLS-AoA-ToA algorithm. Finally the notion of critical distance is introduced and a critical distance equation is derived mathematically and is verified via simulation. Performance enhancement to LLS by WLLS-AoA-ToA and OAS algorithm is shown via Monte Carlo simulation.

Distance estimation can also be achieved via RSS, thus a hybrid AoA-RSS signal

model is presented in the next chapter.

3 Enhanced Positioning Using Angle of Arrival and Received Signal Strength Measurements

The material of this chapter is presented in

i) Naveed Salman, M. W. Khan, A. H. Kemp "Enhanced Hybrid Positioning in Wireless Networks II: AoA-RSS," *IEEE International Conference on Telecommunications and Multimedia* (TEMU), pp. 92-97, July 2014.

ii) **M. W. Khan**, N. Salman, A. H. Kemp, L. Mihaylova "Positioning with Hybrid Measurements in Wireless Sensor Networks," (Submitted to MDPI Sensor journal).

Overview

- In this chapter, we introduce an AoA-RRS signal based approach for static nodes localisation. A LLS estimator is designed, which is further improved by presenting a WLLS-AoA-RSS algorithm based on the noise covariance matrix of the signal. Furthermore, a new zone based two steps optimal ANs selection, TSOAS, scheme is designed to enhance the LLS performance. In order to imitate a more realistic environment, no assumption about the

knowledge of the PLE vector is considered. Thus a joint PLE-coordinate estimation is done for AoA-RSS signal model. Moreover to lower bound the performance of WLLS-AoA-RSS algorithm, a LCRB for AoA-RSS signal model, LCRB-AoA-RSS, is derived. All results and algorithms are verified by simulation.

The rest of the chapter is organised as follows: Section I presents the unbiased AoA-RSS signal model for which an LLS estimator is proposed. Mathematical calculation of bias and theoretical MSE expression for LLS is also presented in section I. Performance enhancement is achieved by proposing: *i*) WLLS-AoA-RSS, *ii*) TSOAS in section II. Section III proposes a novel PLE estimator which is followed by the derivation of LCRB in section IV. All algorithms and derivations are verified via Monte Carlo simulation in section V. Finally, section VI summarizes chapter 3.

3.1 Hybrid AoA-RSS Signal Model

An unbiased hybrid AoA-RSS signal model is presented in this section. A LLS approach is designed to obtain the TN's coordinates and the bias for LLS approach is calculated. In order to predict the performance of the hybrid model a theoretical MSE based on LLS approach is also derived.

3.1.1 LLS solution for Hybrid AoA-RSS Signal Model

The formulation of LLS solution for hybrid AoA-RSS signal model is similar to the formulation of LLS solution for AoA-ToA signal model other than the fact that the range is estimated from the received power of the signal and the unbiasing constant is different because of the introduction of the shadowing effect

in the range estimation. Using the same notations as in chapter 2, the x and y coordinates of the TN, based on angle estimates and range estimates from the received power are given as

$$x = \bar{x}_i + \hat{d}_{R,i} \cos\hat{\theta}_i \delta_{R,i} \tag{3.1}$$

$$y = \bar{y}_i + \hat{d}_{R,i} \sin\hat{\theta}_i \delta_{R,i}, \tag{3.2}$$

where $\hat{d}_{R,i}$ is given by (2.13) and the term $\delta_{R,i}$ represents the unbiasing constant for AoA-RSS signal, associated with i^{th} AN and is given by

$$\delta_{R,i} = \exp\left(\frac{\sigma_{m_i}^2}{2} - \frac{\sigma_{\dot{w}_i}^2}{2\left(\gamma\alpha_i\right)^2}\right). \tag{3.3}$$

In matrix form (3.2) and (3.1) are given as $\mathbf{Au} = \hat{\mathbf{r}}$ where $\mathbf{A}$ and $\mathbf{u}$ are given by

$$\mathbf{A} = \begin{bmatrix} 1_1 & 0 \\ \vdots & \vdots \\ 1_N & 0 \\ 0 & 1_1 \\ \vdots & \vdots \\ 0 & 1_N \end{bmatrix} \in \mathbb{R}^{2N\times 2},\ \mathbf{u} = \begin{bmatrix} x \\ y \end{bmatrix} \in \mathbb{R}^{2\times 1}, \tag{3.4}$$

and $\hat{\mathbf{r}}$ is the erroneous observation matrix given by $\hat{\mathbf{r}} = [\hat{\mathbf{r}}_x,\ \hat{\mathbf{r}}_y]^T$, where

$$\hat{\mathbf{r}}_x = \begin{bmatrix} \bar{x}_1 + \hat{d}_{R,1}\cos\hat{\theta}_1\delta_{R,1} \\ \vdots \\ \bar{x}_N + \hat{d}_{R,N}\cos\hat{\theta}_N\delta_{R,N} \end{bmatrix}, \quad \hat{\mathbf{r}}_y = \begin{bmatrix} \bar{y}_1 + \hat{d}_{R,1}\sin\hat{\theta}_1\delta_{R,1} \\ \vdots \\ \bar{y}_N + \hat{d}_{R,N}\sin\hat{\theta}_N\delta_{R,1} \end{bmatrix}. \tag{3.5}$$

The standard LLS solution is then obtained as

$$\hat{\mathbf{u}} = \mathbf{A}^{\dagger}\hat{\mathbf{r}}, \tag{3.6}$$

where $\mathbf{A}^{\dagger}$ is the Moore Penrose pseudo inverse of matrix $\mathbf{A}$.

3.1.1.1 Bias Calculation

The total bias in the LLS estimator, (3.6), is given as

$$\text{Bias} = E_{\mathbf{w},\mathbf{m}}\left(\mathbf{A}^{\dagger}\hat{\mathbf{r}}\right) - \mathbf{A}^{\dagger}\mathbf{r}, \tag{3.7}$$

where $\hat{\mathbf{r}}$ represent the noisy observations and $\mathbf{r}$ represent noise free observation vector, $\mathbf{w}$ and $\mathbf{m}$ are noise vectors associated with range estimate and angle estimate, respectively. Equ. (3.7) can be written as, Bias $= \mathbf{A}^{\dagger}\left[\boldsymbol{\kappa}\left(x\right)\,\boldsymbol{\kappa}\left(y\right)\right]^{T}$, where $\boldsymbol{\kappa}\left(x\right) = E_{\mathbf{w},\mathbf{m}}\left(\hat{\mathbf{r}}_x\right) - \mathbf{r}_x$ and $\boldsymbol{\kappa}\left(y\right) = E_{\mathbf{w},\mathbf{m}}\left(\hat{\mathbf{r}}_y\right) - \mathbf{r}_y$. Then the i^{th} term of $\boldsymbol{\kappa}\left(x\right)$ is given by

$$\begin{aligned}
\boldsymbol{\kappa}\left(x\right)_i =& E_{\check{w}_i,m_i}\left[\bar{x}_i + d_i\exp\left(\frac{\check{w}_i}{\gamma\alpha_i}\right)\cos\left(\theta_i + m_i\right)\delta_{R,i} - \bar{x}_i - d_i\cos\theta_i\right]. \\
=& E_{\check{w}_i,m_i}\left[d_i\exp\left(\frac{\check{w}_i}{\gamma\alpha_i}\right)\cos\left(\theta_i + m_i\right)\delta_{R,i} - d_i\cos\theta_i\right]. && (3.8) \\
=& d_i E_{\check{w}_i}\left[\exp\left(\frac{\check{w}_i}{\gamma\alpha_i}\right)\right]\cos\theta_i E_{m_i}\left[\cos m_i\right]\delta_{R,i} \\
&+ d_i E_{\check{w}_i}\left[\exp\left(\frac{\check{w}_i}{\gamma\alpha_i}\right)\right]\sin\theta_i E_{m_i}\left[\sin m_i\right]\delta_{R,i} - d_i\cos\theta_i. && (3.9) \\
=& d_i\cos\theta_i\exp\left(\frac{\sigma^2_{\check{w}_i}}{2\left(\gamma\alpha_i\right)^2} - \frac{\sigma^2_{\check{w}_i}}{2\left(\gamma\alpha_i\right)^2} + \frac{\sigma^2_{m_i}}{2} - \frac{\sigma^2_{m_i}}{2}\right) - d_i\cos\theta_i. && (3.10)
\end{aligned}$$

$$\boldsymbol{\kappa}\left(x\right)_i = 0. \tag{3.11}$$

Equ. (3.9) is obtained from (3.8) by using the compound angle formula $\cos\left(\mathrm{A}+\mathrm{B}\right) = \cos\mathrm{A}\cos\mathrm{B} + \sin\mathrm{A}\sin\mathrm{B}$. Finally, (3.10) is obtained by plugging the value of $\delta_{R,i}$ and by taking the expectations given in table. 2.1. Similarly, by replacing the cos function in (3.8) with a sin function it can be shown that $\boldsymbol{\kappa}\left(y\right)_i = 0$ for all $i = 1, ..., N$.

3.1.2 Theoretical MSE for AoA-RSS based LLS

For performance analysis we derive the theoretical MSE expression for the LLS algorithm using AoA-RSS signal model. The theoretical MSE for LLS solution

using AoA-RSS signal can be expressed as

$$MSE(\mathbf{u}) = Tr\left\{E_{\mathbf{w},\mathbf{m}}\left[(\hat{\mathbf{u}}-\mathbf{u})(\hat{\mathbf{u}}-\mathbf{u})^T\right]\right\}. \tag{3.12}$$

Plugging (3.6) in (3.12) and after some mathematical manipulation we obtain

$$MSE(\mathbf{u}) = Tr\left\{\mathbf{A}^{\dagger}\mathbf{C}_{\mathrm{AR}}(\mathbf{u})\left(\mathbf{A}^{\dagger}\right)^T\right\}, \tag{3.13}$$

where $\mathbf{C}_{\mathrm{AR}}(\mathbf{u}) = E_{\mathbf{w},\mathbf{m}}\left[(\hat{\mathbf{r}}-\mathbf{r})(\hat{\mathbf{r}}-\mathbf{r})\right]$, which can be partitioned into submatrices as

$$\mathbf{C}_{\mathrm{AR}}(\mathbf{u}) = \begin{bmatrix} \mathbf{C}^{x}_{\mathrm{AR}} & \mathbf{C}^{xy}_{\mathrm{AR}} \\ \mathbf{C}^{yx}_{\mathrm{AR}} & \mathbf{C}^{y}_{\mathrm{AR}} \end{bmatrix} \in \mathbb{R}^{2N\times 2N}, \tag{3.14}$$

where

$$\begin{aligned} \mathbf{C}^{x}_{\mathrm{AR}} &= E\left[(\hat{\mathbf{r}}_x-\mathbf{r}_x)(\hat{\mathbf{r}}_x-\mathbf{r}_x)^T\right]\in\mathbb{R}^{N\times N} & \mathbf{C}^{xy}_{\mathrm{AR}} &= E\left[(\hat{\mathbf{r}}_x-\mathbf{r}_x)(\hat{\mathbf{r}}_y-\mathbf{r}_y)^T\right]\in\mathbb{R}^{N\times N} \\ \mathbf{C}^{yx}_{\mathrm{AR}} &= E\left[(\hat{\mathbf{r}}_x-\mathbf{r}_x)(\hat{\mathbf{r}}_y-\mathbf{r}_y)^T\right]\in\mathbb{R}^{N\times N} & \mathbf{C}^{y}_{\mathrm{AR}} &= E\left[(\hat{\mathbf{r}}_y-\mathbf{r}_y)(\hat{\mathbf{r}}_y-\mathbf{r}_y)^T\right]\in\mathbb{R}^{N\times N} \end{aligned} \tag{3.15}$$

which for $i=j$ are given as follows

$$\mathbf{C}^{x}_{\mathrm{AR}_{ii}} = \frac{d^2_{R,i}}{2}\exp\left(\frac{\sigma^2_{\breve{w}_i}}{(\gamma\alpha_i)^2}+\sigma^2_{m_i}\right)+\frac{d^2_{R,i}}{2}\cos 2\theta_i\exp\left(\frac{\sigma^2_{\breve{w}_i}}{(\gamma\alpha_i)^2}-\sigma^2_{m_i}\right)-\left(d_{R,i}\cos\theta_i\right)^2. \tag{3.16}$$

$$\mathbf{C}^{y}_{\mathrm{AR}_{ii}} = \frac{d^2_{R,i}}{2}\exp\left(\frac{\sigma^2_{\breve{w}_i}}{(\gamma\alpha_i)^2}+\sigma^2_{m_i}\right)-\frac{d^2_{R,i}}{2}\cos 2\theta_i\exp\left(\frac{\sigma^2_{\breve{w}_i}}{(\gamma\alpha_i)^2}-\sigma^2_{m_i}\right)-\left(d_{R,i}\sin\theta_i\right)^2. \tag{3.17}$$

$$\mathbf{C}^{xy}_{\mathrm{AR}_{ii}} = d^2_{R,i}\cos\theta_i\sin\theta_i\left[\exp\left(\frac{\sigma^2_{\breve{w}_i}}{(\gamma\alpha_i)^2}-\sigma^2_{m_i}\right)-1\right]. \tag{3.18}$$

For $i\neq j$, i.e., $\mathbf{C}^{x}_{\mathrm{AR}_{ij}} = \mathbf{C}^{y}_{\mathrm{AR}_{ij}} = \mathbf{C}^{xy}_{\mathrm{AR}_{ij}} = 0$. The derivation of these expressions is given in appendix III.

3.2 Performance Enhancement

A more reliable estimator based on hybrid AoA-RSS signal model is presented, called the WLLS-AoA-RSS and is based on the noise covariance, (3.14), of the signal. Furthermore, a novel two step optimal ANs selection scheme, TSOAS, is also presented that enhances the performance of the LLS algorithm.

3.2.1 WLLS-AoA-RSS

Performance of LLS solution for hybrid AoA-RSS signal model can be improved by utilizing the information stored in the noise covariance matrix. We use the covariance matrix in a similar fashion as presented in section 2.3.3 and propose a WLLS-AoA-RSS algorithm. The cost function for WLLS-AoA-RSS is given by

$$\varepsilon_{\mathrm{w}} = (\hat{\mathbf{r}} - \mathbf{A}\mathbf{u})^T \mathbf{C}_{\mathrm{AR}}^{-1}(\mathbf{u})(\hat{\mathbf{r}} - \mathbf{A}\mathbf{u}), \tag{3.19}$$

where $\mathbf{C}_{\mathrm{AR}}^{-1}(\mathbf{u})$ is the inverse of the estimated noise covariance matrix for AoA-RSS signal model. It is noted that $\mathbf{C}_{\mathrm{AR}}^{-1}(\mathbf{u})$ depends on the real values of distances and angles, which are not available. Thus we use the noisy estimated values in (3.19) and use the estimated covariance matrix, $\mathbf{C}_{\mathrm{AR}}^{-1}(\hat{\mathbf{u}})$. The WLLS-AoA-RSS solution is then given by

$$\mathbf{u}_{\mathrm{WLLS}} = \mathbf{A}^{\dagger}\hat{\mathbf{r}}^{\dagger},$$

where

$$\mathbf{A}^{\dagger} = \left[\mathbf{A}^T \mathbf{C}_{\mathrm{AR}}^{-1}(\hat{\mathbf{u}})\mathbf{A}\right]^{-1}\mathbf{A}^T \text{ and } \hat{\mathbf{r}}^{\dagger} = \mathbf{C}_{\mathrm{AR}}^{-1}(\hat{\mathbf{u}})\hat{\mathbf{r}}.$$

A second iteration can be performed in which the range and angle estimated from the TN's coordinates obtained from the first iteration are used in the covariance matrix. However, the insignificant performance improvement is not worth the increase in computational complexity of the algorithm.

3.2.2 TSOAS Algorithm

Due to unequal error associated with estimates from different ANs, some ANs may actually deteriorate the positioning accuracy. These ANs may be positioned at a large distance from the TN, may receive signals through multiple paths or may have a poor geometric dilution of precision (GDOP). This scenario is more obvious in a networks where some TNs are outside the convex hull defined by the ANs. Thus, for different TNs in a network there exist an optimal subset of ANs that guarantees optimal accuracy. In this section, we presents TSOAS, a two step optimal AN selection scheme; a pre processing step, called the zone detection, that select different subset of ANs for different TNs followed by the optimal localisation step, where TNs are localized with their respective optimal subsets of ANs.

Step 1: Zone Detection: During this pre processing step the whole network is divided into a grid. The complexity of this step depends on the resolution of the grid and the total number of ANs. However this step needs to be performed only once. Each point on the grid acts as a pseudo TN (PTN). For each of these PTNs the localisation error is calculated for all combinations of ANs using the theoretical MSE presented in the previous section. The combination that shows the lowest MSE is selected as an optimal combination for that point. Thus using this technique, a particular combination is selected for different points on the grid. In this way the whole network is divided into different regions called zones, where each zone has its own optimal subset of ANs that shows the lowest MSE. For the network considered in this chapter, the zones are shown in Fig. 3.3. The optimum combination of ANs for a PTN is calculated by

$$\mathrm{C}^{k}{}_{\mathrm{opt}} = \arg\min_{\mathrm{C}} \left\{ \mathrm{MSE}(\hat{\mathbf{u}}) \right\}.$$

where C represents any combination and $\mathrm{C}^{k}_{\mathrm{opt}}$ is the optimal combination for k^{th}

PTN.

Step II: Optimal Localisation: The second step is also two folds. Firstly a rough estimate of the location of the TN is obtained using all ANs. This rough estimate is necessary to detect the zone where the TN belongs. Once the zone is detected, the location of this TN is refined by localising it again, this time using the optimal combination of ANs for its respective zone.

3.3 Path Loss Exponents (PLEs) Estimation

In order to extract the distance estimate from received path-loss the correct knowledge of PLE associated with each link is necessary. In most of the studies, the PLEs are assumed to be known and are considered to be the same for all links [64], [65]. However, even a small error in PLE vector produces significant error in the final estimate of the coordinates. Recently, some studies propose joint PLE and coordinates estimation [66], [67]. However a same PLE value for all communication links is considered, which is an oversimplification of real conditions. Assuming that ANs and TNs are static, we consider a static but different PLE value for each communication link. For a mobile TN, the PLEs are not static. This scenario is studied in chapter 5. We use the derivative free optimisation technique called generalised pattern search (GenPS) to estimate the PLE vector. These PLE values are then utilised for localisation. According to (2.13), (3.1) and (3.2) can be written as

$$x = \bar{x}_i + \exp\left(\frac{\hat{z}_i}{\gamma\alpha_i}\right)\cos\hat{\theta}_i\delta_{R,i} \quad \text{for } i = 1,\ldots,N \tag{3.20}$$

$$y = \bar{y}_i + \exp\left(\frac{\hat{z}_i}{\gamma\alpha_i}\right)\sin\hat{\theta}_i\delta_{R,i} \quad \text{for } i = 1,\ldots,N \tag{3.21}$$

In matrix form, (3.20) and (3.21) can be written as

$$\mathbf{A}\mathbf{u} = \mathbf{r}_{\alpha}, \tag{3.22}$$

where $\mathbf{A}$ and $\mathbf{u}$ are given by (3.4) and $\mathbf{r}_{\alpha} = [\mathbf{r}_{x,\alpha}, \mathbf{r}_{y,\alpha}]^T$, where

$$\mathbf{r}_{x,\alpha} = \begin{bmatrix} \bar{x}_1 + \exp\left(\frac{\hat{z}_1}{\gamma\alpha_1}\right)\cos\hat{\theta}_1\delta_{R,1} \\ \vdots \\ \bar{x}_N + \exp\left(\frac{\hat{z}_N}{\gamma\alpha_N}\right)\cos\hat{\theta}_N\delta_{R,N} \end{bmatrix}, \ \mathbf{r}_{y,\alpha} = \begin{bmatrix} \bar{x}_1 + \exp\left(\frac{\hat{z}_1}{\gamma\alpha_1}\right)\sin\hat{\theta}_1\delta_{R,1} \\ \vdots \\ \bar{x}_N + \exp\left(\frac{\hat{z}_N}{\gamma\alpha_N}\right)\sin\hat{\theta}_N\delta_{R,N} \end{bmatrix}$$

From (3.22), the cost function for unknown PLE vector can be written as

$$\boldsymbol{\Psi}(\mathbf{u}, \boldsymbol{\alpha}) = \| \mathbf{A}\mathbf{u} - \hat{\mathbf{r}}_{\alpha} \|^2, \tag{3.23}$$

where $\boldsymbol{\alpha}$ is the PLE vector given by $\boldsymbol{\alpha} = [\alpha_1, \ldots, \alpha_N]^T$. The LLS solution to $\mathbf{u}$ is given by $\mathbf{u} = \mathbf{A}^{\dagger}\mathbf{r}_{\alpha}$. Putting $\mathbf{u}$ in (3.23) we get

$$\boldsymbol{\Psi}(\boldsymbol{\alpha}) = \left[\hat{\mathbf{r}}_{\alpha}\left(\mathbf{I}_{2N} - \mathbf{A}\mathbf{A}^{\dagger}\right)\hat{\mathbf{r}}_{\alpha}^{T}\right], \tag{3.24}$$

where $\mathbf{I}_{2N}$ is the identity matrix of dimension $2N$. Equ. (3.24) is unknown only in $\boldsymbol{\alpha}$ which can solved by minimising

$$\hat{\boldsymbol{\alpha}} = \arg\min_{\boldsymbol{\alpha}} \{\boldsymbol{\Psi}(\boldsymbol{\alpha})\}. \tag{3.25}$$

Brute force method can be used to solve (3.25), which is computationally inefficient specially at higher number of ANs. We thus use GenPS technique to minimize (3.25). The GenPS technique is explained in the next subsection.

3.3.1 Generalized Pattern Search

GenPS belongs to a family of derivative-free optimisation technique, originally proposed in [68]. GenPS iteratively updates $\boldsymbol{\alpha}$ such that

$$\boldsymbol{\Psi}(\boldsymbol{\alpha}_k) < \boldsymbol{\Psi}(\boldsymbol{\alpha}_{k-1}), \tag{3.26}$$

where k is the step number. Each iteration consist of an optional search step[1] and a compulsory poll step. During the search step any finite strategy can be employed to choose $\boldsymbol{\alpha}_k$, as long as the condition in (3.26) is satisfied. When search step fails, poll step is invoked during which $\boldsymbol{\Psi}$ is evaluate at all the points adjacent to $\boldsymbol{\alpha}_{k-1}$, i.e., $\boldsymbol{\Psi}$ is evaluated on a mesh $\mathcal{M}_k$, cenetered at $\boldsymbol{\alpha}_{k-1}$. The mesh $\mathcal{M}_k$ can be mathematically represented as

$$\mathcal{M}_k = \{\boldsymbol{\alpha}_k + \Delta_k \mathbf{D}\mathbf{z} : \quad \mathbf{z} \in \mathbb{Z}^q\},$$

where Δ_k is the mesh size parameter that define how far are the neighboring points of $\boldsymbol{\alpha}_k$. $\mathbf{D}$ is a finite set of direction that positively span $\mathbb{R}^N$ and gives the directions of the neighboring points. Each direction $\bar{d_j} \forall j = 1, ..., q$ must be a product of $\mathbf{G}\mathbf{z}_j$, where $\mathbf{G} \in \mathbb{R}^{N \times N}$ is a non singular generating matrix which for the present problem is an identity matrix $\mathbf{G} = \mathbf{I}_N$, which means that $\mathbf{z}_j \in \mathbb{Z}^N$ is an integer vector and belongs to the matrix $\mathbf{D}$. These conditions are necessary for the convergence theory [69].

At the k^{th} poll, the cost function is evaluated at neighboring poll points given by $\mathrm{P_k} = \left\{\boldsymbol{\alpha}_k + \Delta_k \bar{d}, \quad \bar{d} \in \mathbf{D}_k\right\}$. Thus at $(k+1)^{th}$ iteration if the cost function value, i.e., $\boldsymbol{\Psi}(\boldsymbol{\alpha}_{k+1})$ is lower than $\boldsymbol{\Psi}(\boldsymbol{\alpha}_k)$, then the step size is increased by $\Delta_{k+1} = \xi \Delta_k$ for any scalar $\xi > 1$ and $\boldsymbol{\alpha}_{k+1}$ is accepted, i.e., $\mathcal{M}_{k+1}$ is centered at $\boldsymbol{\alpha}_{k+1}$. Otherwise if $\boldsymbol{\Psi}(\boldsymbol{\alpha}_{k+1}) > \boldsymbol{\Psi}(\boldsymbol{\alpha}_k)$ for all the poll points then the step size is decreased by $\Delta_{k+1} = \frac{1}{\xi}\Delta_k$ and $\boldsymbol{\alpha}_{k+1} = \boldsymbol{\alpha}_k$. The algorithm is repeated until a stopping condition is reached e.g., $\boldsymbol{\Psi}\left(\boldsymbol{\alpha}^{k+1}\right) - \boldsymbol{\Psi}\left(\boldsymbol{\alpha}^{k}\right) < \tau$, where τ is some small value. The step by step procedure of GenPS is explained in algorithm 1.

[1]For the present problem of PLE estimation, we don't employ the optional search step.

Algorithm 3.1
Generalized Pattern Search
for $k = 1, ...$
i. Initialize $\boldsymbol{\alpha}_0 \in [2,\ 5]$, Δ_0,τ, ξ, ν.
ii. Evaluate $\boldsymbol{\Psi}(\boldsymbol{\alpha}_{k+1})$ with all poll points from poll set $\left\{\boldsymbol{\alpha}_k + \Delta_k \bar{d}, \bar{d} \in \mathbf{D}\right\}$.
iii-a. If improved poll point is found, accept $\boldsymbol{\alpha}_{k+1}$, set $\Delta_{k+1} = \xi \Delta_k$.
iii-b. If improved poll point cannot be found, set $\boldsymbol{\alpha}_{k+1} = \boldsymbol{\alpha}_k$, set $\Delta_{k+1} = \frac{\Delta_k}{\xi}$.
Repeat until $\boldsymbol{\Psi}(\boldsymbol{\alpha}_{k+1}) - \boldsymbol{\Psi}(\boldsymbol{\alpha}_k) < \tau$.
end

3.4 LCRB-AoA-RSS

The CRB characterizes the best possible accuracy of an unbiased estimator. Conventional localisation CRBs, bounds the performance of ML type algorithms as they are based on individual readings from ANs. On the contrary, the LLS and WLLS-AoA-RSS formulation is based on observation vector, in the present model, $\hat{\mathbf{r}}$. In order to lower bound the performance of WLLS-AoA-RSS we derive the LCRB-AoA-RSS. The maximum accuracy of the two dimensional localisation is characterized by the MSE bound:

$$\mathrm{MSE}(\mathbf{u}) \geq \frac{[\mathbf{I}(\mathbf{u})]_{11} + [\mathbf{I}(\mathbf{u})]_{22}}{\det[\mathbf{I}(\mathbf{u})]}, \tag{3.27}$$

where $[\mathbf{I}(\mathbf{u})]$ is the Fisher information matrix (FIM) whose elements are given by (3.28) [61]. We consider the elements of vector $\hat{\mathbf{r}}$ to be with a Gaussian distribution. This assumption is necessary for the closed form derivation of the LCRB-AoA-RSS.

$$\begin{aligned}[\mathbf{I}(\mathbf{u})]_{ij} = &\left[\frac{\partial \boldsymbol{\mu}(\mathbf{u})}{\partial \mathbf{u}_i}\right] \mathbf{C}_{\mathrm{AR}}^{-1}(\mathbf{u}) \left[\frac{\partial \boldsymbol{\mu}(\mathbf{u})}{\partial \mathbf{u}_j}\right] \\ &+ \frac{1}{2} Tr\left[\left(\mathbf{C}_{\mathrm{AR}}^{-1}(\mathbf{u}) \frac{\partial \mathbf{C}_{\mathrm{AR}}(\mathbf{u})}{\partial \mathbf{u}_i} \mathbf{C}_{\mathrm{AR}}{}^{-1}(\mathbf{u}) \frac{\partial \mathbf{C}_{\mathrm{AR}}(\mathbf{u})}{\partial \mathbf{u}_j}\right)\right], \text{ for } i, j = 1, 2.\end{aligned} \tag{3.28}$$

where $\boldsymbol{\mu}(\mathbf{u})$ is the mean of observation vector and $\frac{\partial \boldsymbol{\mu}(\mathbf{u})}{\partial \mathbf{u}_1}$ is the derivative of the observation vector w.r.t x.

$$\frac{\partial \boldsymbol{\mu}\left(\mathbf{u}\right)}{\partial x} = \left[1_1, 1_2, \cdots 1_N, 0_1, 0_2, \cdots 0_N\right]^T,$$

and $\frac{\partial \boldsymbol{\mu}(\mathbf{u})}{\partial \mathbf{u}_2}$ is the derivative of the mean of the observation vector w.r.t y.

$$\frac{\partial \boldsymbol{\mu}\left(\mathbf{u}\right)}{\partial y} = \left[0_1, 0_2, \cdots 0_N, 1_1, 1_2, \cdots 1_N\right]^T$$

Similarly for the covariance matrix of AoA-RSS signal, i.e., $\mathbf{C}_{\mathrm{AR}}\left(\mathbf{u}\right)$, the derivatives w.r.t x and y are given by

$$\frac{\partial \mathbf{C}_{\mathrm{AR}}\left(\mathbf{u}\right)}{\partial \mathbf{u}_1} = \frac{\partial}{\partial x}\begin{bmatrix} \mathbf{C}_{\mathrm{AR}}^{x} & \mathbf{C}_{\mathrm{AR}}^{xy} \\ \mathbf{C}_{\mathrm{AR}}^{xy} & \mathbf{C}_{\mathrm{AR}}^{y} \end{bmatrix} \tag{3.29}$$

and

$$\frac{\partial \mathbf{C}_{\mathrm{AR}}\left(\mathbf{u}\right)}{\partial \mathbf{u}_2} = \frac{\partial}{\partial y}\begin{bmatrix} \mathbf{C}_{\mathrm{AR}}^{x} & \mathbf{C}_{\mathrm{AR}}^{xy} \\ \mathbf{C}_{\mathrm{AR}}^{xy} & \mathbf{C}_{\mathrm{AR}}^{y} \end{bmatrix} \tag{3.30}$$

The derivates of individual terms in (3.29) and (3.30) are given in table. 3.1, the derivation of which is similar to the derivation of terms in table. 2.2 given in appendix II-B.

Using the derivates in table. 3.1 in (3.29) and (3.30) we obtain

$$\frac{\partial}{\partial x}\mathbf{C}_{\mathrm{AR}_{ii}}^{x} = \left(x - \bar{x}_i\right)\exp\left(\frac{\sigma_{w_i}^2}{\left(\gamma\alpha_i\right)^2} + \sigma_{m_i}^2\right) + \left[\left(y - \bar{y}_i\right)\sin 2\theta_i + \left(x - \bar{x}_i\right)\cos 2\theta_i\right] \times \exp\left(\frac{\sigma_{w_i}^2}{\left(\gamma\alpha_i\right)^2} - \sigma_{m_i}^2\right) - 2\left(x - \bar{x}_i\right). \tag{3.31}$$

Function	**Derivative w.r.t** x	**Derivative w.r.t** y
$\frac{d_{R,i}^2}{2}$	$\Big(x-\bar{x}_i\Big)$	$\Big(y-\bar{y}_i\Big)$
$\Big(\frac{d_{R,i}^2}{2}\cos 2\theta_i\Big)$	$\sin 2\theta_i\Big(y-\bar{y}_i\Big)+\cos 2\theta_i\Big(x-\bar{x}_i\Big)$	$\cos 2\theta_i\Big(y-\bar{y}_i\Big)-\sin 2\theta_i\Big(x-\bar{x}_i\Big)$
$\Big(d_{R,i}\cos\theta_i\Big)^2$	$2\Big(x-\bar{x}_i\Big)$	0
$d_{R,i}^2\cos\theta_i\sin\theta_i$	$(y-\bar{y}_i)$	$(x-\bar{x}_i)$

Table 3.1: Derivate of covariance matrix.

$$\frac{\partial}{\partial y}\mathbf{C}^{x}_{\mathrm{AR}_{ii}} = (y-\bar{y}_i)\exp\left(\frac{\sigma_{w_i}^2}{(\gamma\alpha_i)^2}+\sigma_{m_i}^2\right)+\Big[(y-\bar{y}_i)\cos 2\theta_i-(x-\bar{x}_i)\sin 2\theta_i\Big] \times \exp\left(\frac{\sigma_{w}^2}{(\gamma\alpha_i)^2}-\sigma_{m_i}^2\right). \quad (3.32)$$

$$\frac{\partial}{\partial x}\mathbf{C}^{y}_{\mathrm{AR}_{ii}} = (x-\bar{x}_i)\exp\left(\frac{\sigma_{w_i}^2}{(\gamma\alpha_i)^2}+\sigma_{m_i}^2\right)-\Big[(y-\bar{y}_i)\sin 2\theta_i+(x-\bar{x}_i)\cos 2\theta_i\Big] \times \exp\left(\frac{\sigma_{w_i}^2}{(\gamma\alpha_i)^2}-\sigma_{m_i}^2\right). \quad (3.33)$$

$$\frac{\partial}{\partial y}\mathbf{C}^{y}_{\mathrm{AR}_{ii}} = (y-\bar{y}_i)\exp\left(\frac{\sigma_{w_i}^2}{(\gamma\alpha_i)^2}+\sigma_{m_i}^2\right)-\Big[(y-\bar{y}_i)\cos 2\theta_i-(x-\bar{x}_i)\sin 2\theta_i\Big] \times \exp\left(\frac{\sigma_{w_i}^2}{(\gamma\alpha_i)^2}-\sigma_{m_i}^2\right)-2\,(y-\bar{y}_i). \quad (3.34)$$

$$\frac{\partial}{\partial x}\mathbf{C}^{x,y}_{\mathrm{AR}_{ii}} = (y-\bar{y}_i)\left[\exp\left(\frac{\sigma_{w_i}^2}{(\gamma\alpha_i)^2}-\sigma_{m_i}^2\right)-1\right]. \quad (3.35)$$

$$\frac{\partial}{\partial y}\mathbf{C}^{x,y}_{\mathrm{AR}_{ii}} = (x-\bar{x}_i)\left[\exp\left(\frac{\sigma_{w_i}^2}{(\gamma\alpha_i)^2}-\sigma_{m_i}^2\right)-1\right]. \quad (3.36)$$

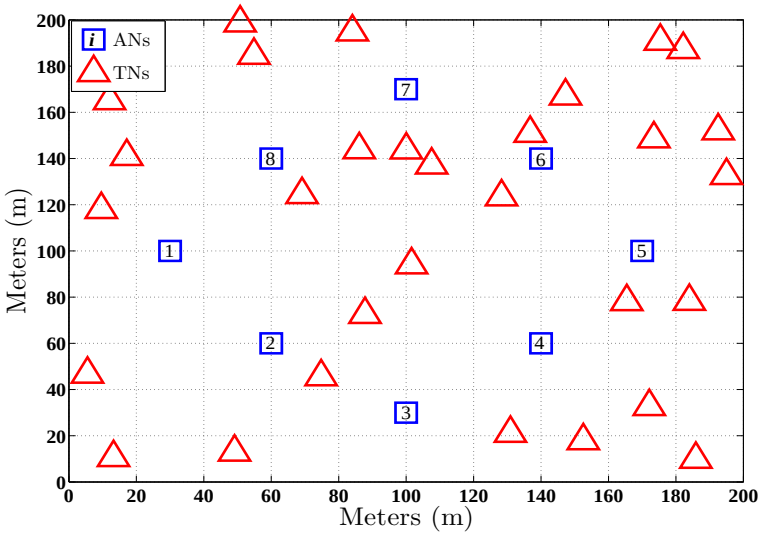

Figure 3.1: Network Deployment.

3.5 Simulation Section

This section, reports simulation results which evaluate the performance of the proposed techniques. Subsets of 8 ANs are considered at fixed and known positions and 30 TNs taken at random and unknown positions. All simulation are run ℓ number of times independently. The network deployment is shown in Fig. 3.1 and is considered for all simulation in this chapter. Though, the performance of the proposed algorithms will be different in different network scenarios, the proposed techniques will always outperform its previous versions.

Figure 3.2, compares the performance of WLLS-AoA-RSS and LLS estimator for AoA-RSS signal. The angle noise variance is kept fixed at $\sigma_m^2 = 4$ deg and the Avg. RMSE is plotted across shadowing noise variance and different PLEs. The x-axis of the figure represents the shadowing variance, σ_w^2 and the y-axis represents the different values of the PLE. As can be seen the WLLS-AoA-RSS show much better performance than LLS estimator.

In Fig.3.3, the network is divided into a number of different zone. Each zone have its own optimal subset of ANs. Each color represents a different combination of

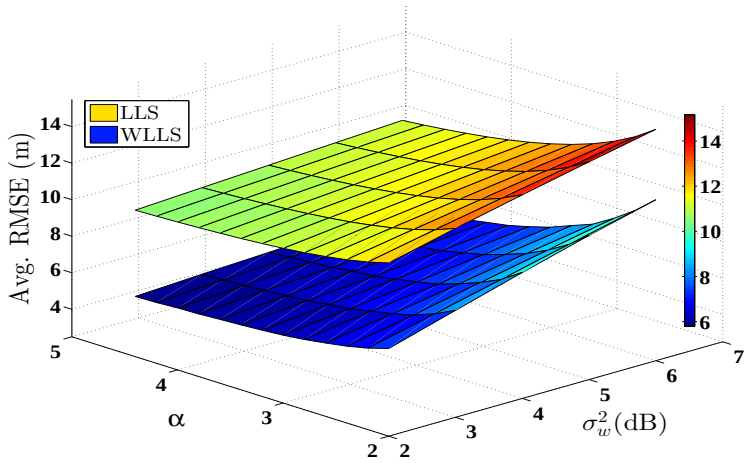

Figure 3.2: Performance comparison between LLS and WLLS-AoA-RSS. $\sigma_m^2 = 4^0$, ANs $= [\text{AN}_1 \text{ ,...,AN}_8]$, $\ell = 2500$.

ANs. It is evident from the figure that using all ANs for all TNs does not show optimal accuracy. The optimal combinations of ANs for the zones shown in Fig.3.3 are given in table. 3.2.

Figure 3.4 shows the Avg. RMSE obtained while using optimal subsets of ANs for

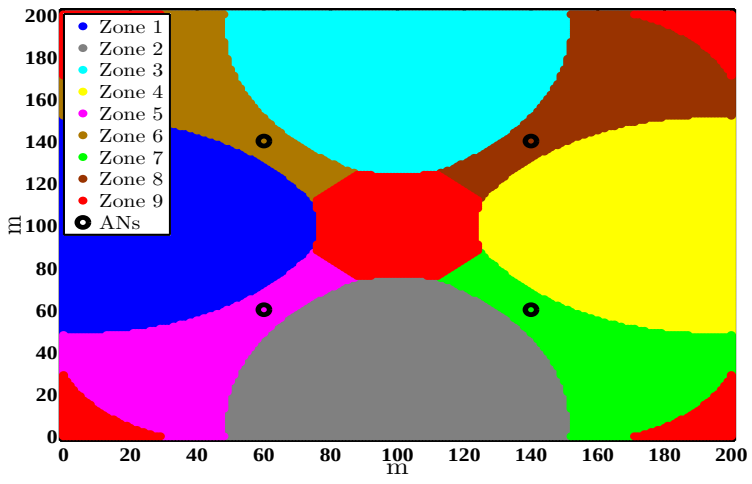

Figure 3.3: Division of network into different zone based theoretical MSE. AN $= [2, 4, 6, 8]$.

Zones	Optimal AN combination
Zone 1	$i = 2, 8$
Zone 2	$i = 2, 4$
Zone 3	$i = 6, 8$
Zone 4	$i = 4, 6$
Zone 5	$i = 2, 4, 8$
Zone 6	$i = 2, 6, 8$
Zone 7	$i = 2, 4, 6$
Zone 8	$i = 4, 6, 8$
Zone 9	$i = 2, 4, 6, 8$

Table 3.2: Optimal combinations of ANs for zones shown in Fig. 3.3.

their respective zones, which is compared with the Avg. RMSE obtained while using all ANs simultaneously. It is evident from the figure that selecting optimal subsets improve the accuracy significantly.

Figure 3.5 plots the analytical MSE with the Avg. RMSE obtained by simulation. It is observed from the figure that the analytical MSE derived in section 3.1.2 coincides with the Monte Carlo simulation obtained for LLS hybrid AoA-RSS signal model.

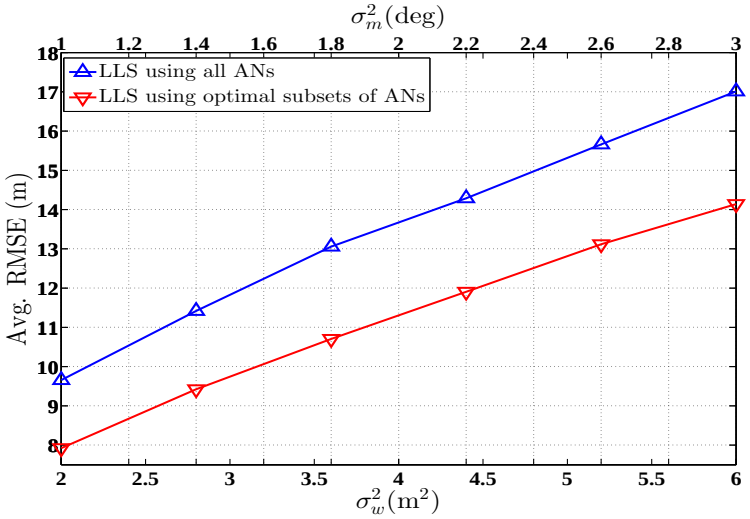

Figure 3.4: Performance comparison in terms of Avg. RMSE, using optimal subsets of ANs and using all ANs simultaneously. ANs $= [2, 4, 6, 8]$, $\ell = 1000$, $\alpha_i = 2.5 \; \forall \, i$.

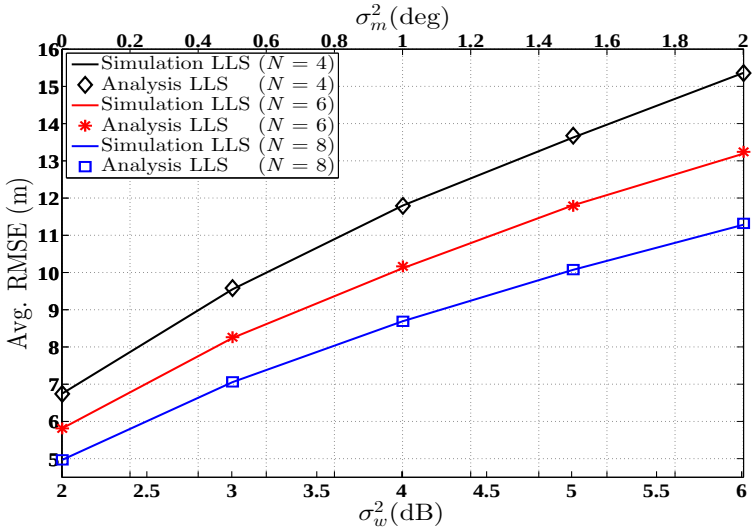

Figure 3.5: Performance comparison between theoretical MSE and simulation LLS for AoA-RSS signal. ANs =[$(\mathrm{AN}_2, \mathrm{AN}_4, \mathrm{AN}_6, \mathrm{AN}_8)$, $(\mathrm{AN}_1, \mathrm{AN}_2, \mathrm{AN}_3, \mathrm{AN}_5, \mathrm{AN}_6, \mathrm{AN}_7)$, $(\mathrm{AN}_1, \cdots, \mathrm{AN}_8)$], $\ell = 1500$, $\alpha_i = 2.5\ \forall\, i$.

Figure 3.6 demonstrates the performance of the hybrid AoA-RSS signal model based on the LLS approach when the PLE vector is estimated via GenPS. Each AN-TN link is associated with a different PLE, which is taken at random between 2-5. The LLS using erroneous PLEs is also plotted for comparison, i.e., when $\bar{\alpha}_i = \alpha_i + p_i$, where $\bar{\alpha}_i$ is the erroneous PLE and p_i is the error associated with the true PLE α_i. p_i is considered to be with Gaussian distribution with the standard deviation σ_{p_i}, i.e., $p_i \sim \mathcal{N}\left(0, \sigma_{p_i}^2\right)$. For this simulation, σ_{p_i} has a value of 0.2. It is observed that even such a small error in the PLE vector produces considerable error in the final estimate of the location of the TN, while localisation using estimated PLEs, produces considerably better estimates.

Comparison of the LLS, WLLS-AoA-RSS with its corresponding LCRB-AoA-RSS is given in Fig. 3.7. In this case, the PLE is kept fixed at 2.5. The Avg. RMSE of all TNs is plotted across both noise variances. Again it can be seen from Fig. 3.7 that the WLLS-AoA-RSS outperforms the LLS model and that LCRB-AoA-RSS tightly bounds WLLS-AoA-RSS.

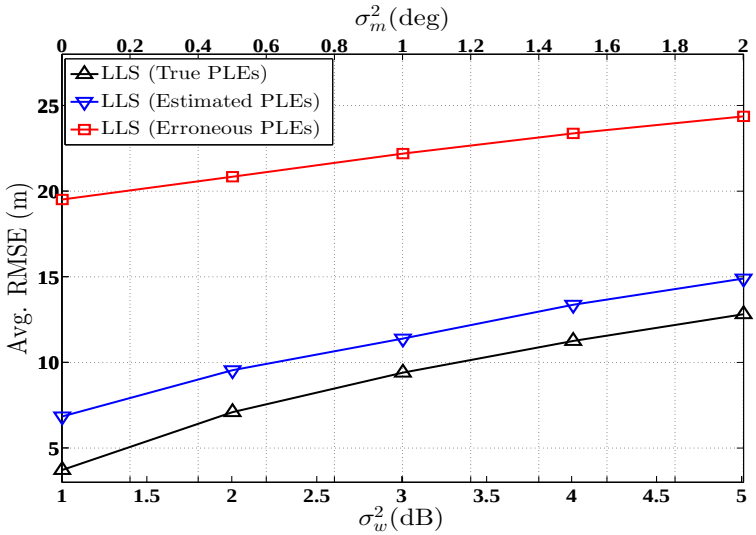

Figure 3.6: Avg. RMSE comparison using estimated PLEs and true PLE's. ANs $= [1-8]$ $\ell = 2000$, τ=1, $\xi = 2$, $\Delta_0 = 0.5$, $v = 10$, $\alpha_i \in \mathcal{U}[2\ 5]$, $\alpha_0 \in \mathcal{U}[2\ 5]$, $\sigma_p = 0.2$.

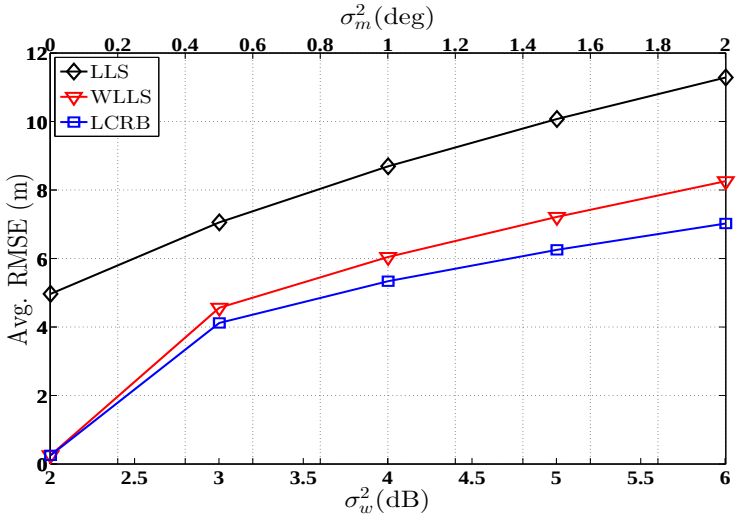

Figure 3.7: Performance comparison between LLS, WLLS-AoA-RSS and LCRB-AoA-RSS. ANs $= [\mathrm{AN}_1, ..., \mathrm{AN}_8]$, $\alpha_i = 2.5\ \forall\, i$, $\ell = 2000$.

3.6 Summary

A hybrid AoA-RSS signal model was presented in this chapter. A LLS, WLLS-AoA-RSS estimators were designed for the mentioned signal model. Optimisation was achieved by designing a two step zone based optimal ANs combination scheme. A novel estimator for the estimation of the PLE vector is also proposed, that utilises the GenPS algorithm. Finally, to bound the performance of the WLLS-AoA-RSS algorithm a LCRB-AoA-RSS is derived that tightly bounds the performance of WLLS-AoA-RSS technique. The simulation results confirms the analysis presented in this chapter.

To take the hybrid signal models one step further, cooperative communication links between TNs are established. Thus in the next chapter, a new cooperative localisation scheme is presented based on both hybrid AoA-ToA and hybrid AoA-RSS signal models. Optimisation, computational complexities and different realistic scenarios like unhybrid TNs with hybrid ANs and partial connectivity is also discussed in the next chapter

4 Optimised Localisation with Cooperation In Wireless Networks

The material of this chapter is presented in

i) M. W. Khan, Naveed Salman, A. H. Kemp "Cooperative Positioning Using Angle of Arrival and Time of Arrival," *in Sensor Signal Processing for Defence (SSPD)*, pp.1-5, 8-9 Sept. 2014.

ii) M. W. Khan, Naveed Salman, A. H. Kemp, L. Mihaylova "Optimized Hybrid Localisation with Cooperation in Wireless Sensor Networks," *IET Signal Processing* (Accepted, awaiting publication).

4.1 Overview

- Two hybrid signal models namely, the AoA-ToA and the AoA-RSS signal models were introduced in the last two chapters. LLS, WLLS and two optimal ANs selection schemes were also proposed for the mentioned signal models. In this chapter, a cooperative version of the hybrid signal models is presented for static nodes. Cooperative LLS estimators are proposed and

optimisation is achieved by utilizing the noise covariance matrices. This chapter also explores a more realistic scenario in which only ANs are capable of hybrid angle and range estimation while TNs, which usually are low on resources are capable of distance estimation only. Also networks with limited connectivity is considered and the effect of limited connectivity on estimation accuracy is studied. Furthermore the complexity comparison is done for non-cooperative LLS, cooperative LLS and optimised cooperative LLS.

4.2 Cooperative Localisation

In large scale networks some TNs may be situated in an area where they can not be reached by the ANs. Localisation of such nodes presents a serious problem in positioning systems. One way to resolve the issue is to use TN to TN communication [70], [71], i.e., some TN can act as pseudo-anchors to localise out of range TNs. Furthermore this cooperation between TNs improves the localisation accuracy as more measurements are available for estimation. Cooperative localisation is studied in [72] for RSS, [73] for ToA, [74] for AoA and in [75], [76] for hybrid signal models.

4.3 Cooperative Hybrid Localisation

For future use we define the following parameters: Let $\hat{\theta}_{ij}$ and $\hat{d}_{ij}$ be the measured angle and distance between i^{th} AN and j^{th} TN, respectively. On the other hand, let $\hat{D}_{jk}$ be the measured distance between j^{th} and k^{th} TN, and $\hat{\Phi}_{jk}$ is the AoA impinging at j^{th} TN from k^{th} TN. Furthermore, we use the notation of $\bar{x}_i$ and $\bar{y}_i$ for the x and y coordinate of i^{th} AN while x_j and y_j for the x and y coordinates

of j^{th} TN. Incorporating the readings from k^{th} TN together with readings from the ANs, the x and y coordinates of j^{th} TN is estimated as [77]

$$\hat{x}_j = \bar{x}_i + \hat{d}_{ik}\cos\hat{\theta}_{ik}\delta_{ik} - \hat{D}_{jk}\cos\hat{\Phi}_{jk}\delta_{jk} \text{ for } i = 1,\ldots,N \quad k = 1,\ldots,M \tag{4.1}$$

$$\hat{y}_j = \bar{y}_i + \hat{d}_{ik}\sin\hat{\theta}_{ik}\delta_{ik} - \hat{D}_{jk}\sin\hat{\Phi}_{jk}\delta_{jk} \text{ for } i = 1,\ldots,N \quad k = 1,\ldots,M \tag{4.2}$$

where δ_{ij} and δ_{jk} are the bias reducing constants for AoA-ToA and AoA-RSS signal, respectively. It should be noted that for $j = k$, the terms $\left(\hat{D}_{jk}\cos\hat{\Phi}_{jk}\delta_{jk}\right)$ and $\left(\hat{D}_{jk}\sin\hat{\Phi}_{jk}\delta_{jk}\right)$ are equal to zero. Hence (4.1) and (4.2) reduces to

$$\hat{x}_j = \bar{x}_i + \hat{d}_{ij}\cos\hat{\theta}_{ij}\delta_{ij} \quad \text{for } i = 1,\ldots,N \tag{4.3}$$

$$\hat{y}_j = \bar{y}_i + \hat{d}_{ij}\sin\hat{\theta}_{ij}\delta_{ij} \quad \text{for } i = 1,\ldots,N \tag{4.4}$$

Equ. (4.3) and (4.4) are the same as (2.40), (2.39) and (3.2), (3.1) for AoA-ToA and AoA-RSS, repectively, which is the estimated location from the readings of the AN only while (4.1) and (4.2) represents the estimated location from the readings of ANs and TNs simultaneously. In (4.1) and (4.2) the terms $\hat{d}_{ik}\cos\hat{\theta}_{ik}$ and $\hat{d}_{ik}\sin\hat{\theta}_{ik}$ are the projections of $\hat{d}_{ik}$ on the x and $y-$axis, respectively from which the projections $\hat{D}_{jk}\cos\hat{\Phi}_{jk}$ and $\hat{D}_{jk}\sin\hat{\Phi}_{jk}$ are subtracted, respectively, constituting the cooperation step. These operations can be understood from Fig. 4.1 in which the geometry of the i^{th} AN and that of j^{th} and k^{th} TN is illustrated. To write (4.1) and (4.2) in matrix form we first define the vectors in table. 4.1:

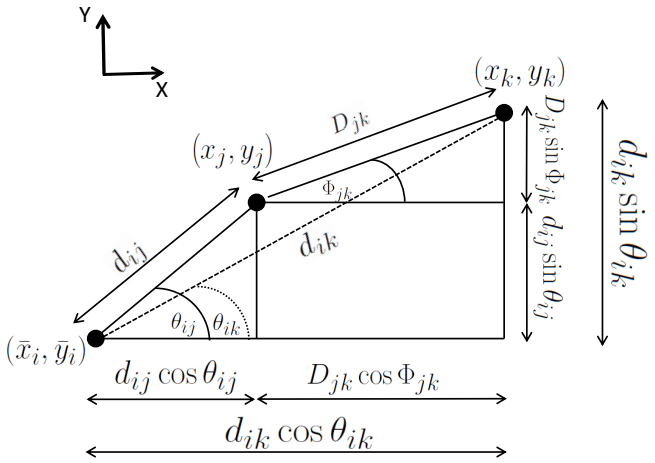

Figure 4.1: AN and TN geometry

Equ. (4.1) and (4.2) can then be represented in matrix form as

$$\mathbf{A}_{\mathrm{c}}\hat{\mathbf{u}} = \hat{\mathbf{b}}, \tag{4.5}$$

where $\hat{\mathbf{b}} = [\mathbf{b}_{x_1}, ..., \mathbf{b}_{x_N}, \mathbf{b}_{y_1}, ..., \mathbf{b}_{y_N}]^T$, where

$$\mathbf{b}_{x_j} = \begin{bmatrix} \mathbf{A}_x + \mathbf{d}_1 \cos\boldsymbol{\theta}_1\boldsymbol{\delta}_1 - \check{\mathbf{d}}_{j1}\cos\boldsymbol{\Phi}_{j1}\boldsymbol{\delta}_{j1} \\ \mathbf{A}_x + \mathbf{d}_2 \cos\boldsymbol{\theta}_2\boldsymbol{\delta}_2 - \check{\mathbf{d}}_{j2}\cos\boldsymbol{\Phi}_{j2}\boldsymbol{\delta}_{j2} \\ \vdots \\ \mathbf{A}_x + \mathbf{d}_N \cos\boldsymbol{\theta}_N\boldsymbol{\delta}_N - \check{\mathbf{d}}_{jN}\cos\boldsymbol{\Phi}_{jN}\boldsymbol{\delta}_{jN} \end{bmatrix},$$

$$\mathbf{b}_{y_j} = \begin{bmatrix} \mathbf{A}_y + \mathbf{d}_1 \sin\boldsymbol{\theta}_1\boldsymbol{\delta}_1 - \check{\mathbf{d}}_{j1}\sin\boldsymbol{\Phi}_{j1}\boldsymbol{\delta}_{j1} \\ \mathbf{A}_y + \mathbf{d}_2 \sin\boldsymbol{\theta}_2\boldsymbol{\delta}_2 - \check{\mathbf{d}}_{j2}\sin\boldsymbol{\Phi}_{j2}\boldsymbol{\delta}_{j2} \\ \vdots \\ \mathbf{A}_y + \mathbf{d}_N \sin\boldsymbol{\theta}_N\boldsymbol{\delta}_N - \check{\mathbf{d}}_{jN}\sin\boldsymbol{\Phi}_{jN}\boldsymbol{\delta}_{jN} \end{bmatrix}.$$

The LLS solution for the linear system is given by

$$\hat{\mathbf{u}} = \mathbf{A}_{\mathrm{c}}^{\dagger}\hat{\mathbf{b}}, \tag{4.6}$$

where $\mathbf{A}_{\mathrm{c}}^{\dagger}$ is the Moore–Penrose pseudo inverse of $\mathbf{A}_{\mathrm{c}}$ and is given by $\mathbf{A}_{\mathrm{c}}^{\dagger} = \left(\mathbf{A}_{\mathrm{c}}^T\mathbf{A}_{\mathrm{c}}\right)^{-1}\mathbf{A}_{\mathrm{c}}^T$. Matrix $\mathbf{A}_{\mathrm{c}}^{\dagger}$ can be calculated directly without taking the pseudo

Table 4.1: Notation.

Vector	Description	Mathematical form	Dimension ($\mathbb{R}^X$)
$\mathbf{E}_\kappa$	Column vector of κ ones.	$\mathbf{E}_\kappa = [1_1, 1_2, \ldots, 1_\kappa]^T$	$\mathbb{R}^{\kappa \times 1}$
$\mathbf{A}_\mathrm{c}$	Averaging matrix, composed $2M$ $\mathbf{E}_{MN}$ vectors on the diagonal.	$\mathbf{A} = \mathrm{diag}[\mathbf{E}_{MN}, \ldots, \mathbf{E}_{MN}]$	$\mathbb{R}^{2NM^2 \times 2M}$
$\mathbf{u}$	Unknown vector, composed of x and y coordinates of M TNs.	$\mathbf{u} = [x_1, \ldots x_M, y_1, \ldots y_M]^T$	$\mathbb{R}^{2M \times 1}$
$\mathbf{A}_x$	Column vector composed of the x coordinates of N ANs	$\mathbf{A}_x = [\bar{x}_1, \ldots, \bar{x}_N]^T$	$\mathbb{R}^{N \times 1}$
$\mathbf{A}_y$	Vector composed of the y coordinates of N AN	$\mathbf{A}_y = [\bar{y}_1, \ldots, \bar{y}_N]^T$	$\mathbb{R}^{N \times 1}$
$\mathbf{d}_k$	Range vector, composed of noisy distance estimates between N ANs and k^{th} TN	$\mathbf{d}_k = \left[\hat{d}_{1k}, \ldots, \hat{d}_{Nk}\right]^T$	$\mathbb{R}^{N \times 1}$
$\check{\mathbf{d}}_{jk}$	Column vector, composed of noisy distance between j^{th} TN to k^{th} TN	$\check{\mathbf{d}}_{jk} = \hat{D}_{jk}\mathbf{E}_N$	$\mathbb{R}^{N \times 1}$
$\boldsymbol{\theta}_j$	Gradient vector, composed of noisy angle estimates from j^{th} TN to N ANs	$\boldsymbol{\theta}_j = \left[\hat{\theta}_{1j}, \ldots, \hat{\theta}_{Nj}\right]^T$	$\mathbb{R}^{N \times 1}$
$\boldsymbol{\Phi}_{jk}$	Gradient vector, composed of noisy angle estimate from k^{th} TN to j^{th} TN	$\boldsymbol{\Phi}_{jk} = \hat{\Phi}_{jk}\mathbf{E}_N$	$\mathbb{R}^{N \times 1}$
$\boldsymbol{\delta}_j$	Unbiasing vector, composed of unbiasing constants associated with j^{th} TN and N AN	$\boldsymbol{\delta}_j = [\delta_{1j}, \ldots, \delta_{Nj}]^T$	$\mathbb{R}^{N \times 1}$
$\boldsymbol{\delta}_{jk}$	Unbiasing vector, composed of unbiasing constants associated with j^{th} TN and k^{th} TNs	$\boldsymbol{\delta}_{jk} = \delta_{jk}\mathbf{E}_N$	$\mathbb{R}^{N \times 1}$

inverse if the number of TNs and ANs are known, i.e.,

$$\mathbf{A}_{\mathrm{c}}^{\dagger} = \mathrm{diag}\left[\boldsymbol{\eta}, \boldsymbol{\eta}, \cdots, \boldsymbol{\eta}\right] \in \mathbb{R}^{2M \times 2NM^2}, \tag{4.7}$$

where $\boldsymbol{\eta}$ is a row matrix of MN elements, the value of each element is given by $\frac{1}{MN}$. This cooperative LLS estimator (4.6) shall be referred to as LLS-Coop in the rest of the thesis.

4.3.1 Distributed Approach

If only one or a subset of all the TNs is desired to be localised while capitalising on the cooperation with all TNs but avoiding the complexity of the centralised algorithm as in the previous case, a distributed approach can be employed. The distributed cooperative localisation, localizes a single TN (This can be easily extended to estimate the location of a subset of all TNs) and reduces the complexity of the system without affecting the accuracy of localisation. The location estimate of the j^{th} TN is given by

$$\mathbf{A}_j \hat{\mathbf{u}}_j = \hat{\mathbf{b}}_j,$$

where

$$\mathbf{A}_j = \mathrm{diag}\left[\mathbf{E}_{MN}, \mathbf{E}_{MN}\right] \in \mathbb{R}^{2MN \times 2},\ \mathbf{u}_j = \left[x_j, y_j\right]^T \in \mathbb{R}^{2\times 1},\ \hat{\mathbf{b}}_j = \left[\mathbf{b}_{x_j}, \mathbf{b}_{y_j}\right]^T \in \mathbb{R}^{2MN \times 1}.$$

The LLS solution is then given by

$$\hat{\mathbf{u}}_j = \mathbf{A}_j^{\dagger} \hat{\mathbf{b}_j}$$

for $\mathbf{A}_j^{\dagger} = \mathrm{diag}\left[\boldsymbol{\eta}, \boldsymbol{\eta}\right] \in \mathbb{R}^{2\times 2MN}$.

4.3.2 Cooperative Hybrid AoA-ToA

From here onwards, for cooperative hybrid AoA-ToA, $\hat{d}_{ij}$, $\hat{D}_{ij}$ and δ_{ij} will be represented by $\hat{d}_{T,ij}$, $\hat{D}_{T,ij}$ and $\delta_{T,ij}$ respectively, and are given by

$$\hat{d}_{T,ij} = d_{ij} + n_{ij}, \quad \hat{D}_{T,jk} = D_{jk} + n_{jk}, \quad \delta_{T,ij} = \exp\left(\frac{\sigma^2_{m_{ij}}}{2}\right),$$

where $d_{ij} = \sqrt{(\bar{x}_i - x_j)^2 + (\bar{y}_i - y_j)^2}$ and $D_{jk} = \sqrt{(x_j - x_k)^2 + (y_j - y_k)^2}$, n_{ij} and n_{jk} represent the zero mean Gaussian errors in distance estimates, i.e., $n_{ij} \sim \mathcal{N}\left(0, \sigma^2_{n_{ij}}\right)$ and $n_{jk} \sim \mathcal{N}\left(0, \sigma^2_{n_{jk}}\right)$. The angle measurement $\hat{\theta}_{ij}$ from the j^{th} TN to i^{th} AN is given by

$$\hat{\theta}_{ij} = \arctan\left[\frac{(y_j - \bar{y}_i)}{(x_j - \bar{x}_i)}\right] + m_{ij}, \tag{4.8}$$

where m_{ij} represents the zero mean Gaussian error in angle estimates, i.e., $m_{ij} \sim \mathcal{N}\left(0, \sigma^2_{m_{ij}}\right)$. On the other hand, the angle measurement between from k^{th} to j^{th}, i.e., $\hat{\Phi}_{jk}$ can be obtained in one of the following ways.

Case 1. If all TNs are capable of estimating their relative angles then $\hat{\Phi}_{jk}$ can be modeled as

$$\hat{\Phi}_{jk} = \arctan\left[\frac{(y_k - y_j)}{(x_k - x_j)}\right] + m_{jk}, \tag{4.9}$$

where m_{jk} represents the zero mean Gaussian noise in angle estimate, i.e., $m_{jk} \sim \mathcal{N}\left(0, \sigma^2_{m_{jk}}\right)$.

Case 2. In many cases, only the AN are capable of AoA measurements while the TNs are low in resources and hence can only estimate their relative distances, in other words the TNs are not hybrid then for the formulation in (4.5), $\hat{\Phi}_{jk}$ can be estimated as follows

$$\hat{\Phi}_{jk} = \arctan\left[\frac{(\hat{y}_k - \hat{y}_j)}{(\hat{x}_k - \hat{x}_j)}\right], \tag{4.10}$$

where the $(\hat{y}_k - \hat{y}_j)$ and $(\hat{x}_k - \hat{x}_j)$ in (4.10) are estimated using (1.5) and (1.7) respectively. The accuracy of estimation deteriorate in this case as the number

of observations decreases. These systems where the TNs are not hybrid will be referred to as LLS-Coop-X.

4.3.3 Cooperative Hybrid AoA-RSS

For hybrid AoA-RSS $\hat{d}_{ij}$, $\hat{D}_{jk}$ and δ_{ij} are represented by $\hat{d}_{R,ij}$, $\hat{D}_{R,ij}$ and $\delta_{R,ij}$ respectively and are estimated from the RSS measurements as in [78].

$$\hat{d}_{R,ij} = d_{ij} \exp\left(\frac{w_{ij}}{\gamma\alpha}\right), \quad \hat{D}_{R,jk} = D_{jk} \exp\left(\frac{w_{jk}}{\gamma\alpha}\right), \quad \delta_{R,ij} = \exp\left(\frac{\sigma^2_{m_{ij}}}{2} - \frac{\sigma^2_{w_{ij}}}{2\left(\gamma\alpha\right)^2}\right),$$

where w_{ij} is the zero mean Gaussian random variable representing the shadowing effects, i.e., $w_{ij} \sim \mathcal{N}\left(0, \sigma^2_{w_{ij}}\right)$, where $\hat{\theta}_{ij}$ and $\hat{\Phi}_{jk}$ are the same for both models given by (4.8), (4.9) and (4.10).

4.4 Cooperative LLS Optimisation

In this section we improve the performance of the LLS by preparing an optimisation step. In order to localise node j with coordinates (x_j, y_j), the cooperation steps with TN k with coordinates (x_k, y_k) are represented by (4.1) and (4.2), where $\hat{d}_{ik}\cos\hat{\theta}_{ik}$ is the projection of $\hat{d}_{ik}$ on the $x-$axis and $\hat{d}_{ik}\sin\hat{\theta}_{ik}$ is the projection on $y-$axis. In the formulation (4.1) and (4.2), the projection of $\hat{D}_{jk}$, i.e., $\hat{D}_{jk}\cos\hat{\Phi}_{jk}$ and $\hat{D}_{jk}\sin\hat{\Phi}_{jk}$ are subtracted from $\hat{d}_{ik}\cos\hat{\theta}_{ik}$ and $\hat{d}_{ik}\sin\hat{\theta}_{ik}$ respectively for all M ANs. Since the combined error in hybrid distance and angle measurements is inherently distance dependent, step (4.1) and (4.2), may introduce large error if some ANs are positioned far away from the TS. Thus, instead of using all ANs, a pair of optimal ANs could be selected that guarantees minimum error or the ANs with the least error in the projection $\hat{d}_{ik}\cos\hat{\theta}_{ik}$ and $\hat{d}_{ik}\sin\hat{\theta}_{ik}$. In this section, we propose an optimisation scheme that will select such a pair of ANs. Let the total

number of ANs be represented by the set $\overline{\text{AN}} = \{\text{AN}_1, \text{AN}_2, \cdots, \text{AN}_M\}$, then the number of 2-subsets $\text{AN}_{\text{sub}} \subset \overline{\text{AN}}$ is given by the permutation with repetition, i.e., M^2. Then to localise the j^{th} TN in cooperation with the k^{th} TN, the first optimal anchor $\text{AN}_{\text{opt(1)}}$ of AN_{sub} is selected as the one that minimizes the approximate variance of the projection $\hat{d}_{ik} \cos \hat{\theta}_{ik}$ such that

$$\text{AN}_{\text{opt(1)}} = \arg \min_{\text{AN} \in \overline{\text{AN}}} \{c_{x,k}\}, \tag{4.11}$$

and the second anchor $\text{AN}_{\text{opt(2)}}$ is selected as the one that minimizes the projection $\hat{d}_{ik} \sin \hat{\theta}_{ik}$ such that

$$\text{AN}_{\text{opt(2)}} = \arg \min_{\text{AN} \in \overline{\text{AN}}} \{c_{y,k}\}. \tag{4.12}$$

$c_{x,k}$ and $c_{y,k}$ represent the approximate variance of the respective projections of $\hat{d}_{ik}$. They are represented by $c^t_{x,k}$ and $c^t_{y,k}$ and given by (4.13) and (4.14) for AoA-ToA respectively. On the other hand, they are represented by $c^R_{x,k}$ and $c^R_{y,k}$ and given by (4.15) and (4.16) for AoA-RSS respectively. Since the actual value of the distance in (4.13)-(4.16) is unknown its measured value is used. It should be noted that the same AN could serve as the optimal AN to minimize both (4.11) and (4.12). The LLS estimator with this optimisation shall be referred to as LLS-Opt-Coop.

4.5 Complexity Analysis

This section present the complexity analysis of the proposed algorithms. Following [79], the CPU cycle count is used to compare the computational complexities by considering the individual cycle counts for addition (ADD), multiplication (MUL), and comparison (CMP) operations. Thus using cycle count 1, 3 and 1 for ADD, MUL and CMP, respectively, the complexities of LLS-NoCoop, LLS-Coop and LLS-Opt-Coop are given in table 4.2. For LLS-NoCoop the complexity

$$c_{x,k}^{t} = \left(\frac{d_{T,ik}^2}{2} + \frac{\sigma_{n_{ik}}^2}{2}\right)\exp\left(\sigma_{m_{ik}}^2\right) + \left(\frac{d_{T,ik}^2}{2}\cos 2\theta_{ik} + \frac{\sigma_{n_{ik}}^2}{2}\cos 2\theta_{ik}\right)\exp\left(-\sigma_{m_{ik}}^2\right) - (d_{T,ik}\cos\theta_{ik})^2 \tag{4.13}$$

$$c_{y,k}^{t} = \left(\frac{d_{T,ik}^2}{2} + \frac{\sigma_{n_{ik}}^2}{2}\right)\exp\left(\sigma_{m_{ik}}^2\right) - \left(\frac{d_{T,ik}^2}{2}\cos 2\theta_{ik} + \frac{\sigma_{n_{ik}}^2}{2}\cos 2\theta_{ik}\right)\exp\left(-\sigma_{m_{ik}}^2\right) - (d_{T,ik}\sin\theta_{ik})^2 \tag{4.14}$$

$$c_{x,k}^{R} = \frac{d_{R,ik}^2}{2}\exp\left(\frac{\sigma_{w_{ik}}^2}{(\gamma\alpha)^2} + \sigma_{m_{ik}}^2\right) + \frac{d_{R,ik}^2}{2}\cos 2\theta_{ik}\exp\left(\frac{\sigma_{w_{ik}}^2}{(\gamma\alpha)^2} - \sigma_{m_{ik}}^2\right) - (d_{R,ik}\cos\theta_{ik})^2 \tag{4.15}$$

$$c_{y,k}^{R} = \frac{d_{R,ik}^2}{2}\exp\left(\frac{\sigma_{w_{ik}}^2}{(\gamma\alpha)^2} + \sigma_{m_{ik}}^2\right) - \frac{d_{R,ik}^2}{2}\cos 2\theta_{ik}\exp\left(\frac{\sigma_{w_{ik}}^2}{(\gamma\alpha)^2} - \sigma_{m_{ik}}^2\right) - (d_{R,ik}\sin\theta_{ik})^2 \tag{4.16}$$

shown in table 4.2 is for all N TNs localised individually without cooperation. The CMP operator is only used in LLS-Opt-Coop to compare the approximate variances given by (4.13), (4.14) and (4.15), (4.16) for AoA-ToA and AoA-RSS signal models, respectively. The number of comparison required for each model are $2MN$. Number of cycles counts for calculating approximate variance is given by App. Var in table 4.2. For complexity analysis given in 4.2, 4 ANs and 5 TNs are considered. Table 4.2 shows that the CPU cycle count for LLS-NoCoop is the lowest, followed by LLS-Coop and then LLS-Opt-Coop.

4.6 Partial Connectivity

Full connectivity can not always be achieved in large networks due to limited communication range of resource constraint sensor nodes. Hence the assumption of full connectivity becomes unrealistic in large networks. This section explores the issue of partial connectivity in cooperative hybrid networks. In this scenario a $\mathrm{TN_A}$(TN that is to be localised) first broadcasts a location request message

Table 4.2: Computation complexity.

Operation	MUL		ADD		CMP	CPU cycles ($M = 3, N = 5$)	
	AoA-ToA	AoA-RSS	AoA-ToA	AoA-RSS		AoA-ToA	AoA-RSS
LLS-NoCoop							
$\mathbf{A}^\dagger$	1	1	0	0	NA	3	3
$\mathbf{b}$	$22MN$	$26MN$	$10MN$	$12MN$		1140	1350
$\mathbf{A}^\dagger\mathbf{b}$	$4MN$	$4MN$	$(4MN - 2N)$	$(4MN - 2N)$		230	230
LLS-Coop							
$\mathbf{A}^\dagger$	2	2	0	0	NA	6	6
$\mathbf{b}$	$22N(M+N-1)$	$26N(M+N-1)$	$10N\,(M + N - 1)$	$12N\,(M + N - 1)$		2660	3150
$\mathbf{A}^\dagger\mathbf{b}$	$4MN^3$	$4MN^3$	$\left(4MN^3 - 2N\right)$	$\left(4MN^3 - 2N\right)$		5990	5990
LLS-Opt-Coop							
$\mathbf{A}^\dagger$	1	1	2	2	$2MN$	5	5
$\mathbf{b}$	$22N(M+N-1)$	$26N(M+N-1)$	$10N\,(M + N - 1)$	$12N\,(M + N - 1)$		2660	3150
$\mathbf{A}^\dagger\mathbf{b}$	$4N^2(M+N-1)$	$4N^2(M+N-1)$	$4N^2(M+N-1)-2N$	$4N^2(M+N-1)-2N$		2790	2790
App. Var	$74MN$	$62MN$	$36MN$	$24MN$		3870	3150
CMP	-	-	-	-		30	30

(LOC request), which is picked up by other TNs, ANs or in most cases both. The second step is, if an AN receives the LOC request it measures the range and the angle of the impinging signal and sends the measurements back to $\mathrm{TN_A}$. On the other hand if other TNs receive the LOC request it them have to check for the availability of ANs in its own range. If no ANs are available, the LOC request is discarded by the TNs. In case of availability of one or more ANs, the measurements (AN-$\mathrm{TN_A}$ and TN-$\mathrm{TN_A}$ observations) are passed to $\mathrm{TN_A}$. If the LOC request is not picked by any sensor node, then $\mathrm{TN_A}$ is out of communication range of the network and cannot be localised. These steps can be understood from Fig. 4.2. A pseudocode for the localisation of $\mathrm{TN_A}$ is given in Algorithm 4.1.

4.7 Simulation Results

We consider a 120m×120m network with 4 ANs at $(20, 20)\,, (20, 100)\,, (100, 20)$ and $(100, 100)$ while 30 TNs are arbitrarily deployed at random locations within

Algorithm 4.1 Pseudocode for localisation of TN_A.

PROGRAM : Partial connectivity

1. TN_A broadcasts LOC
2. Pause(time)
3. **IF** TN_A receive measurements from ANs or TNs.
4. identify transmitter
5. **IF** transmitters are only ANs
6. Localise via (4.3) and (4.4) only.
7. **ELSE IF** transmitters are TNs
8. Localise via (4.1) and (4.2) only.
9. **ELSE IF** transmitters are ANs and TNs.
10. Localise via(4.1), (4.2), (4.3) and (4.4).
11. **ENDIF**
12. **ELSE**
13. TN_A is outside the networks range.
14. **END**

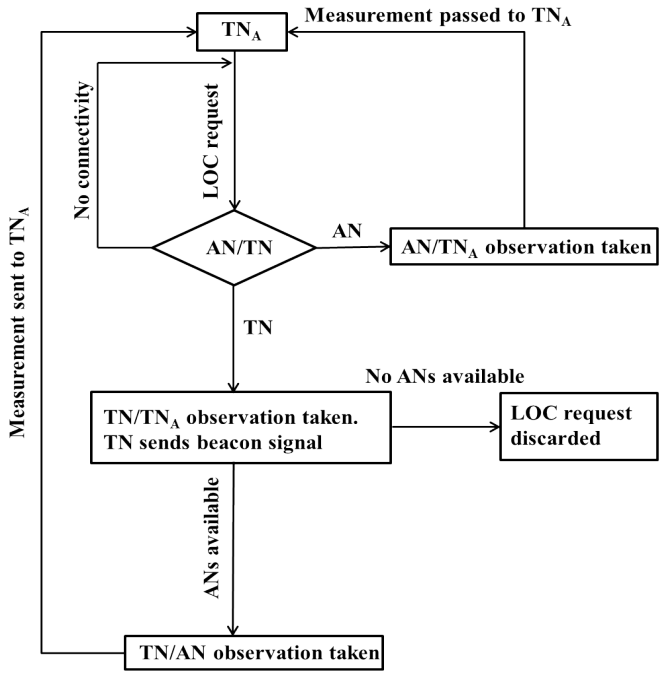

Figure 4.2: Flowchart for localisation of TN_A in case of full and partial connectivity.

and outside the convex hull of the network. All the simulations are run independently ℓ number of times. The network deployment is shown in Fig. 4.3 and is considered for all simulation in this chapter. Though, the performance of the proposed algorithms will be different in different network scenarios, the proposed techniques will always outperform its previous versions.

In Fig. 4.4, the hybrid AoA-ToA algorithms are compared. For simplicity, the same noise variance in distance and angle measurements is used for all AN-TN and TN-TN links i.e $\sigma^2_{n_{ij}} = \sigma^2_{n_{jk}} = \sigma^2_n$ and $\sigma^2_{m_{ij}} = \sigma^2_{m_{jk}} = \sigma^2_m$. The performance in terms of the average root means square error (Avg. RMSE) is compared while the variance in distance and angle estimates is increased gradually. It is seen that the performance of the LLS estimator with no cooperation (LLS-NoCoop) is worst of all. Considerable performance improvement is observed with cooperation between the TNs; with the LLS-Opt-Coop estimator showing the lowest RMSE.

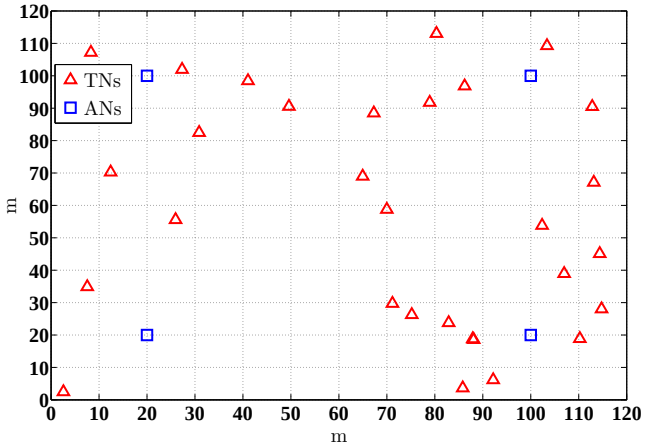

Figure 4.3: Network deployment.

Next is the LLS-Coop when both TNs and ANs are hybrid. While performance degradation is observed for LLS-Coop-X, i.e., when the TNs are not hybrid.

Fig. 4.5 presents the performance of AoA-RSS hybrid systems, the RMSE in location estimates is compared when the shadowing variance and the angle error variance is incremented in the links. Shadowing variance is kept the same for all links, i.e., $\sigma^2_{w_{ij}} = \sigma^2_{w_{jk}} = \sigma^2_w$. Altogether the performance is worse than the AoA-ToA case, this is due to the fact that the RSS distance estimates are

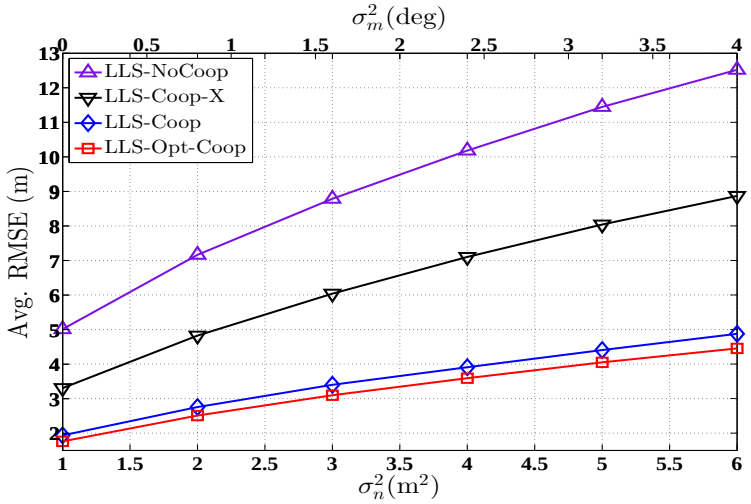

Figure 4.4: Performance comparison between LLS-NoCoop, LLS-Coop, LLS-Coop-X, LLS-Opt-Coop hybrid AoA-ToA localisation. ANs=4, TNs=30, $\ell = 1500$.

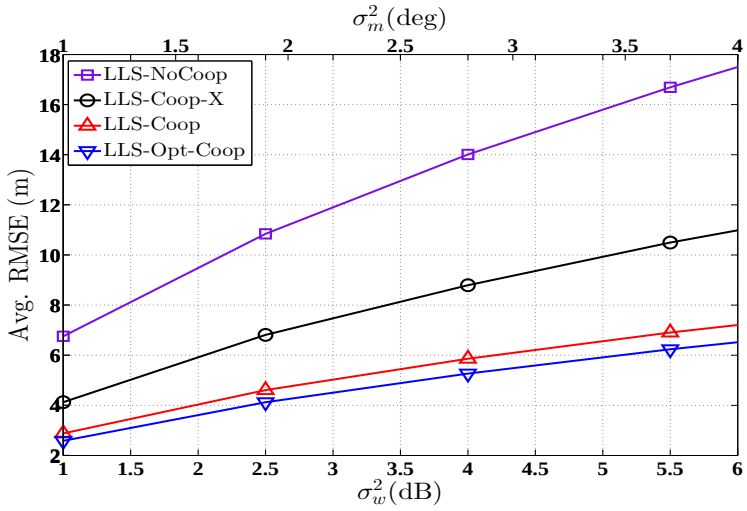

Figure 4.5: Performance comparison between LLS-NoCoop, LLS-Coop, LLS-Coop-X, LLS-Opt-Coop hybrid AoA-RSS localisation. ANs=4, TNs=30, $\ell = 1500$, $\alpha_i \forall i = 2.5$.

more erroneous then the ToA distance estimates, especially at longer inter-node distance. The PLE value considered is 2.5, and is the same for all links. A similar trend as in Fig. 4.4 is observed in this case, with LLS-Opt-Coop performing the best followed by LLS-Coop and then LLS-Coop-X while the LLS-NoCoop performs the worst.

Fig. 4.6 shows the performance of LLS-Coop for AoA-ToA signal model when the network is not fully connected. It is noted that full connectivity does not give the best performance. This is because the angle noise variance is distance dependent, hence in case of full connectivity the noisy links with far away sensor nodes are also utilised which degrades the overall performance of the system. However the difference in accuracy is not significant.

A similar trend is seen in Fig. 4.7 where the performance of LLS-Coop for AoA-RSS model is compared for different connectivity ranges. In this case both angle and range noise variance are distance dependent. A full connectivity does not show the best performance in this case either.

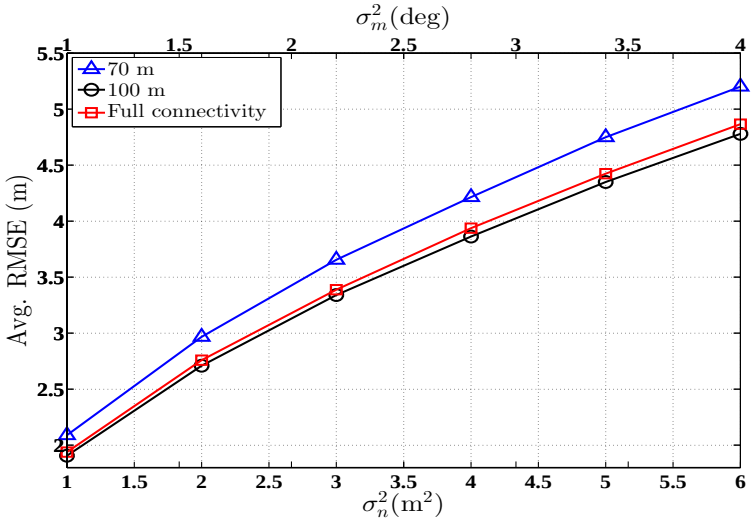

Figure 4.6: Performance comparison for LLS-Coop AoA-ToA model with partial connectivity, $\sigma^2_{n_{ij}} = \sigma^2_{n_{jk}} = \sigma^2_n$, $\sigma^2_{m_{ij}} = \sigma^2_{m_{jk}} = \sigma^2_m$, ANs=4, TNs=30, $\ell = 1500$.

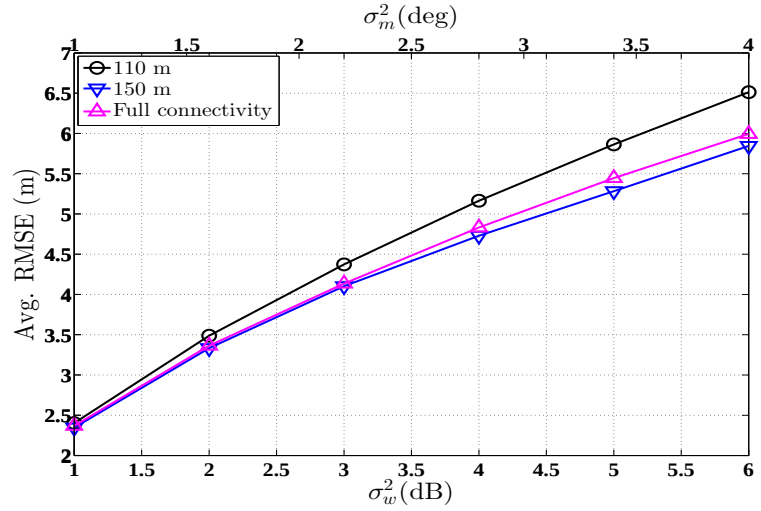

Figure 4.7: Performance comparison for LLS-Coop AoA-RSS model with partial connectivity, $\sigma^2_{w_{ij}} = \sigma^2_{w_{jk}} = \sigma^2_w$, $\sigma^2_{m_{ij}} = \sigma^2_{m_{jk}} = \sigma^2_m$, ANs=4, TNs=30, $\ell = 1500$, $\alpha_i \forall i = 2.5$.

4.8 Summary

This chapter presented a novel cooperative version of hybrid signal based localisation. Two hybrid signal, i.e., AoA-ToA and AoA-RSS are under focus. To achieve localisation, a cooperative LLS estimators based on both hybrid signals were designed. A distributed approach was presented, which can be used when a subset of TNs are required to be localised. In order to demonstrate a more realistic environment, non hybrid TNs were considered. Furthermore, full connectivity is not always achieved in practical scenarios, therefore the case of partial connectivity was considered. For all algorithms presented, computational complexities was calculated. Finally all algorithms proposed were verified via Monte Carlo simulations. Accurate results are demonstrated.

In the next chapter, a moving TN will be considered. Tracking algorithms based on Kalman filter (KF), extended Kalman filter (EKF) and particle filter (PF) will be designed and a thorough performance comparison for the mentioned filters will be presented.

5 Tracking of Mobile Wireless Nodes.

The material of this chapter is presented in

i) M. W. Khan; A. H. Kemp; N. Salman; L. Mihaylova, "Tracking of wireless mobile nodes in the presence of unknown path-loss characteristics," *18th International Conference on Information Fusion (Fusion 2015)* , pp.104-111, 6-9 July 2015.

ii) **M. W. Khan**; N. Salman; A. M. Khan; A.Ali; A. H. Kemp, "A Comparative Study of Target Tracking With Kalman Filter, Extended Kalman Filter and Particle Filter Using Received Signal Strength Measurements," *IEEE International Conference on Emerging Technologies (ICET), pp. 1-6, 2015.*

5.1 Overview

- In the previous chapters, different localisation algorithms for static TNs were developed. TNs are not always static in practical scenarios. Thus new algorithms need to be designed for the mobility of the TNs. Some highly celebrated techniques for tracking of mobile TNs are based on the Kalman filter (KF) [80], [81], the extended Kalman filter (EKF) [82], [83] and the

particle filter (PF) [84], [85]. Two system models are under focus in this chapter, for tracking purpose: *i*) the RSS signal model and *ii*) the hybrid AoA-RSS signal model. In order to analyse the impact of using incorrect PLE on location estimate, a theoretical MSE expression is derived. Furthermore, a continuously changing PLE vector is considered and is estimated at each time step and then utilised in AoA-RSS signal model for tracking purpose. Performance comparison is done for tracking of wireless node using hybrid AoA-RSS signal model with estimated PLE vector and by using RSS of the signal only.

5.2 Signal Models for Moving Target Node

Applications of a mobile TN include, robot tracking, wildlife tracking, pets, elderly and toddler tracking [86], [87]. Tracking of these mobile TNs present new challenges for researchers. The motion of TNs can be represented by its position, velocity and acceleration [88]. Different types of motion models are studied in literature. These include random walk, the constant velocity model and the constant acceleration model [89]. In this thesis, the constant velocity model is considered [90]. However to demonstrate a more realistic scenario, sudden changes in the direction of the motion of the TN are accepted. In the following subsections, two signal models that will be used with KF, EKF and PF are explained. These signal model are RSS based and Hybrid AoA-RSS based. It should be noted that these signal models were explained in previous chapters for static TNs. In this chapter, they are revisited again for mobile TN. It should also be noted that as the TN is moving, the observation model is dynamic and changes at every time step. Thus, the subscript t will represent the observations at time step t.

5.2.1 The RSS Signal Model

In this chapter, we consider a two dimensional network consisting N static ANs with known locations, $\bar{\mathbf{u}}_i = [\bar{x}_i, \bar{y}_i]^T (\bar{\mathbf{u}}_i \in \mathbb{R}^2)$ for $i = 1, ..., N$ and a TN which has unknown coordinates, $\mathbf{u}_t = [x_t,\ y_t]^T$ $(\mathbf{u}_t \in \mathbb{R}^2)$ and velocity, $\mathbf{v}_t = [v_x,\ v_y]^T$, at time step t. At any time step, a minimum of 3 distance estimates, $d_{i,t}$ are required to track a TN in 2-D. These distance estimates can be readily extracted from the received path-loss as

$$\mathcal{L}_{i,t} = \mathcal{L}_0 + 10\alpha_{i,t} \log_{10} \frac{d_{i,t}}{d_0} + \check{w}_{i,t}, \tag{5.1}$$

where $\mathcal{L}_{i,t}$ is the received path-loss at i^{th} AN, $\mathcal{L}_0$ is the path-loss at reference distance d_0 usually taken as 1m, $\alpha_{i,t}$ is the PLE associated with i^{th} AN at time step t, which for the RSS signal model is assumed to be known for all ANs, $d_{i,t}$ is the true distance between i^{th} AN and TN at time step t, given by $d_{i,t} = \sqrt{(x_t - \bar{x}_i)^2 + (y_t - \bar{y}_i)^2}$ and $\check{w}_{i,t}$ represents the log normal shadowing which is modelled as Gaussian random variable with mean zero and variance $\sigma^2_{\check{w}_{i,t}}$, i.e., $\check{w}_{i,t} \sim \mathcal{N}\left(0, \sigma^2_{\check{w}_{i,t}}\right)$. The path-loss is the difference between the observed power at the AN and transmit power at the TN and can be represented as

$$\mathcal{L}_{i,t} = 10 \log_{10} P - 10 \log_{10} P_{i,t}, \tag{5.2}$$

where P is the transmit power at TN which is known to all ANs and $P_{i,t}$ is the received power at i^{th} AN. The path-loss $z_{i,t}$ from d_0 to $d_{i,t}$ at time step t, observed at i^{th} AN can be represented as

$$\hat{z}_{i,t} = \gamma \alpha_{i,t} \ln d_{i,t} + \check{w}_{i,t}, \tag{5.3}$$

where $\gamma = \frac{10}{\ln 10}$. Equ. (5.3) can be presented in matrix form as

$$\hat{\mathbf{z}}_t = \mathbf{z}_t + \mathbf{w}_t, \tag{5.4}$$

where $\hat{\mathbf{z}}_t = [\hat{z}_{1,t}, ..., \hat{z}_{N,t}]^T$, $\mathbf{z}_t = [\gamma\alpha_{1,t} \ln d_{1,t}, ...,\ \gamma\alpha_{N,t} \ln d_{N,t}]^T$ and $\mathbf{w}_t = [\check{w}_{1,t}, ..., \check{w}_{N,t}]^T$.

Since (5.4) is non linear in terms of x_t and y_t, the KF can not be implemented directly. It should be noted that the EKF is directly applied to the Taylor series expansion of observation model presented by (5.4).

Linearisation of Observation Model: For a ToA based system, the linearisation idea was first given in [56]. We follow a similar approach here to linearise (5.4). After some mathematical manipulation (5.3) can be written as

$$\exp\left(\frac{2\hat{z}_{i,t}}{\gamma\alpha_{i,t}}\right) \approx \hat{d}_{i,t}^2. \tag{5.5}$$

Equ. (5.5) represents the biased distance estimate via RSS at time step t. To make the model unbiased we introduce an unbiasing constant $1/\beta_{i,t}$, such that

$$E\left[\frac{1}{\beta_{i,t}}\exp\left(\frac{2\hat{z}_{i,t}}{\gamma\alpha_{i,t}}\right)\right] = d_{i,t}^2, \tag{5.6}$$

where $\beta_{i,t} = \exp\left(\frac{2\sigma_{\tilde{w}_{i,t}}^2}{(\gamma\alpha_{i,t})}\right)$. To linearise (5.6), we subtract the distance equation of i^{th} AN, $d_{i,t}^2$ for $i = 1, ..., N-1$ $(i \neq r)$ from the distance equation of reference AN $d_{r,t}^2$. This reference AN can be chosen at random or some special criteria can be designed to select the optimum reference AN. The selection of optimum reference AN and the idea of unbiasing constant, $\frac{1}{\beta_{i,t}}$, is detailed in [60]. We have

$$\begin{aligned}\left[(x_t-\bar{x}_r)^2+(y_t-\bar{y}_r)^2\right] - \left[(x_t-\bar{x}_i)^2+(y_t-\bar{y}_i)^2\right] \\ = \frac{1}{\beta_{r,t}}\exp\left(\frac{2\hat{z}_{r,t}}{\gamma\alpha_{r,t}}\right) - \frac{1}{\beta_{i,t}}\exp\left(\frac{2\hat{z}_{i,t}}{\gamma\alpha_{i,t}}\right),\end{aligned} \tag{5.7}$$

which can be simplified to

$$\begin{aligned}(\bar{x}_i-\bar{x}_r)\,x_t + (\bar{y}_i-\bar{y}_r)\,y_t = 0.5\Bigg[\varepsilon_i-\varepsilon_r \\ + \frac{1}{\beta_{r,t}}\exp\left(\frac{2\hat{z}_{r,t}}{\gamma\alpha_{r,t}}\right) - \frac{1}{\beta_{i,t}}\exp\left(\frac{2\hat{z}_{i,t}}{\gamma\alpha_{i,t}}\right)\Bigg],\end{aligned} \tag{5.8}$$

where $\varepsilon_r = (\bar{x}_r^2 + \bar{y}_r^2)$ and $\varepsilon_i = (\bar{x}_i^2 + \bar{y}_i^2)$. (5.8) can be written in matrix form as

$$\mathbf{A}_{RSS}\mathbf{u}_t = 0.5\mathbf{r}_t, \tag{5.9}$$

where

$$\mathbf{A}_{RSS} = \begin{bmatrix} \bar{x}_1 - \bar{x}_r & \bar{y}_1 - \bar{y}_r \\ \bar{x}_2 - \bar{x}_r & \bar{y}_2 - \bar{y}_r \\ \vdots & \vdots \\ \bar{x}_{N-1} - \bar{x}_r & \bar{y}_{N-1} - \bar{y}_r \end{bmatrix}, \quad \mathbf{u}_t = \begin{bmatrix} x_t \\ y_t \end{bmatrix} \tag{5.10}$$

$$\mathbf{r}_t = \begin{bmatrix} \frac{1}{\beta_{r,t}} \exp\left(\frac{2\hat{z}_{r,t}}{\gamma\alpha_{r,t}}\right) - \frac{1}{\beta_{1,t}} \exp\left(\frac{2\hat{z}_{1,t}}{\gamma\alpha_{1,t}}\right) - \varepsilon_r + \varepsilon_1 \\ \frac{1}{\beta_{r,t}} \exp\left(\frac{2\hat{z}_{r,t}}{\gamma\alpha_{r,t}}\right) - \frac{1}{\beta_{2,t}} \exp\left(\frac{2\hat{z}_{2,t}}{\gamma\alpha_{2,t}}\right) - \varepsilon_r + \varepsilon_2 \\ \vdots \\ \frac{1}{\beta_{r,t}} \exp\left(\frac{2\hat{z}_{r,t}}{\gamma\alpha_{r,t}}\right) - \frac{1}{\beta_{(N-1),t}} \exp\left(\frac{2\hat{z}_{(N-1),t}}{\gamma\alpha_{(N-1),t}}\right) - \varepsilon_r + \varepsilon_{N-1} \end{bmatrix} \tag{5.11}$$

With (5.10) and (5.11), the KF can be implemented. It should be noted that for a total of N measurements from N ANs, we can utilise only $(N-1)$ observation as given by the dimension of (5.11). Which means that some of the information is lost during the linearisation steps.

5.2.2 The Hybrid AoA-RSS Signal Model

The hybrid AoA-RSS signal model was introduced in chapter 3 for static nodes. Here we detail it in the context of mobile nodes. With both distance and angle measurements at hand, the coordinates of the TN at the t^{th} time step can be computed as follows

$$\hat{x}_t = \bar{x}_i + \hat{d}_{i,t} \cos\hat{\theta}_{i,t}\delta_{i,t}, \tag{5.12}$$

$$\hat{y}_t = \bar{y}_i + \hat{d}_{i,t} \sin\hat{\theta}_{i,t}\delta_{i,t}, \tag{5.13}$$

The estimated distance $\hat{d}_{i,t}$ is given by(5.5). On the other hand, the estimated angle of arrival at time step t, $\hat{\theta}_{i,t}$, is given by

$$\hat{\theta}_{i,t} = \arctan\left(\frac{(y_t - \bar{y}_i)}{(x_t - \bar{x}_i)}\right) + m_{i,t}, \tag{5.14}$$

where $m_{i,t}$ is the zero mean Gaussian random variable representing the noise in angle estimate, i.e., $m_{i,t} \sim \mathcal{N}\left(0, \sigma^2_{m_{i,t}}\right)$. With the above observations, (5.12) and (5.13) can be written in a vector form as

$$\mathbf{A}\mathbf{u}_t = \hat{\mathbf{b}}_t, \tag{5.15}$$

where $\mathbf{A}^\dagger$ is the Moore–Penrose pseudo-inverse of $\mathbf{A}$ and $\mathbf{A} = \text{diag}\left(\mathbf{e}_1, \mathbf{e}_1\right)$, where $\mathbf{e}_1$ is a column vector of N ones. The observation matrix $\hat{\mathbf{b}}$ is given by

$$\hat{\mathbf{b}}_t = \begin{bmatrix}\hat{\mathbf{b}}_{x,t} & \hat{\mathbf{b}}_{y,t}\end{bmatrix}^T, \tag{5.16}$$

$$\hat{\mathbf{b}}_{x,t} = \begin{bmatrix} \bar{x}_1 + \hat{d}_{1,t}\cos\hat{\theta}_{1,t}\delta_{1,t} \\ \vdots \\ \bar{x}_N + \hat{d}_{N,t}\cos\hat{\theta}_{N,t}\delta_{N,t} \end{bmatrix}, \hat{\mathbf{b}}_{y,t} = \begin{bmatrix} \bar{y}_1 + \hat{d}_{1,t}\sin\hat{\theta}_{1,t}\delta_{1,t} \\ \vdots \\ \bar{y}_N + \hat{d}_{N,t}\sin\hat{\theta}_{N,t}\delta_{N,t} \end{bmatrix},$$

where δ_i is the unbiasing constant for the hybrid AoA-RSS signal and is given by

$$\delta_{i,t} = \beta_{i,t}\rho_{i,t}, \tag{5.17}$$

and $\rho_{i,t} = \exp\left(\sigma^2_{m_{i,t}}/2\right)$.

5.3 Theoretical MSE for Erroneous PLEs

In this section, we derive the theoretical MSE to observe the impact of incorrect PLE assumption on location estimation while using AoA-RSS signal model [91]. First, we use the observed path-loss (5.3) to extract the range between AN and TN when the true values of PLEs are not known. For ease of understanding we will drop the subscript t in this section. Using the erroneous PLE values we have from (5.3)

$$\frac{z_i}{\gamma\check{\alpha}_i} = \frac{\alpha_i}{\check{\alpha}_i}\ln d_i + \frac{\check{w}_i}{\gamma\check{\alpha}_i}, \tag{5.18}$$

where $\check{\alpha}_i$ is the incorrect PLE for the i^{th} AN, i.e., $\check{\alpha}_i = \alpha_i + e_i$, and e_i represents the error in PLE associated with i^{th} AN. Taking exponential on both side of (5.18), the unbiased distance estimate using and erroneous PLE is obtained as

$$\check{d}_i = d_i^{\kappa_i} \exp\left(\frac{\check{w}_i}{\gamma \check{\alpha}_i}\right) \Lambda_i, \tag{5.19}$$

where $\kappa_i = \alpha_i / \check{\alpha}_i$ and $\Lambda_i = \exp\left(-\frac{\sigma^2_{\check{w}_i}}{2(\gamma\check{\alpha}_i)^2}\right)$.

For the aforementioned hybrid AoA-RSS signal model, (5.19) is taken as the distance estimate in (5.16), i.e., we use $\check{d}_i$ instead of $\hat{d}_i$. Also the unbiasing constant δ_i is changed to $\check{\delta}_i = \Lambda_i \rho_i$, where $\check{\delta}_i$ represents the unbiasing constant with incorrect PLE. Thus, (5.12) and (5.13) are written as follows

$$\hat{x}_t = \bar{x}_i + \check{d}_i \cos\hat{\theta}_{i,t} \check{\delta}_i$$

$$\hat{y}_t = \bar{y}_i + \check{d}_i \sin\hat{\theta}_{i,t} \check{\delta}_i$$

which in matrix form is written as

$$\mathbf{u}_\alpha = \mathbf{A}^\dagger \hat{\mathbf{b}}_\alpha,$$

where

$$\hat{\mathbf{b}}_\alpha = \begin{bmatrix} \hat{\mathbf{b}}_{x,\alpha} & \hat{\mathbf{b}}_{y,\alpha} \end{bmatrix}$$

$$\hat{\mathbf{b}}_{x,\alpha} = \begin{bmatrix} \bar{x}_1 + \check{d}_1 \cos\hat{\theta}_{1,t} \check{\delta}_1 \\ \vdots \\ \bar{x}_N + \check{d}_N \cos\hat{\theta}_{N,t} \check{\delta}_N \end{bmatrix}, \hat{\mathbf{b}}_{y,\alpha} = \begin{bmatrix} \bar{y}_1 + \check{d}_1 \sin\hat{\theta}_1 \check{\delta}_1 \\ \vdots \\ \bar{y}_N + \check{d}_N \sin\hat{\theta}_N \check{\delta}_N \end{bmatrix},$$

The theoretical MSE is then given by [61]

$$\text{MSE} = Tr\left\{ E_{\mathbf{w},\mathbf{m}} \left[\left(\check{\mathbf{u}}_\alpha - \mathbf{u}_\alpha\right) \left(\check{\mathbf{u}}_\alpha - \mathbf{u}_\alpha\right)^T \right] \right\}, \tag{5.20}$$

where $\check{\mathbf{u}}_\alpha$ is the estimated location using noisy angle estimates and noisy range

estimates with incorrect PLEs, while $\mathbf{u}_\alpha$ is the ground truth. Thus (5.20) can be simplified to

$$\mathrm{MSE}\left(\mathbf{u}\right) = Tr\left\{\mathbf{A}^{\dagger}\mathbf{C}_\alpha\left(\mathbf{u}\right)\mathbf{A}^{\dagger^T}\right\}, \tag{5.21}$$

where $\mathbf{C}_\alpha\left(\mathbf{u}\right) = E_{\mathbf{w},\mathbf{m}}\left[\left(\check{\mathbf{b}}_\alpha - \mathbf{b}_\alpha\right)\left(\check{\mathbf{b}}_\alpha - \mathbf{b}_\alpha\right)^T\right]$, for $\mathbf{b}_\alpha$ representing the noise-free observation, $\check{\mathbf{b}}_\alpha$ representing the noisy observation and incorrect PLEs and $E_{\mathbf{w},\mathbf{m}}$ is the expectation w.r.t. shadowing noise and noise associated with angle estimates. The covariance $\mathbf{C}_\alpha\left(\mathbf{u}\right)$, can be partitioned into separate sub-matrices as follows

$$\mathbf{C}_\alpha\left(\mathbf{u}\right) = \begin{bmatrix} \mathbf{C}_\alpha\left(x\right) & \mathbf{C}_\alpha\left(xy\right) \\ \mathbf{C}_\alpha\left(xy\right) & \mathbf{C}_\alpha\left(y\right) \end{bmatrix}, \tag{5.22}$$

where

$$\mathbf{C}_\alpha\left(x\right) = E_{\mathbf{w},\mathbf{m}}\left[\left(\hat{\mathbf{b}}_{x,\alpha} - \mathbf{b}_{x,\alpha}\right)\left(\hat{\mathbf{b}}_{x,\alpha} - \mathbf{b}_{x,\alpha}\right)^T\right] \in \mathbb{R}^{N\times N} \tag{5.23}$$

$$\mathbf{C}_\alpha\left(y\right) = E_{\mathbf{w},\mathbf{m}}\left[\left(\hat{\mathbf{b}}_{y,\alpha} - \mathbf{b}_{y,\alpha}\right)\left(\hat{\mathbf{b}}_{y,\alpha} - \mathbf{b}_{y,\alpha}\right)^T\right] \in \mathbb{R}^{N\times N} \tag{5.24}$$

$$\mathbf{C}_\alpha\left(xy\right) = E_{\mathbf{w},\mathbf{m}}\left[\left(\hat{\mathbf{b}}_{x,\alpha} - \mathbf{b}_{x,\alpha}\right)\left(\hat{\mathbf{b}}_{y,\alpha} - \mathbf{b}_{y,\alpha}\right)^T\right] \in \mathbb{R}^{N\times N} \tag{5.25}$$

$\mathbf{C}_\alpha\left(x\right)$, $\mathbf{C}_\alpha\left(y\right)$ and $\mathbf{C}_\alpha\left(xy\right)$ reduces to (5.26), (5.27) and (5.28), respectively, for $i = j$ and (5.29), (5.30) and (5.31), respectively for $i \neq j$. Derivation is given in Appendix IV.

5.4 Target Tracking

A detailed performance comparison is presented in this section between KF, EKF and PF, first using RRS measurements and then AoA-RSS signal model. The PF performance will be analysed for different number of particles. As already mentioned a constant velocity model is considered. However to imitate a more realistic environment sudden changes in direction of TNs are considered.

Algorithm 5.1

$$\mathbf{C}_{\alpha}\left(x\right)_{ii} = d_i^{2\kappa_i}\left(\frac{\sigma_{\check{w}_i}^2}{\left(\gamma\check{\alpha}_i\right)^2} + \sigma_{m_i}^2\right) + \frac{d_i^{2\kappa_i}}{2}\cos\left(2\theta_i\right)\exp\left(\frac{\sigma_{\check{w}_i}^2}{\left(\gamma\check{\alpha}_i\right)^2} - \sigma_{m_i}^2\right) + \left(d_i\cos\theta_i\right)^2 - 2d_i d_i^{\kappa_i}\cos^2\theta_i \quad (5.26)$$

$$\mathbf{C}_{\alpha}\left(y\right)_{ii} = d_i^{2\kappa_i}\left(\frac{\sigma_{\check{w}_i}^2}{\left(\gamma\check{\alpha}_i\right)^2} + \sigma_{m_i}^2\right) - \frac{d_i^{2\kappa_i}}{2}\cos\left(2\theta_i\right)\exp\left(\frac{\sigma_{\check{w}_i}^2}{\left(\gamma\check{\alpha}_i\right)^2} - \sigma_{m_i}^2\right) + \left(d_i\sin\theta_i\right)^2 - 2d_i d_i^{\kappa_i}\sin^2\theta_i \quad (5.27)$$

$$\mathbf{C}_{\alpha}\left(xy\right)_{ii} = d_i^{2\kappa_i}\cos\theta_i\sin\theta_i\exp\left(\frac{\sigma_{\check{w}_i}^2}{\left(\gamma\check{\alpha}_i\right)^2} - \sigma_{m_i}^2\right) - 2d_i^{\kappa_i}\cos\theta_i\sin\theta_i + d_i^2\cos\theta_i\sin\theta_i \quad (5.28)$$

$$\mathbf{C}_{\alpha}\left(x\right)_{ij} = \left(d_i^{\kappa_i}d_j^{\kappa_j} - d_i^{\kappa_i}d_j - d_i d_j^{\kappa_j} + d_i d_j\right)\cos\theta_i\cos\theta_j \quad (5.29)$$

$$\mathbf{C}_{\alpha}\left(y\right)_{ij} = \left(d_i^{\kappa_i}d_j^{\kappa_j} - d_i^{\kappa_i}d_j - d_i d_j^{\kappa_j} + d_i d_j\right)\sin\theta_i\sin\theta_j \quad (5.30)$$

$$\mathbf{C}_{\alpha}\left(xy\right)_{ij} = \left(d_i^{\kappa_i}d_j^{\kappa_j} - d_i^{\kappa_i} - d_j^{\kappa_j} + d_i d_j\right)\cos\theta_i\sin\theta_j \quad (5.31)$$

5.4.1 The Kalman Filter

The KF, named after Rudolf E Kalman, a Hungarian researcher, is an algorithm that is based a sequence of noisy observations and is used to estimate unknown parameters which in tracking of wireless nodes are positions and velocities of the nodes. It is observed that the estimate based on the series of observation produce better estimates than those based on individual readings. For its simplicity the KF is one of the most widely used tracking algorithm. However the requirement of linear observation models corrupted with Gaussian noise for its implementation is one of the drawbacks of KF. KF is based on the fact that the state of the system at time step t is evolved from the state of the system at $t-1$. The KF involves alternative predict and update steps. Thus starting from an initial guess state $\boldsymbol{s}_0$ and initial error covariance matrix $\mathbf{W}_0$ the KF propagates the first two moments, i.e., mean and covariance of the state vector $\boldsymbol{s}_t$ at every time step.

Consider a linear dynamic system where the state and observation model is represented by the following equations

$$\boldsymbol{s}_t = \mathbf{S}\,\boldsymbol{s}_{(t-1)} + \mathbf{q}_t, \tag{5.32}$$

$$\mathbf{p}_t = \mathbf{H}\boldsymbol{s}_t + \mathbf{m}_t, \tag{5.33}$$

where $\mathbf{S}$ represents the transition matrix and is dependent on the motion of the TN, $\mathbf{p}_t$ is the measurements received from the sensors,$\mathbf{H}$ is the data matrix and is dependent on the observation model in question (In this thesis we use RSS and AoA-RSS observation models), $\boldsymbol{s}_{(t-1)}$ is the state vector at previous time step, i.e., the position and velocity of TN at previous time step, $\mathbf{r}_t$ is the process noise due to modeling error which is assumed to be zero mean Gaussian process with covariance $\mathbf{Q}_t$, i.e., $\mathbf{r}_t \sim \mathcal{N}(0, \mathbf{Q}_t)$, $\mathbf{m}_t$ is the measurement noise that is assumed to be zero mean Gaussian random process with covariance $\mathbf{C}_t$, i.e.,

$\mathbf{m}_t \sim \mathcal{N}(0, \mathbf{C}_t)$. Then the prediction and measurement update steps involved in KF's implementation are as follows

5.4.1.1 Prediction

The first step involve the prediction of the state one step ahead based on the motion model. Thus starting from the initial state $\hat{\boldsymbol{s}}_0$ and initial error covariance matrix $\mathbf{W}_0$, and using a constant velocity model the KF updates $\hat{\boldsymbol{s}}_0$ and $\mathbf{W}_0$ according to following equations.

$$\boldsymbol{s}_t^p = \mathbf{S}\,\hat{\boldsymbol{s}}_{(t-1)} + \boldsymbol{\epsilon}_t, \tag{5.34}$$

$$\bar{\mathbf{W}}_t = \mathbf{S}\,\mathbf{W}_{(t-1)}\mathbf{S} + \mathbf{Q}_t, \tag{5.35}$$

where $\boldsymbol{\epsilon}_t$ is a random noise simulating the modeling error at time step t, $\boldsymbol{s}_t^p$ is the predicted state at time step t, given by $\boldsymbol{s}_t^p = [x_t^p,\, y_t^p,\, v_x,\, v_y]$, x^p and y^p are the predicted coordinates, v_x and v_y are the velocities in x and y directions. $\bar{\mathbf{W}}_t$ is the predicted error covariance and $\mathbf{S}$ is called the transition matrix given by

$$\mathbf{S} = \begin{bmatrix} 1 & 0 & T_s & 0 \\ 0 & 1 & 0 & T_s \\ 0 & 0 & 1 & 0 \\ 0 & 0 & 0 & 1 \end{bmatrix}, \tag{5.36}$$

where T_s is the time interval between two time steps. The value of T_s may change between states, however for simplicity we assume a constant time step which makes matrix $\mathbf{S}$ a constant matrix.

5.4.1.2 Measurement Update

In the measurement update step, the predicted state vector and the error covariance are refined based on the observation model (5.33) and the measurements

from the sensors. The state vector is updated according to

$$\hat{\boldsymbol{s}}_t = \boldsymbol{s}_t^p + \mathbf{K}_t \left(\mathbf{p}_t - \mathbf{H}\boldsymbol{s}_t^p \right). \tag{5.37}$$

where $\mathbf{K}_t$ is the Kalman gain, a weighting matrix that determines how reliable are the measurements from the sensors as compared with the predicted state. The Kalman gain makes this decision based on the predicted error covariance ($\bar{\mathbf{W}}_t$) and the measurement error covariance ($\mathbf{C}_t$). So, for example in scalar parameter estimation, a Kalman gain of 0.5 suggests that the predicted state and the measurements are equally realiable. Thus the final output estimate will be a simple average of both. The Kalman gain at time step t is given by

$$\mathbf{K}_t = \bar{\mathbf{W}}_t \mathbf{H}^T \left(\mathbf{H}\, \bar{\mathbf{W}}_t\, \mathbf{H}^T + \mathbf{C}_t \right). \tag{5.38}$$

The error covariance is also dependent on Kalman gain and is update according to

$$\mathbf{W}_t = \left(\mathbf{I}_4 - \mathbf{K}_t \mathbf{H} \right) \bar{\mathbf{W}}_t. \tag{5.39}$$

The complete derivation of KF filter is detailed in [92]. The data matrix $\mathbf{H}$ and the observation vector $\mathbf{p}_t$ for KF are defined next.

RSS Signal Model: For RSS based systems, the observation model is given by (5.19), thus $\mathbf{p}_t$ is equivalent to $\mathbf{r}_t$. The data matrix for RSS based measurement model is given by $\mathbf{A}_{RSS}$ in (5.19). However, in order for $\mathbf{H}$ to have correct dimensions, to be used in (5.37), (5.38) and (5.39), the data matrix $\mathbf{H}$ is given by $\mathbf{H} = [\mathbf{A}_{RSS}\, \mathbf{Z}]$ where $\mathbf{Z}$ is a zero matrix of dimension $(N-1) \times 2$. The only purpose of adding the zero matrix, $\mathbf{Z}$ to the data matrix, $\mathbf{H}$ is to make $\mathbf{H}$ dimensionally consistent with other matrices used in KF.

AoA-RSS Signal Model: For AoA-RSS signal model, the observation model is given by 5.15. Thus, the observation vector, $\mathbf{p}_t$ is equivalent to $\mathbf{b}_t$. The data matrix, $\mathbf{H}=\left[\mathbf{A}\ \bar{\mathbf{Z}}\right]$, where $\bar{\mathbf{Z}}$ is a zero matrix of dimension $2N \times 2$, and is included

in data matrix, $\mathbf{H}$ to make it dimensionally consistent with other matrices used in filtering process.

5.4.2 Extended Kalman Filter

For EKF no compulsion of linear transition or linear observation model is required. The EKF approximates the non linear model with the first order Taylor series expansion of the observation model. Thus considering a non linear dynamical system of the form

$$\boldsymbol{s}_t = f\left(\boldsymbol{s}_{(t-1)}\right) + \mathbf{r}_t, \tag{5.40}$$

$$\mathbf{p}_t = g\left(\boldsymbol{s}_t\right) + \mathbf{m}_t. \tag{5.41}$$

Equ. (5.40) and (5.41) represents the state transition and observation model, respectively. Where $f\left(.\right)$ and $g\left(.\right)$ are non linear differentiable functions. The prediction and measurement update steps are presented as follows

5.4.2.1 Prediction

The state vector is predicted according to the following equation

$$\boldsymbol{s}_t^p = f\left(\hat{\boldsymbol{s}}_{(t-1)}\right) + \boldsymbol{\epsilon}_t. \tag{5.42}$$

The function $f\left(.\right)$ can be directly used to compute the predicted state. However the same is not true for error covariance prediction. Thus the partial derivative of $f\left(.\right)$ is used instead. The predicted error covariance for the non linear system is given as

$$\bar{\mathbf{M}} = \mathbf{J}_f\Big|_{\hat{\boldsymbol{s}}_{(t-1)}} \quad \mathbf{M}_{(t-1)} \quad \mathbf{J}_f^T\Big|_{\hat{\boldsymbol{s}}_{(t-1)}} + \mathbf{Q}_t, \tag{5.43}$$

where $\mathbf{J}_f|_{\hat{\boldsymbol{s}}_{(t-1)}}$ is the Jacobian of $f\ (\boldsymbol{s})$ evaluated at $\hat{\boldsymbol{s}}_{(t-1)}$, i.e., $\frac{\partial f}{\partial \boldsymbol{s}}\Big|_{\hat{\boldsymbol{s}}_{(t-1)}}$. In most scenarios the state transition model is linear, which is also the case in constant velocity model. Thus (5.34) will be used to predict the state while using EKF.

5.4.2.2 Measurement Update

The predicted error covariance is used at the measurement update stage to calculate the Kalman gain. The Kalman gain and the measurements from the sensors are then utilised to refine the predicted state vector. The predicted state vector is updated by

$$\hat{\boldsymbol{s}}_t = \boldsymbol{s}_t^p + \mathbf{K}_t \left(\mathbf{p}_t - g\left(\boldsymbol{s}_t^p\right)\right), \tag{5.44}$$

and the Kalman gain is computed as

$$\mathbf{K}_t = \bar{\mathbf{M}}_t \mathbf{B}^T \left(\mathbf{B}\, \bar{\mathbf{M}}_t\, \mathbf{B}^T + \mathbf{C}_t\right), \tag{5.45}$$

where $\mathbf{B} = \left[\mathbf{J}_g|_{\boldsymbol{s}_t^p}\right]$ and $\mathbf{J}_g|_{\boldsymbol{s}_t^p}$ is the Jacobian of $g\left(\boldsymbol{s}\right)$ evaluated at $\boldsymbol{s}_t^p$. The error covariance matrix is updated as

$$\mathbf{M}_t = \left(\mathbf{I}_4 - \mathbf{K}_t \mathbf{B}\right) \bar{\mathbf{M}}_t. \tag{5.46}$$

The complete derivation of EKF and smoothing equations is given in [93].

For RSS Signal Model: For RSS signal model, $\mathbf{p}_t$ is equivalent to $\mathbf{z}_t$ in 5.4 and $\mathbf{B} = \left[\mathbf{J}_g|_{\boldsymbol{s}_t^p}\ \mathbf{Z}_{N\times 2}\right]$ and $\mathbf{J}_g|_{\boldsymbol{s}_t^p}$ is the Jacobian of $g\left(\boldsymbol{s}\right)$ evaluated at $\boldsymbol{s}_t^p$ and is given by

$$\mathbf{J}_g\Big|_{\boldsymbol{s}_t^p} = \begin{bmatrix} \frac{\gamma\alpha_{1,t}\left(x_t^p - \bar{x}_1\right)}{d_{1,t}^p} & \frac{\gamma\alpha_{1,t}\left(y_t^p - \bar{y}_1\right)}{d_{1,t}^p} \\ \vdots & \vdots \\ \frac{\gamma\alpha_{N,t}\left(x_t^p - \bar{x}_N\right)}{d_{N,t}^p} & \frac{\gamma\alpha_{N,t}\left(y_t^p - \bar{y}_N\right)}{d_{N,t}^p} \end{bmatrix}, \tag{5.47}$$

where $d_i^p = \left(\left(x_t^p - \bar{x}_i\right)^2 + \left(y_t^p - \bar{y}_i\right)\right)$.

5.4.3 Particle Filter

Though computationally more expensive, the PF unlike KF does not require the noise to be Gaussian or the observation model to be linear. The PF is a recursive sequential Monte Carlo estimator that approximates the posterior density of the state vector with randomly drawn points also called particles and updates the state vector as new observations become available. The accuracy of the filter is directly and computational cost is inversely proportional to the number of particle N_s used.

According to Bayesian statistics the posterior state probability density function (PDF) is given as

$$p\left(\boldsymbol{s}_t \mid \mathbf{p}_{(1:t)}\right) = \frac{p\left(\mathbf{p}_t \mid \boldsymbol{s}_t\right) p\left(\boldsymbol{s}_t \mid \boldsymbol{s}_{(t-1)}\right)}{p\left(\mathbf{p}_t \mid \mathbf{p}_{(t-1)}\right)} p\left(\boldsymbol{s}_{(1:t-1)} \mid \mathbf{p}_{(1:t-1)}\right), \tag{5.48}$$

where $\mathbf{p}_{(1:t)} = (\mathbf{p}_1, \mathbf{p}_2, ..., \mathbf{p}_t)$ are the observations upto time step t. The posterior PDF can be approximated by N_s particle in two dimension $\boldsymbol{s}_{j,t}$ for $j = 1, ..., N_s$. Each particle is associated with weight $w_{j,t}$.

$$p\left(\boldsymbol{s}_{1:t}^{j} \mid \mathbf{p}_{1:t}\right) = \Sigma_{j=1}^{N_s} w_t^j \delta\left(\boldsymbol{s}_{1:t} - \boldsymbol{s}_{(1:t)}^{j}\right). \tag{5.49}$$

The particles are generated from the proposal density also called importance function $g\left(\boldsymbol{s}_{1:t} \mid \mathbf{p}_{1:t}\right)$ and the weights are given by

$$w_t^j = \frac{p\left(\boldsymbol{s}_{1:t} \mid \mathbf{p}_{1:t}\right)}{g\left(\boldsymbol{s}_{1:t} \mid \mathbf{p}_{1:t}\right)}. \tag{5.50}$$

The proposal density is chosen as

$$g\left(\boldsymbol{s}_{1:t} \mid \mathbf{p}_{1:t}\right) = g\left(\boldsymbol{s}_t \mid \boldsymbol{s}_{t-1}, \mathbf{p}_t\right) g\left(\boldsymbol{s}_{1:(t-1)} \mid \mathbf{p}_{1:(t-1)}\right), \tag{5.51}$$

then from (5.48)-(5.51) we get

$$w_t^j \propto \frac{p\left(\mathbf{p}_t \mid \boldsymbol{s}_t^j\right) p\left(\boldsymbol{s}_t^j \mid \boldsymbol{s}_{(t-1)}^j\right)}{g\left(\boldsymbol{s}_t^j \mid \boldsymbol{s}_{(t-1)}^j, \mathbf{p}_{(t-1)}^j\right)} w_{(t-1)}^j. \tag{5.52}$$

A special criteria can be designed to select the proposal density [94]. However a straightforward approach is to select the prior as the proposal density, i.e., $g\left(\boldsymbol{s}_t^j \mid \boldsymbol{s}_{(t-1)}^j, \mathbf{p}_t\right) = p\left(\boldsymbol{s}_t^j \mid \boldsymbol{s}_{(t-1)}^j\right)$ which reduces (5.52) to

$$w_t^j = p\left(\mathbf{p}_t \mid \boldsymbol{s}_t^j\right) w_{(t-1)}^j. \tag{5.53}$$

The marginalized density of the state vector is given by

$$p\left(\boldsymbol{s}_t \mid \mathbf{p}_t\right) = \Sigma_{j=1}^{N_s} w_t^j \delta\left(\boldsymbol{s}_t - \boldsymbol{s}_t^j\right). \tag{5.54}$$

Degeneracy of Particle Filters: One of the drawback of PF is degeneracy of the particles. During degeneracy a large portion of particles are given negligible weights. Thus only those particles with significant weights called effective particles contributes in approximating the posterior PDF. This scenario can be avoided by the process of resampling. When the number of effective particle N_{eff} drops below a predefined threshold N_{thr}, a resampling procedure is invoked. During resampling, N_s particles are selected from effective particles with repetition, where the probability of selecting a particle is directly proportional to its weight. These selected particles are then given equal weights of $1/N_s$. The number of effective particles can be calculated according to the following equation.

$$N_{eff} = \frac{1}{\Sigma_{j=1}^{N_s} \left(w^j\right)^2}. \tag{5.55}$$

5.5 PLE Estimation

A novel PLE estimator was presented in chapter 3, where static TNs and thus a static PLE vector was considered. However when the TN is moving the PLE vector changes continuously. We consider a varying PLE vector and then use GenPS algorithm to estimate the PLE vector at every time step, before employing KF or PF for tracking. The GenPS algorithm is explained in section 3.3. However

Algorithm 5.2 : Initialization and GenPS

for time step $t = 1$,...
  for $i = 1, ..., N$
    estimate the path-loss $\hat{z}_{i,t}$ and the AoA $\hat{\theta}_{i,t}$.
  end
  for $k = 1, ...$
    i. Initialize $\boldsymbol{\alpha}_0 \in [2\ 5]$, Δ_0,τ, ξ, ν.
    ii. Evaluate cost function with all poll points from poll set $\left\{\boldsymbol{\alpha}^k + \Delta_k \bar{d}, \bar{d} \in \mathbf{D}\right\}$.
    iii-a. If improved poll point is found, accept $\boldsymbol{\alpha}^{k+1}$, set $\Delta_{k+1} = \xi \Delta_k$.
    iii-b. If improved poll point cannot be found, set $\boldsymbol{\alpha}^{k+1} = \boldsymbol{\alpha}^k$, set $\Delta_{k+1} = \frac{\Delta_k}{\xi}$.
    Repeat until $\Omega\left(\boldsymbol{\alpha}^{k+1}\right) - \Omega\left(\boldsymbol{\alpha}^k\right) < \tau$.
  end
    Goto algorithm 2 or algorithm 3.
end

in this section we give a step by step procedure to estimate PLE vector in the context of tracking via KF or PF. The steps involved in PLE estimation, KF and PF are given in algorithm 5.2, 5.3 and 5.4.

5.6 Simulation Results

Through extensive Monte Carlo simulation we analyse the perofrmance of all filters discussed in this chapter using RSS signal model and AoA-RSS signal model with estimated PLE vectors. All simulation are run for ℓ number of times independently for η Monte Carlo runs.

5.6.1 Performance Analysis for RSS Signal Model

A 2-D network of dimension 60×60 metres is considered with a single TN moving with a constant velocity of 1 m/s. To make the scenario more realistic the TN encounters sudden changes in direction. For simplicity the noise variance, and

Algorithm 5.3 : Kalman Filter

Generate initial state $\boldsymbol{s}_0$ and initial Covariance matrix $\mathbf{W}_0$.

i. Prediction.

Predict $\bar{\boldsymbol{v}}_t$ by propagating $\boldsymbol{s}_0$ through the motion model.

$$\bar{\boldsymbol{s}}_t = \mathbf{S}\hat{\boldsymbol{s}}_{t-1} + \mathbf{r}_t$$

Predict $\bar{\mathbf{W}}_t$ by

$$\bar{\mathbf{W}}_t = \mathbf{S}\mathbf{W}_{t-1}\mathbf{S}^T + \mathbf{Q}$$

ii. Measurement update

Estimate Kalman gain

$$\mathbf{K}_t = \bar{\mathbf{W}}_t\mathbf{H}^T\left(\mathbf{H}\bar{\mathbf{W}}_t\mathbf{H}^T + \mathbf{C}\right)$$

Update the predicted state vector and predicted error covariance matrix.

$$\hat{\boldsymbol{s}}_t = \bar{\boldsymbol{s}}_t + \mathbf{K}_t\left(\hat{\mathbf{b}}_t - \mathbf{H}\bar{\boldsymbol{p}}_t\right)$$

$$\mathbf{W}_t = \left(\mathbf{I}_4 - \mathbf{K}_t\mathbf{H}\right)\bar{\mathbf{W}}_t$$

Set $t = t + 1$. Go to Algorithm 1.

Algorithm 5.4 : Particle Filter

Initialization:
Generate samples $\left\{\boldsymbol{s}_0^{j*} \sim \mathcal{N}\left(\mu_0, \sigma_0^2\right)\right\}$, $j = 1, ..., N_s$. Set $w_0^{j*} = \frac{1}{N_s}$.
i. Prediction:
For $j = 1, ..., N_s$, predict according to

$$\boldsymbol{s}_t^j = p\left(\boldsymbol{s}_t \mid \boldsymbol{s}_{t-1}^{j*}\right)$$

ii. Weight update
Update the weights according to

$$w_t^j = p\left(\mathbf{b}_t \mid \boldsymbol{s}_t^j\right) w_{t-1}^j$$

Normalize weights by

$$\tilde{w}_t^j = \frac{w_t^j}{\Sigma_{j=1}^{Ns} w_t^j}$$

iii. Estimate Output
The state is estimated by the mean of posterior i.e

$$\hat{\mathbf{s}}_t = E\left[p\left(\boldsymbol{s}_t \mid \mathbf{b}_t\right)\right]$$

or

$$\hat{\mathbf{s}}_t = \frac{1}{N_s} \Sigma_{j=1}^{N_s} \tilde{w}_t^j \boldsymbol{s}_t^j$$

resample if required. Set $t = t + 1$ and $w_t^j = \frac{1}{N_s}$. Go to algorithm 1.

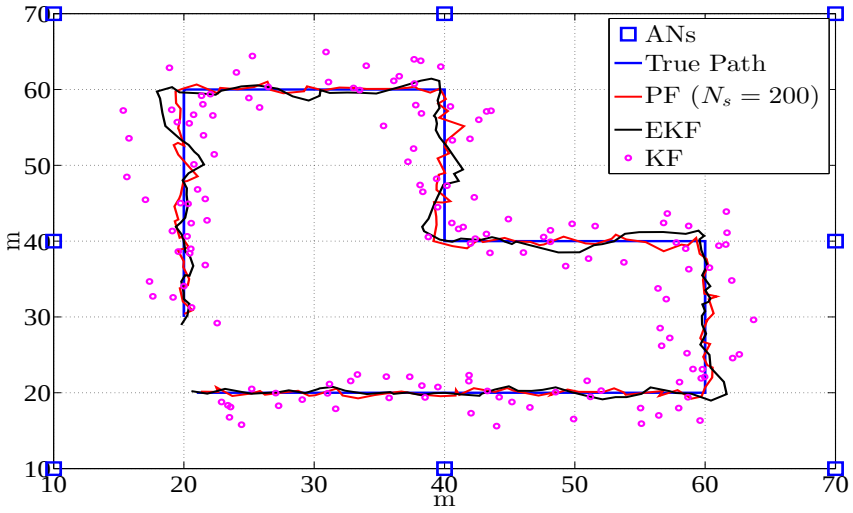

Figure 5.1: True trajectory comparison with estimated trajectory via KF, EKF and PF. $N = 8$, $N_s = 200$, $N_{thr} = {}^{N_s}/_{4}$, $\alpha_{i,t} = 2.5 \,\forall\, i \wedge t$, $T_s = 1\,\text{sec}$, $\sigma^2_{\breve{w}_{i,t}} = 0.5\,\text{dB} \,\forall\, i \wedge t$.

PLE values are considered fixed and same for all ANs.

Fig. 5.1 shows the true trajectory of the TN along with the estimated trajectory with KF, EKF and PF. The number of particle used for this demonstration are kept fixed at $N_s = 200$. From Fig. 5.1 it can be clearly seen that the EKF outperforms the the KF by a high margin. Moreover the PF has superior performance than the EKF. This superior performance of PF is presented more clearly in the next demonstration.

In Fig. 5.2, the performance of the filters are compared in terms of root mean square error (RMSE). The superior performance of EKF over KF is evident from Fig. 5.2. It is also observed that the PF's performance is approximately the same as EKF for small number of particles. However PF outperforms EKF for large number of particles. The rise and fall in the RMSE of KF is due to the selection of random reference AN as explained in section 5.2.1. As the TN moves away from the reference AN, the reference distance increases and the performance of the filter deteriorate and improves again when the TN moves towards the reference

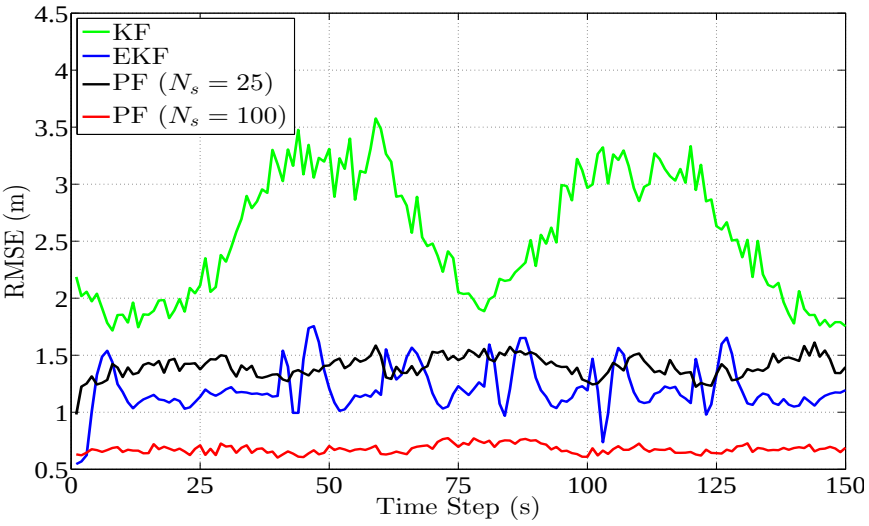

Figure 5.2: RMSE comparison between the KF, EKF and the PF. $\eta = 200$, $N = 8$, $N_s = 100$, $N_{thr} = {}^{N_s}/_4$, $\alpha_{i,t} = 2.5 \forall\, i \wedge t$, $T_s = 1\,\text{sec}$, $\sigma^2_{\breve{w}_{i,t}} = 0.5\,\text{dB} \forall\, i \wedge t$.

AN.

The accuracy of PF is directly proportional to number of particle considered. In Fig. 5.3 the performance of PF is compared for different number of particles. It is observed that the performance of PF improves with higher number of particles.

Fig. 5.4 shows the particle distribution across the network. Initially no prior information about the TN's position is available. Thus the Initial particles are randomly distributed throughout the network at $t = 1$. At $t = 2$ a sudden decrease in number of effective particles is observed. This is because most of the particles at $t = 1$ are given negligible weights due their random and incorrect positions. At $t = 10$ most of the particles have converged at the true position of the TN. A similar behavior is observed at $t = 30$.

5.6.2 Performance Analysis for AoA-RSS Signal Model

A fully connected 2-dimensional network of 150m $\times$ 150m with a single TN, with constant velocity, changing directions and unknown coordinates is considered.

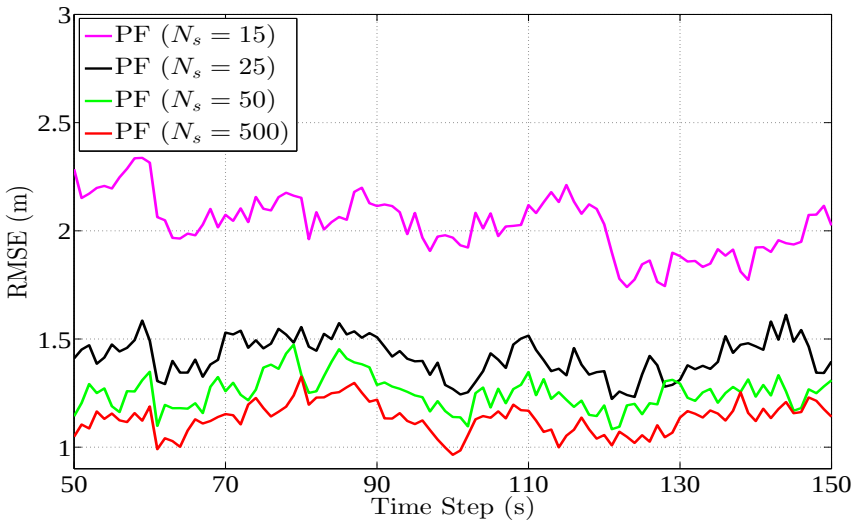

Figure 5.3: RMSE comparison of PF using different number of particles. $\eta = 200$, $N = 8$, $N_s = [15, 25, 50, 500]$, $N_{thr} = {}^{N_s}/_4$, $\alpha_{i,t} = 2.5\,\forall\, i \wedge t$, $T_s = 1\,\text{sec}$, $\sigma^2_{\breve{w}_{i,t}} = 0.5\,\text{dB}\,\forall\, i \wedge t$.

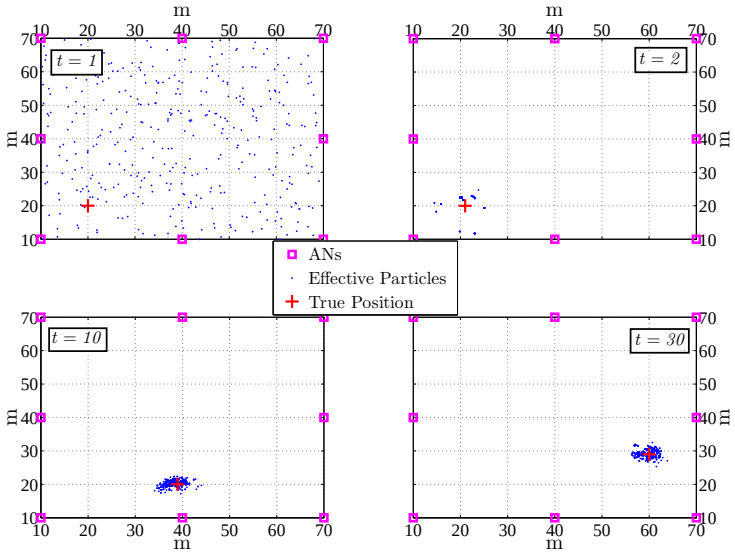

Figure 5.4: Distribution of particles across the network at different time steps. $N = 8$, $N_s = 500$, $N_{thr} = {}^{N_s}/_4$, $\alpha_{i,t} = 2.5\,\forall\, i \wedge t$, $T_s = 1\,\text{sec}$, $\sigma^2_{\breve{w}_{i,t}} = 0.5\,\text{dB}\,\forall\, i \wedge t$.

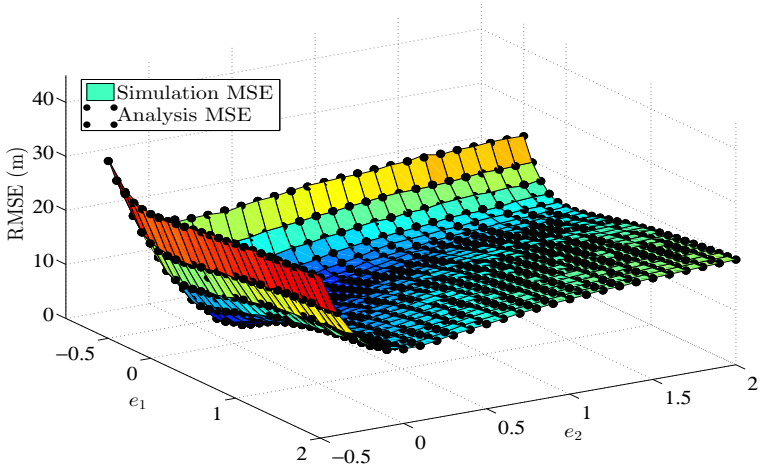

Figure 5.5: Performance comparison between simulation and analytical MSE. ANs $= [0\,0, 0\,50]^T$, $e_i = \check{\alpha}_i - \alpha_i$, $\alpha_1 = 2.5$, $\alpha_2 = 3$, $N = 2$, $\sigma^2_{\check{w}_i} = 1$ dB$\forall\, i$, $\sigma^2_{m_i} = 1^0\, \forall\, i$, $\ell = 500$.

In Fig.5.5, the theoretical RMSE and simulation RMSE of location estimates are compared in a scenario where erroneous PLE values are used. For simplicity only two ANs are considered. Two different values of PLE, i.e., $\alpha_1 = 2.5$ and $\alpha_2 = 3$ are considered for each AN-TN link. The error $e_1 = \check{\alpha}_1 - \alpha_1$ and $e_2 = \check{\alpha}_2 - \alpha_2$ in the PLEs are shown on the x and y axis, while the z coordinates represents the RMSE in location estimate. The shadowing variance is $\sigma^2_{\check{w}_i} = 1$ dB $\forall\, i$ while the error in angle estimates is $\sigma^2_{m_i} = 1^0\, \forall\, i$. The simulation results are averaged over $\epsilon = 500$ independent runs. It is clear from the plot that even a small error in PLEs has a significant impact on localisation accuracy. Futhermore, it is evident from Fig. 5.5 that the theoretical MSE accurately predicts the system performance.

Fig. 5.6 shows the true trajectory of TN's motion and performance comparison of tracking via KF for erroneous PLE values and estimated PLEs. The true values of the PLEs are considered to be changing at every time step and drawn randomly from a uniform distribution, i.e., $\alpha \in \mathcal{U}\,[2\ 5]$. The erroneous PLEs are generated by adding a random noise with a Gaussian distribution of variance σ^2_α

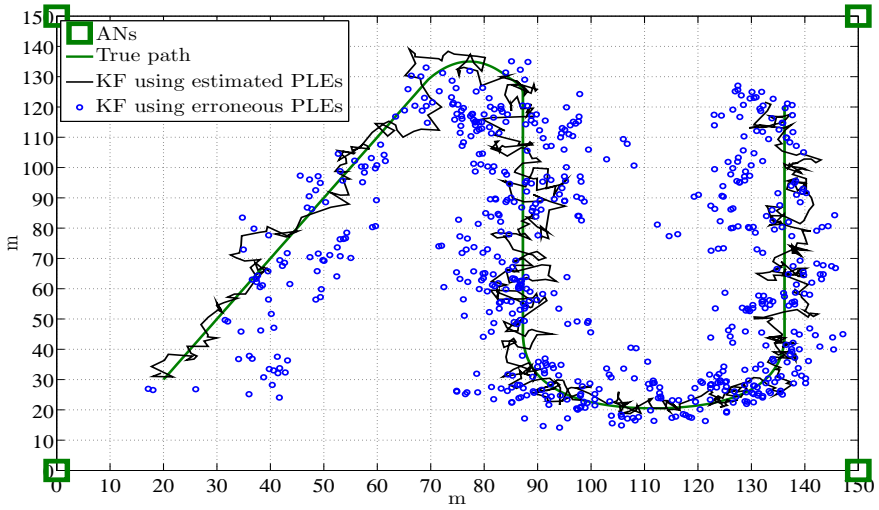

Figure 5.6: Performance comparison of KF using erroneous PLEs and estimated PLEs. $T_s = 1$ sec, $\sigma^2_{m_i} = 5^0 \; \forall \; i$, $\sigma^2_{\breve{w}_i} = 5$ dB $\forall \; i$, $\alpha \in \mathcal{U}\,[2\;5]$, $\sigma^2_\alpha = 0.2$, $\Delta_0 = 0.1$, $v = 10$, $\xi = 2$, $\tau = 3$, $\eta = 1$, $N = 4$.

and mean zero at every time step. However, it is assumed that the realization of the added noise does not change within each time step. For Fig. 5.6, $\sigma^2_\alpha = 0.2$. The estimated angle and the shadowing variance is kept fixed at $\sigma^2_{m_i} = 5^0$ and $\sigma^2_{\breve{w}_i} = 5$ dB $\forall \; i$ respectively. The GenPS algorithm estimates the PLEs before the filtering process at every time step of $T_s = 1$s, the parameters of the GenPS algorithm are given at the bottom of Fig. 5.6. It is evident from the trajectories in Fig. 5.6 that KF with PLE estimation via GenPS performs considerably better than the KF with incorrectly assumed PLEs.

Fig. 5.7 keeps the same parameters as in Fig. 5.6 and compares the RMSE at every time step using KF with an erroneous and estimated PLE vector. The RMSE values are an average over $\eta = 30$ independent runs. A performance improvement of 25%-30% is observed when using estimated PLEs.

Fig. 5.8 shows the true trajectory of the motion of the TN, the estimated trajectory with PF using erroneous PLEs and the trajectory of the PF with estimated PLEs. The estimated angle and the shadowing variance is kept fixed at $\sigma^2_{m_i} = 5^0$

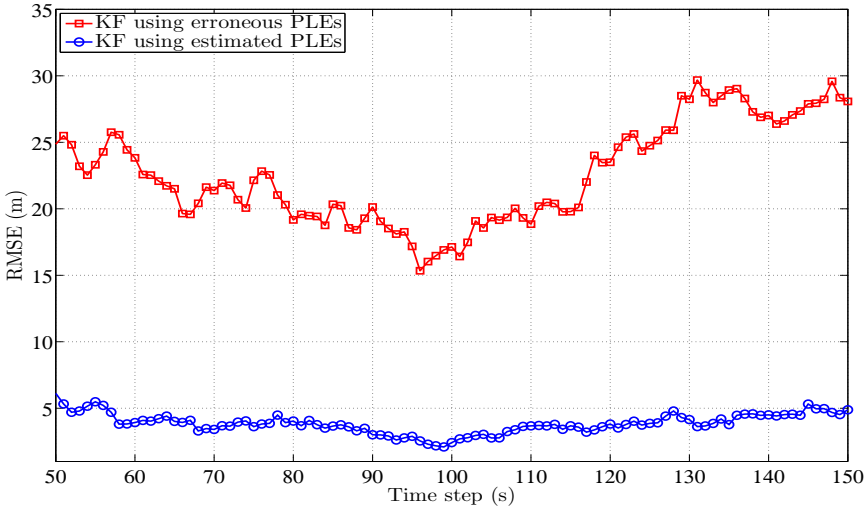

Figure 5.7: RMSE comparison of tracking via KF using estimated and erroneous PLE values. $T_s = 1$ sec, $\sigma^2_{m_i} = 5^0 \; \forall \, i$, $\sigma^2_{\check{w}_i} = 5$ dB $\forall \, i$, $\alpha \in \mathcal{U}\,[2\;5]$, $\sigma^2_{\alpha} = 0.5$, $\Delta_0 = 0.1$, $v = 10$, $\xi = 2$, $\tau = 3$, $\eta = 30$, $N = 4$.

$\forall \, i$ and $\sigma^2_{\check{w}_i} = 5$ dB $\forall \, i$ respectively. Similar to Fig. 5.6 and Fig. 5.7, $\alpha \sim \mathcal{U}\,[2\;5]$ and $\check{\alpha} \sim \mathcal{U}\,[2\;5]$. For the PF, we consider $N_s = 2000$ particles. Following the pattern set by the KF in Fig. 5.6 and 5.7, the PF with PLE estimation exhibits superior performance to the same with erroneous PLEs.

Keeping the parameters the same as in Fig. 5.8, Fig. 5.9 compares the RMSE between of the PF with and without PLE estimation. The simulations are run $\eta = 30$ times. For both cases, two different sets of particles, i.e., $N_s = 1000$ and $N_s = 2000$ are used. It is seen that the performance of PF with incorrect PLEs does not vary with different N_s values, this is because the incorrect PLEs induces such a large error in the observation vector that the PF does not converge even with a large numbers of particles. On the other hand, it is seen that while estimating the PLEs with GenPS, 30%-35% improvement in accuracy is achieved.

Fig. 5.10 compares the performance of both KF and PF using GenPS for PLE estimation. Two different values of the number of particles, i.e., $N_s = 1000$, and 2000 are taken for PF tracking. Also two sets of shadowing variance and

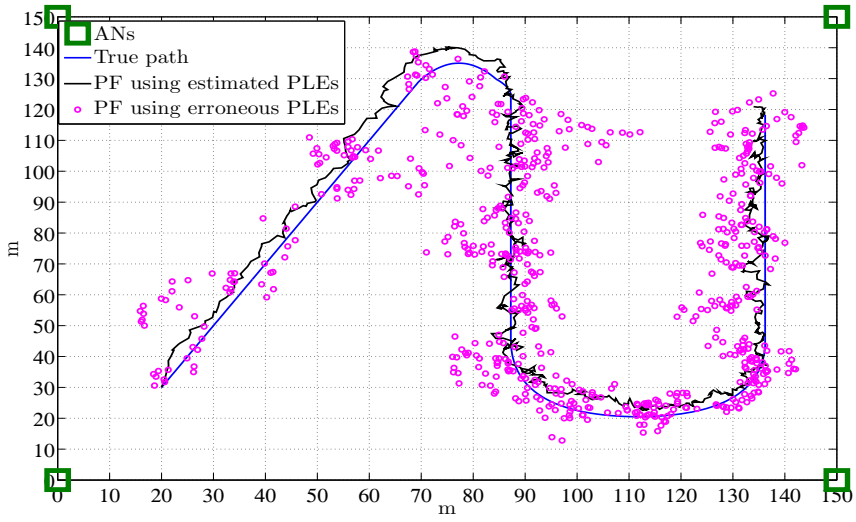

Figure 5.8: Performance comparison of tracking via PF while using erroneous and estimated PLE values. $T_s = 1$ sec, $N_s = 2000$, $N_{thr} = N_s/4$, $\sigma^2_{m_i} = 5^0 \; \forall \, i$, $\sigma^2_{\breve{w}_i} = 5$ dB $\forall \, i$, $\alpha \in \mathcal{U}\,[2\ 5]$, $\sigma^2_{\alpha} = 0.2$, $\Delta_0 = 0.1$, $v = 10$, $\xi = 2$, $\tau = 3$, $\eta = 1$.

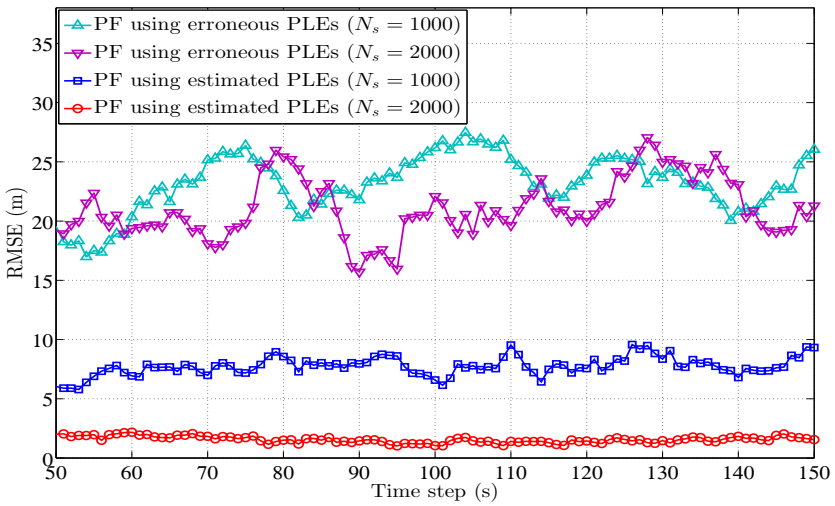

Figure 5.9: RMSE in location estimate utilizing PF, using estimated and erroneous PLE values. $T_s = 1$ sec, $\sigma^2_{m_i} = 5^0 \; \forall \, i$, $\sigma^2_{\breve{w}_i} = 5$ dB $\forall \, i$, $N_{thr} = N_s/10$, $\alpha \in \mathcal{U}\,[2\ 5]$, $\sigma^2_{\alpha} = 0.5$, $\Delta_0 = 0.1$, $v = 10$, $\xi = 2$, $\tau = 3$, $\eta = 30$.

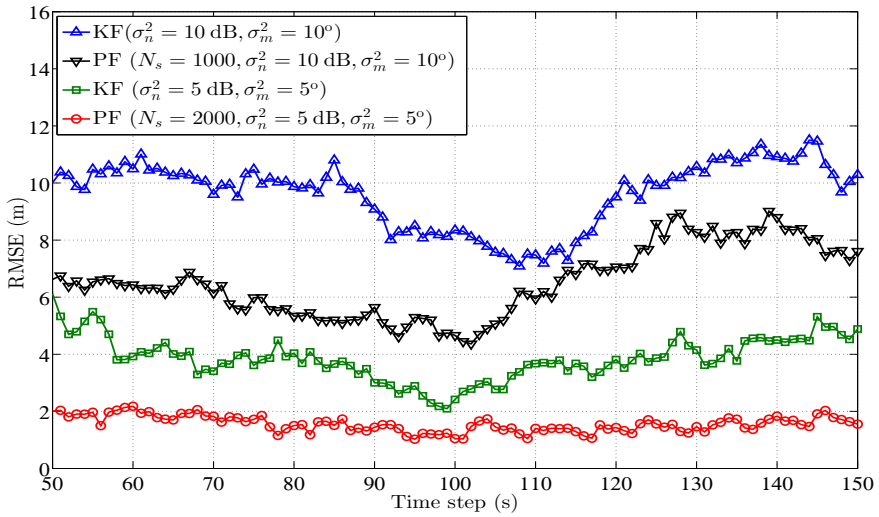

Figure 5.10: Performance comparison between PF and KF using estimated PLE. $T_s = 1$ sec, $N_{thr} = N_s/10$, $\alpha \in \mathcal{U}[2\ 5]$, $\sigma_\alpha^2 = 0.5$ $\Delta_0 = 0.1$, $v = 10$, $\xi = 2$, $\tau = 3$, $\eta = 30$.

angle noise variance, i.e., $\sigma_{\dot{w}_i}^2 = 5\,\text{dB}$, $\sigma_{m_i}^2 = 5^0$ and $\sigma_{\dot{w}_i}^2 = 10\,\text{dB}$, $\sigma_{m_i}^2 = 10^0$ are considered for both KF and PF. In both scenarios the PF performs better than the KF.

5.7 Summary

In this chapter we analysed the performance of some of the most widely used tracking filters to date. These are KF, EKF and PF. Two signal models were under focus, RSS and AoA-RSS. The RSS reading from the ANs are non linear in nature. Thus its linearised version is used for tracking via KF and a Taylor series expansion of the non linear observation model is used for EKF. It is shown that EKF performs considerably better than KF, while the PF outperforms the EKF for RSS signal model. Furthermore throughout literature the PLE vector, which is essential for range estimation via RSS is assumed to be known. To demonstrate the effect of incorrect PLE vector on location coordinates of the

TN, a theoretical MSE expression is derived for AoA-RSS signal model. Then using the GenPS method the PLE vector is estimated at every time step before employing KF, EKF or PF for tracking of wireless node. Similarly for AoA-RSS signal model with estimated PLEs, EKF dominates KF in terms of RMSE performance and PF outperforming EKF.

6 Conclusions and Future Work

6.1 Conclusions

This thesis focused on improving the estimation accuracy of localisation in WSN. A major portion of the thesis covers the utilisation of hybrid signal models with range and bearing measurement. A number of enhanced algorithms based on hybrid signals are proposed. The thesis also focuses on tracking of wireless node, in a network with unknown path-loss characteristics and presents a thorough performance analysis of target tracking via KF, EKF and PF based on the received strength of the signal.

With the increasing demand of accurate positioning system, hybrid signal based localisation is getting considerable attention. Thus, in this thesis a highly celebrated hybrid signal model is studied that is based on the AoA and the ToA of the signal. The hybrid estimator is improved by rendering the model unbiased and improving the estimation accuracy. In order to analyse the LLS estimator's performance utilising the hybrid AoA-ToA signal, a theoretical MSE expression is derived that accurately predicts the system performance. It is observed that the system performance in terms of RMSE is different while using different combinations of ANs. Thus, by designing an optimal AN selection step, called OAS that is based on the theoretical MSE, the combination of ANs that shows minimum

error is chosen for localisation.

Due to different level of noise and different AN-TN separations associated with different links, some ANs are more reliable than other. Thus weights are given to ANs which are directly proportional to the link quality. The covariance matrix stores all the information of signal quality. Hence the noise covariance matrix is first derived and a WLLS-AoA-ToA algorithm is proposed which is more accurate than the LLS estimator.

Finally, in order to lower bound the performance of WLLS-AoA-ToA algorithm, LCRB-AoA-ToA, which is used extensively in literature as a benchmark for system performance, is derived.

The estimation of ToA of the signal requires the nodes to be equipped with synchronised high frequency clocks. Of course this will increase the over all cost of the network. Since the RSS is already available at the receiving node without any additional hardware, it can be utilised to estimate the range, rather than using ToA. Thus another hybrid signal that is based on AoA and RSS of the signal is studied. Following a similar trend as for AoA-ToA signal model, first the theoretical MSE for LLS solution is derived that accurately predicts the LLS performance. This is followed by deriving the noise covariance matrix for AoA-RSS signal model, to be utilised in the WLLS-AoA-RSS algorithm.

Due to bad GDoP and because some TNs may be placed outside the convex hull defined by the ANs, some ANs may actually deteriorate the overall accuracy of estimation. In order to utilise these ANs in an optimum fashion, a two step optimised AN selection algorithm, called TSOAS, is designed. In TSOAS, the whole network is divided into different zones and then for each zone an optimal combination of ANs is selected that has the lowest MSE for that particular zone. This optimal combination is selected on the basis of theoretical MSE. In the

second step, all TNs are localised with their respective optimal combination of ANs which depends on the zone the TN lies in.

The extraction of range from RSS requires the correct knowledge of PLE values associated with each link. In order to consider a more realistic environment, the PLE vector is estimated before localisation, rather than assuming that it is known. This is done with the help of GenPS algorithm, a derivative free optimisation technique. Together with WLLS-AoA-RSS algorithm a more realistic and accurate estimator is obtained. Finally to lower bound the performance of WLLS-AoA-RSS algorithm a LCRB-AoA-RSS is derived.

In large networks a good number of TNs fails to communicate with ANs because of their distant position from the ANs. These out of range TNs are totally dependent on neighbouring TNs to localise themselves. Thus the hybrid schemes are taken one step further and cooperative links are established between the TNs. Three cooperative localisation schemes are proposed *i*) LLS Coop *ii*) low complexity LLS Coop and *iii*) optimised LLS Coop. Significant performance improvement is observed when cooperative links are established between the TNs. But to implement such networks all TNs must be capable of distance and angle estimation. This significantly increase the overall cost of the network. For this reason a low complexity LLS Coop is proposed which eliminates the need for hybrid TNs. Cooperative localisation algorithms are usually computationally more expensive than non cooperative algorithms. In order to analyse the increase in computational load, a complexity analysis is presented between LLS, LLS Coop, low complexity LLS Coop and optimised LLS Coop.

In order to estimate range from RSS, the value of the PLE is required. In order to realise the impact of using incorrect PLE on estimation accuracy, a theoretical MSE expression is derived for LLS while using erroneous PLE values. To make

the scenario more realistic a mobile TN is considered which make the PLE vector change continuously. Then using GenPS, the PLE vector is first estimated, which followed by the tracking of mobile TN using the KF or the PF. A significant improvement is observed in the accuracy when utilising the estimated PLE vector rather than erroneous PLE vector, even if a very small error is added to the true PLE values. This is followed by an extensive performance comparison between KF, EKF and PF based on the RSS of the signal. It is observed that the accuracy of PF is the best subject to high number of particles, followed by the EKF and followed by the KF. It is also observed that for small number of particles (around 25-50), the performance of PF is similar to the EKF.

6.2 Future Work

Although localisation of wireless nodes has been a well studied subject, there still remains room for further research. Some current trends and topics for future research are highlighted below.

Divergence due to bad GDOP

It is observed that the performance of a positioning system deteriorate significantly when the TNs are outside the convex hull defined by the ANs. Optimisation methods such as Gauss-Newton fails to converge in these scenarios while LLS based algorithm shows an unacceptable accuracy. This problem can be addressed with other optimisation methods like genetic algorithms (GA), simulated annealing (SA), Markov chain Monte-Carlo (MCMC) and GenPS. Further studies are required for the efficiency of these methods for location of nodes outside the convex hull.

Multiple TN Localisation and Tracking

Tracking of a mobile wireless node has been studied extensively in literature. However tracking of multiple nodes is a fairly new area of research. Some recent studies propose multiple objects tracking that are based on video captured from a stationary camera. This require significant image processing. However Multiple node tracking using RF signals is an open area of research.

Optimum AN positioning for a moving TN

The optimum AN selection presented in this thesis is highly dependent on the GDOP of AN and TN. If a TN is moving then the GDOP will change continuously. Thus a particular AN can perform optimally at one instance but not at other instance due the motion of TN. An algorithm can be developed based on the motion of ANs in which the ANs can change their position according to the positions of TNs.

Hybrid RSS-ToA

We already have RSS information available in a ToA based localisation system. Thus in order to improve performance both measurement can be utilised simultaneously. Very little work has been done on this issue. Both RSS based and ToA based systems perform differently in different scenario for example ToA based system are found to be more accurate than RSS based system at higher inter node distances while RSS based localisation systems are preferred at small inter node distances. Thus one can be used instead of the other depending upon the nature of the network. Or perhaps some weighting strategy can be devised to give different weights to RSS and ToA measurement based on their performance in a

particular network.

Additive and Multiplicative Noise

Two types of noise models for distance estimate (for ToA) are available in literature. The additive noise model which is independent of the actual distance between the nodes and the multiplicative noise model which is distance dependent. Extensive range estimates on real time systems are required to obtain conclusive results on the type of noise model that best fits the range estimates [95].

7 Appendices

This section presents the derivations of all the mathematical expressions discussed in this thesis. These include: The derivations of all the expectation taken in table. 2.1, derivation of covariance matrix for AoA-ToA signal model, derivation of covariance matrix for AoA-RSS signal model, Derivation of FIM for AoA-ToA and AoA-RSS signal model and derivation of covariance matrix for AoA-RSS signal model with incorrect PLE assumption.

Appendix I

This appendix presents the derivation of all the expectations taken in table. 2.1.

Let τ be a Gaussian random variable with zero mean and σ_τ^2 variance i.e. $\tau \sim \mathcal{N}\left(0, \sigma_\tau^2\right)$, also a and b are assumed to be constants.

- $E_\tau\left(\cos\tau\right) = \exp\left(-\frac{\sigma_\tau^2}{2}\right)$

$E_\tau\left(\cos\tau\right)$ can be written in the form of its infinite series as

$$E_\tau\Big[\cos\tau\Big]=1-E_\tau\left[\frac{\tau^2}{2!}\right]+E_\tau\left[\frac{\tau^4}{4!}\right]-E_\tau\left[\frac{\tau^6}{6!}\right]+\cdots, \tag{7.1}$$

where (7.1) is Maclaurin series expansion of the cos function. Taking the expectation of individual terms.

$$E_\tau\Big[\cos\tau\Big] = 1 - \frac{\sigma_\tau^2}{2} + \frac{\sigma_\tau^4}{8} - \frac{\sigma_\tau^6}{48} + \cdots \tag{7.2}$$

Equation (7.2) is power series expansion of $\exp\left(-\frac{\sigma_\tau^2}{2}\right)$. Thus,

$$E_\tau\Big[\cos\tau\Big] = \exp\left(-\frac{\sigma_\tau^2}{2}\right). \tag{7.3}$$

- $E_\tau\left[\cos 2\tau\right] = \exp\left(-2\sigma_\tau^2\right)$

Expanding $E_\tau\left[\cos 2\tau\right]$ with Maclaurin series

$$E_\tau\left[\cos 2\tau\right] = 1 - E_\tau\left[\frac{(2\tau)^2}{2!}\right] + E_\tau\left[\frac{(2\tau)^4}{4!}\right] - E_\tau\left[\frac{(2\tau)^6}{6!}\right] + \cdots$$

$$E_\tau\left[\cos 2\tau\right] = 1 - E_\tau\left[\frac{4\tau^2}{2}\right] + E_\tau\left[\frac{16\tau^4}{24}\right] - E_\tau\left[\frac{64\tau^6}{720}\right] + \cdots$$

$$E_\tau\left[\cos 2\tau\right] = 1 - 2E_\tau\Big[\tau^2\Big] + \frac{2}{3}E_\tau\Big[\tau^4\Big] - \frac{4}{45}E_\tau\Big[\tau^6\Big] + \cdots. \tag{7.4}$$

The second, fourth and sixth moment of a Gaussain random variable, τ , is given

by σ_τ^2, $3\sigma_\tau^4$ and $15\sigma_\tau^6$, respectively. Putting in (7.4) we get,

$$E_\tau\left[\cos 2\tau\right] = 1 - 2\sigma^2 + \frac{2}{3}\left(3\sigma^4\right) - \frac{4}{45}\left(15\sigma^6\right) + \cdots$$

$$E_\tau\left[\cos 2\tau\right] = 1 - 2\sigma^2 + 2\sigma^4 - \frac{4}{3}15\sigma^6 + \cdots. \tag{7.5}$$

Equation (7.5) is power series expansion of $\exp\left(-2\sigma_\tau^2\right)$. Thus,

$$E_\tau\left[\cos 2\tau\right] = \exp\left(-2\sigma_\tau^2\right). \tag{7.6}$$

- $E_\tau\Big[\sin\tau\Big] = 0$

$E_\tau\Big[\sin\tau\Big]$ can be written in the form of its infinite series as

$$E_\tau\Big[\sin\tau\Big] = E_\tau\left[\tau - \frac{\tau^3}{3!} + \frac{\tau^5}{5!} - \frac{\tau^7}{7!} + \cdots\right] \tag{7.7}$$

since all odd moments of a Gaussian random variable are zero, thus

$$E_{m_i}\Big[\sin m_i\Big] = 0. \tag{7.8}$$

- $E_\tau\Big[\sin 2\tau\Big] = 0$

$E_\tau\Big[\sin 2\tau\Big]$ can be written in the form of its infinite series as

$$E_\tau\Big[\sin 2\tau\Big] = E_\tau\left[2\tau - \frac{8\tau^3}{3!} + \frac{32\tau^5}{5!} - \frac{128\tau^7}{7!} + \cdots\right]$$

Since all odd moments of a Gaussian random variable are zero, thus

$$E_\tau\Big[\sin 2\tau\Big] = 0. \tag{7.9}$$

- $E_\tau\left[\exp\left(\frac{\tau}{ab}\right)\right] = \exp\left(\frac{\sigma_\tau^2}{2(ab)^2}\right)$

Mathematically the expectation can be presented as

$$E_\tau\Big[\exp\left(\frac{\tau}{ab}\right)\Big] = \int_{-\infty}^{\infty} \exp\left(\frac{\tau}{ab}\right) \frac{1}{\sigma_\tau^2\sqrt{2\pi}} \exp\left(-\frac{\tau^2}{2\sigma_\tau^2}\right) d\tau.$$

$$= \int_{-\infty}^{\infty} \frac{1}{\sigma_\tau^2\sqrt{2\pi}} \exp\left(-\frac{\tau^2 - \frac{\tau}{ab}\left(2\sigma_\tau^2\right)}{2\sigma_\tau^2}\right) d\tau.$$

By completing squares,

$$E_{w_i}\left[\exp\left(\frac{\tau}{ab}\right)\right] = \int_{-\infty}^{\infty} \frac{1}{\sigma_\tau^2\sqrt{2\pi}} \exp\left(-\frac{\tau^2 - \frac{\tau}{ab}\left(2\sigma_\tau^2\right) + \left(\frac{\sigma_\tau^2}{(ab)}\right)^2}{2\sigma_\tau^2}\right) \exp\left\{\frac{1}{2\sigma_\tau^2}\left(\frac{\sigma_\tau^2}{(ab)}\right)^2\right\} d\tau,$$

or

$$E_\tau\left[\exp\left(\frac{\tau}{ab}\right)\right] = \int_{-\infty}^{\infty} \frac{1}{\sigma_\tau^2\sqrt{2\pi}} \exp\left(-\frac{\left(\tau - \frac{\sigma_\tau^2}{(ab)}\right)^2}{2\sigma_\tau^2}\right) \exp\left(\frac{\sigma_\tau^2}{2\left(ab\right)^2}\right) d\tau. \tag{7.10}$$

The first portion of (7.10) (in red) is the probability density function whose integral is equal to 1, hence we conclude

$$E_\tau\left[\exp\left(\frac{\tau}{ab}\right)\right] = \exp\left(\frac{\sigma_\tau^2}{2\left(ab\right)^2}\right). \tag{7.11}$$

Appendix II-A: Derivation Of Covariance Matrix For AoA-ToA Signal

This appendix presents the covariance matrix derivation.

Derivation of Equation (2.51). From (2.50), we have $\mathbf{C}_{\mathrm{AT}}^{x} = E\left[\left(\hat{\mathbf{t}}_x - \mathbf{t}_x\right)\left(\hat{\mathbf{t}}_x - \mathbf{t}_x\right)^T\right]$, putting the value of $\hat{\mathbf{t}}_x$ and $\mathbf{t}_x$ for $i = j$, we get

$$\mathbf{C}^{x}_{\mathrm{AT}_{ii}} = E_{m_i,n_i}\left[\left(\Big(d_{T,i}+n_i\Big)\cos\Big(\theta_i+m_i\Big)\delta_{T,i}-d_{T,i}\cos\theta_i\right)^2\right]$$

$$\begin{aligned}\mathbf{C}^{x}_{\mathrm{AT}_{ii}} = E_{m_i,n_i}\Bigg[\Bigg(\Big(d_{T,i}+n_i\Big)^2\cos^2\Big(\theta_i+m_i\Big)\Bigg)\delta^2_{T,i}+\Big(d_{T,i}\cos\theta_i\Big)^2\\ -2\delta_{T,i}\Big(d_{T,i}\cos\theta_i\Big)\Big(d_{T,i}+n_i\Big)\cos\Big(\theta_i+m_i\Big)\Bigg]\end{aligned} \tag{7.12}$$

$$\begin{aligned}\mathbf{C}^{x}_{\mathrm{AT}_{ii}} = E_{m_i,n_i}\Bigg[\Big(d^2_{T,i}+n_i^2+2d_{T,i}n_i\Big)\Big(0.5+0.5\Big(\cos 2\theta_i\cos 2m_i\\ -\sin 2\theta_i\sin 2m_i\Big)\Big)\delta^2_{T,i}+\Big(d_{T,i}\cos\theta_i\Big)^2-2\delta_{T,i}\Big(d^2_{T,i}+d_{T,i}n_i\Big)\\ \Big(\cos^2\theta_i\cos m_i-\cos\theta_i\sin\theta_i\sin m_i\Big)\Bigg]\end{aligned} \tag{7.13}$$

(7.13) is obtained from (7.12) by using the identity $\cos^2(a) = 0.5 + 0.5\cos(2a)$. Also using the expectations (7.8) and (7.9), (7.14) is obtained.

$$\begin{aligned}\mathbf{C}^{x}_{\mathrm{AT}_{ii}} =&\Bigg[\Big(\frac{d^2_{T,i}}{2}\Big)+\Big(\frac{d^2_{T,i}}{2}\Big)\cos 2\theta_i E_{m_i}\Big(\cos 2m_i\Big)+E_{n_i}\left(\frac{n_i^2}{2}\right)+E_{n_i}\left(\frac{n_i^2}{2}\right)\\ &E_{m_i}\Big(\cos 2m_i\Big)\Bigg]\delta^2_{T,i}+\Big(d_{T,i}\cos\theta_i\Big)^2-2\delta_{T,i}\Big(d_{T,i}\cos\theta_i\Big)^2E_{m_i}\Big(\cos m_i\Big).\end{aligned} \tag{7.14}$$

Finally by using (7.3) and (7.6), we conclude the proof by obtaining (2.51).

For non-diagonal terms of $\mathbf{C}^{x}_{\mathrm{AT}} = E\left[\left(\hat{\mathbf{t}}_x-\mathbf{t}_x\right)\left(\hat{\mathbf{t}}_x-\mathbf{t}_x\right)^T\right]$, i.e. $i \neq j$, putting the

value of $\hat{\mathbf{t}}_x$ and $\mathbf{t}_x$ we get

$$\mathbf{C}^x_{\mathrm{AT}_{ij}} = E_{m_{ij},n_{ij}}\Bigg[\bigg(\Big(d_{T,j}+n_i\Big)\cos\Big(\theta_i+m_i\Big)\delta_{T,i}-d_{Ti}\cos\theta_i\bigg) \times\bigg(\Big(d_{T,j}+n_j\Big)\cos\Big(\theta_j+m_j\Big)\delta_{T,j}-d_{T,j}\cos\theta_j\bigg)\Bigg]$$

$$\begin{aligned}\mathbf{C}^x_{\mathrm{AT}_{ij}} = E_{m_{ij},n_{ij}}\Bigg[&\Big(\Big(d_{T,i}d_{T,j}+d_{T,i}n_j+d_{T,j}n_i+n_in_j\Big)\Big(\cos\theta_i\cos m_i+\sin\theta_i\sin m_i\Big)\\ &\Big(\cos\theta_j\cos m_j+\sin\theta_j\sin m_j\Big)\delta_{T,ij}\Big)\Big(\Big(d_{T,i}d_{T,j}+d_{T,j}n_i\Big)\Big(\cos\theta_i\cos\theta_j\\ &\cos m_i+\sin\theta_i\cos\theta_j\sin m_i\Big)\delta_{T,i}\Big)-\Big(\Big(d_{T,i}d_{T,j}+d_{T,i}n_j\Big)\Big(\cos\theta_i\cos\theta_j\\ &\cos m_j+\sin\theta_i\cos\theta_j\sin m_j\Big)\delta_{T,j}\Big)+d_{T,i}d_{T,j}\cos\theta_i\cos\theta_j\Bigg],\end{aligned}\tag{7.15}$$

where $\delta_{T,ij}=\delta_{T,i}\delta_{T,j}$. Taking expectations in (7.15), we obtain

$$\begin{aligned}\mathbf{C}^x_{\mathrm{AT}_{ij}} =&d_{T,i}d_{T,j}\cos\theta_i\cos\theta_j-d_{T,i}d_{T,j}\cos\theta_i\cos\theta_j\\ &-d_{T,i}d_{T,j}\cos\theta_i\cos\theta_j+d_{T,i}d_{T,j}\cos\theta_i\cos\theta_j\\ =&0.\end{aligned}$$

The derivation of $\mathbf{C}^y_{\mathrm{AT}}$ is similar to $\mathbf{C}^x_{\mathrm{AT}}$ other than that x coordinates are replaced by y i.e cos function is replaced by sin .

Derivation of Equation (2.53). From (2.50), we have $\mathbf{C}^{xy}_{\mathrm{AT}} = E\Big[\Big(\hat{\mathbf{t}}_x-\mathbf{t}_x\Big)\Big(\hat{\mathbf{t}}_y-\mathbf{t}_y\Big)^T\Big]$, putting the value of $\hat{\mathbf{t}}_x$, $\mathbf{t}_x$, $\hat{\mathbf{t}}_y$ and $\mathbf{t}_y$ for $i=j$, we get

$$\mathbf{C}^{xy}_{\mathrm{AT}_{ii}} = E_{m_i,n_i}\Bigg[\bigg(\Big(d_{T,i}+n_i\Big)\cos\Big(\theta_i+m_i\Big)\delta_{T,i} - d_{T,i}\cos\theta_i\bigg) \times \bigg(\Big(d_{T,i}+n_i\Big)\sin\Big(\theta_i+m_i\Big)\delta_{T,i} - d_{T,i}\sin\theta_i\bigg)\Bigg]$$

$$\mathbf{C}^{xy}_{\mathrm{AT}_{ii}} = E_{m_i,n_i}\Bigg[\bigg(\Big(d_{T,i}+n_i\Big)^2\cos\Big(\theta_i+m_i\Big)\sin\Big(\theta_i+m_i\Big)\bigg)\delta^2_{T,i} - \bigg(d_{T,i}\Big(d_{T,i}+n_i\Big)\cos\Big(\theta_i+m_i\Big)\sin\theta_i\bigg)\delta_{T,i} - \bigg(d_{T,i}\Big(d_{T,i}+n_i\Big)\sin\Big(\theta_i+m_i\Big)\cos\theta_i\bigg)\delta_{T,i} + d^2_{T,i}\cos\theta_i\sin\theta_i\Bigg]. \tag{7.16}$$

Using the identities $\cos(a+b) = \cos(a)\cos(b) - \sin(a)\sin(b)$, $\sin(a+b) = \sin(a)\cos(b)+\cos(a)\sin(b)$, $\cos^2 a - \sin^2 a = \cos 2a$ and then taking expectation, (7.8), (7.16) is obtained.

$$\mathbf{C}^{xy}_{\mathrm{AT}_{ii}} = \bigg(\Big(d^2_{T,i} + E_{n_i}\Big[n_i^2\Big]\Big)\cos\theta_i\sin\theta_i E_{m_i}\Big[\cos 2m_i\Big]\bigg)\delta^2_{T,i} - \bigg(d^2_{T,i}\cos\theta_i E_{m_i}\Big[\cos m_i\Big]\sin\theta_i\bigg)\delta_{T,i} - \bigg(d^2_{T,i}\sin\theta_i E_{m_i}\Big[\cos m_i\Big]\cos\theta_i\bigg)\delta_{T,i} + d^2_{T,i}\cos\theta_i\sin\theta_i$$

Finally, using expectation (7.3) and (7.6) we conclude the proof by obtaining (2.53).

For non-diagonal terms of $\mathbf{C}^{xy}_{\mathrm{AT}} = E\left[\left(\hat{\mathbf{t}}_x - \mathbf{t}_x\right)\left(\hat{\mathbf{t}}_y - \mathbf{t}_y\right)^T\right]$, putting the value of $\hat{\mathbf{t}}_x$, $\mathbf{t}_x$, $\hat{\mathbf{t}}_y$ and $\mathbf{t}_y$ for $i \neq j$.

$$\mathbf{C}^{xy}_{\mathrm{AT}_{ij}} = E_{m_{ij},n_{ij}}\Bigg[\bigg(\Big(d_{T,i}+n_i\Big)\cos\Big(\theta_i+m_i\Big)\delta_{T,i} - d_{T,i}\cos\theta_i\bigg) \times\bigg(\Big(d_{T,j}+n_j\Big)\sin\Big(\theta_j+m_j\Big)\delta_{T,j} - d_{T,j}\sin\theta_j\bigg)\Bigg]$$

$$\begin{aligned}\mathbf{C}^{xy}_{\mathrm{AT}_{ij}} = E_{m_{ij},n_{ij}}\Bigg[\bigg(\Big(d_{T,i}d_{T,j}+d_{T,i}n_j+d_{T,j}n_i+n_in_j\Big)\Big(\cos\theta_i\cos m_i-\sin\theta_i\sin m_i\Big)\\ \Big(\sin\theta_j\cos m_j+\cos\theta_j\sin m_j\Big)\delta_{T,ij}\bigg)-\bigg(\Big(d_{T,i}d_{T,j}+d_{T,j}n_i\Big)\\ \Big(\cos\theta_i\sin\theta_j\cos m_i+\sin\theta_i\sin\theta_j\sin m_i\Big)\delta_{T,i}\bigg)-\bigg(\Big(d_{T,i}d_{T,j}+d_{T,i}n_j\Big)\\ \Big(\cos\theta_i\sin\theta_j\cos m_j+\cos\theta_i\cos\theta_j\sin m_j\Big)\delta_{T,j}\bigg)+d_{T,i}d_{T,j}\cos\theta_i\sin\theta_j\Bigg].\end{aligned} \tag{7.17}$$

Taking expectations in (7.17), weget

$$\begin{aligned}\mathbf{C}^{xy}_{\mathrm{AT}_{ij}} =& d_{T,i}d_{T,j}\cos\theta_i\sin\theta_j - d_{T,i}d_{T,j}\cos\theta_i\sin\theta_j\\ &- d_{T,i}d_{T,j}\cos\theta_i\sin\theta_j + d_{T,i}d_{T,j}\cos\theta_i\sin\theta_j\\ =& 0.\end{aligned}$$

Appendix II-B: Derivation Of FIM For AoA-ToA Signal

This appendix presents the derivation of elements of F.I.M. for AoA-ToA signal model.

Taking derivative of (2.51), (2.52) and (2.53) w.r.t x i.e.

$$\frac{\partial \mathbf{C}_{\mathrm{AT}}^{x}}{\partial x} = \left[\frac{\partial}{\partial x}\left(\frac{d_{T,i}^{2}}{2}\right)+\frac{\partial}{\partial x}\left(\frac{\sigma_{n_i}^{2}}{2}\right)\right]\exp\left(\sigma_{m_i}^{2}\right)+\left[\frac{\partial}{\partial x}\left(\frac{d_{T,i}^{2}}{2}\cos 2\theta_i\right)+\frac{\partial}{\partial x}\left(\frac{\sigma_{n_i}^{2}}{2}\cos 2\theta_i\right)\right] \times \exp\left(-\sigma_{m_i}^{2}\right)-\frac{\partial}{\partial x}\left[\left(d_{T,i}\cos\theta_i\right)^{2}\right] \tag{7.18}$$

$$\frac{\partial \mathbf{C}_{\mathrm{AT}}^{y}}{\partial x} = \left[\frac{\partial}{\partial x}\left(\frac{d_{T,i}^{2}}{2}\right)+\frac{\partial}{\partial x}\left(\frac{\sigma_{n_i}^{2}}{2}\right)\right]\exp\left(\sigma_{m_i}^{2}\right)-\left[\frac{\partial}{\partial x}\left(\frac{d_{T,i}^{2}}{2}\cos 2\theta_i\right)+\frac{\partial}{\partial x}\left(\frac{\sigma_{n_i}^{2}}{2}\cos 2\theta_i\right)\right] \times \exp\left(-\sigma_{m_i}^{2}\right)-\frac{\partial}{\partial x}\left(d_{T,i}\sin\theta_i\right)^{2}, \tag{7.19}$$

$$\frac{\partial \mathbf{C}_{\mathrm{AT}}^{xy}}{\partial x} = \frac{\partial}{\partial x}\left(d_{T,i}^{2}\cos\theta_i\sin\theta_i\right)\left[\exp\left(-\sigma_{m_i}^{2}\right)-1\right]+\frac{\partial}{\partial x}\left(\cos\theta_i\sin\theta_i\right)\left[\sigma_{n_i}^{2}\exp\left(-\sigma_{m_i}^{2}\right)\right]. \tag{7.20}$$

The derivates in (7.18), (7.19) and (7.20) are given below

1. $$\begin{aligned}\frac{\partial}{\partial x}\left(\frac{d_{T,i}^2}{2}\right) =& \frac{1}{2}\frac{\partial\left(d_{T,i}^2\right)}{\partial x}\\ =& \frac{1}{2}\left(\frac{\partial}{\partial x}\left(x-\bar{x}_i\right)^2+\cancelto{0}{\frac{\partial}{\partial x}\left(y-\bar{y}_i\right)^2}\right)\\ =& \frac{1}{2}\left(2\left(x-\bar{x}_i\right)\frac{\partial}{\partial x}\left(x-\bar{x}_i\right)\right)\\ =& \left(x-\bar{x}_i\right)\end{aligned}$$

$$\boxed{\frac{\partial}{\partial x}\left(\frac{d_{T,i}^2}{2}\right) = \left(x-\bar{x}_i\right)}$$

2. $$\begin{aligned}\frac{\partial}{\partial x}\left(\frac{d_{T,i}^2}{2}\cos 2\theta_i\right) =& \frac{d_{T,i}^2}{2}\frac{\partial}{\partial x}\cos 2\theta_i+\cos 2\theta_i\frac{\partial}{\partial x}\frac{d_{T,i}^2}{2}\\ =& -\frac{d_{T,i}^2}{2}\sin 2\theta_i\frac{\partial}{\partial x}\left(2\theta_i\right)+\cos 2\theta_i\Big(x-\bar{x}_i\Big)\\ =& -\frac{d_{T,i}^2}{2}\sin 2\theta_i 2\frac{\partial}{\partial x}\arctan\left(\frac{y-\bar{y}_i}{x-\bar{x}_i}\right)+\cos 2\theta_i\Big(x-\bar{x}_i\Big) \qquad (7.21)\\ =& -d_{T,i}^2\sin 2\theta_i\left(\frac{1}{1+\left(\frac{y-\bar{y}_i}{x-\bar{x}_i}\right)^2}\right)\frac{\partial}{\partial x}\left(\frac{y-\bar{y}_i}{x-\bar{x}_i}\right)+\cos 2\theta_i\Big(x-\bar{x}_i\Big)\end{aligned}$$

(7.22)

where (7.22) is obtained from (7.21) by using the derivative of inverse tangent function i.e. $\frac{\partial}{\partial x}\arctan f\left(x\right)=\frac{1}{1+f(x)^2}\frac{\partial}{\partial x}f\left(x\right)$.

$$\begin{aligned}\frac{\partial}{\partial x}\left(\frac{d_{T,i}^2}{2}\cos 2\theta_i\right) =& -d_{T,i}^2\sin 2\theta_i\frac{\left(x-\bar{x}_i\right)^2}{\left(x-\bar{x}_i\right)^2+\left(y-\bar{y}_i\right)^2}\left(-\frac{y-\bar{y}_i}{\left(x-\bar{x}_i\right)^2}\right)+\cos 2\theta_i\Big(x-\bar{x}_i\Big)\\ =& \left(y-\bar{y}_i\right)\sin\left(2\theta_i\right)+\cos\Big(2\theta_i\Big)\Big(x-\bar{x}_i\Big)\end{aligned}$$

$$\frac{\partial}{\partial x}\left(\frac{d_{T,i}^2}{2}\cos 2\theta_i\right) = (y-\bar{y}_i)\sin(2\theta_i) + \cos\left(2\theta_i\right)\left(x-\bar{x}_i\right)$$

3. $$\begin{aligned}
\frac{\partial}{\partial x}\left(\frac{\sigma_{n_i}^2}{2}\cos 2\theta_i\right) &= \frac{\sigma_{n_i}^2}{2}\frac{\partial}{\partial x}\cos\left(2\theta_i\right) \\
&= -\frac{\sigma_{n_i}^2}{2}\sin 2\theta_i \frac{\partial}{\partial x}(2\theta_i) \\
&= -\sigma_{n_i}^2 \sin 2\theta_i \frac{\partial}{\partial x}\arctan\left(\frac{y-\bar{y}_i}{x-\bar{x}_i}\right) \\
&= -\sigma_{n_i}^2 \sin 2\theta_i \left(\frac{1}{1+\left(\frac{y-\bar{y}_i}{x-\bar{x}_i}\right)^2}\right)\frac{\partial}{\partial x}\left(\frac{y-\bar{y}_i}{x-\bar{x}_i}\right) \\
&= -\sigma_{n_i}^2 \sin 2\theta_i \left(\frac{(x-\bar{x}_i)^2}{(x-\bar{x}_i)^2+(y-\bar{y}_i)^2}\right)\left(-\frac{(y-\bar{y}_i)}{(x-\bar{x}_i)^2}\right) \\
&= \sigma_{n_i}^2 \sin\left(2\theta_i\right)\frac{(y-\bar{y}_i)}{d_{T,i}^2}.
\end{aligned}$$

$$\frac{\partial}{\partial x}\left(\frac{\sigma_{n_i}^2}{2}\cos 2\theta_i\right) = \sigma_{n_i}^2 \sin\left(2\theta_i\right)\frac{(y-\bar{y}_i)}{d_{T,i}^2}$$

4. $$\begin{aligned}
\frac{\partial}{\partial x}\left(d_{T,i}\cos\theta_i\right)^2 =& \frac{\partial}{\partial x}\left(d_{T,i}\left(\frac{1}{2}+\frac{1}{2}\cos 2\theta_i\right)\right)\\
=& \frac{\partial}{\partial x}\left(\frac{d_{T,i}^2}{2}\right)+\frac{\partial}{\partial x}\left(\frac{d_{T,i}^2}{2}\cos 2\theta_i\right)\\
=& \frac{\partial}{\partial x}\left(\frac{d_{T,i}^2}{2}\right)+\left(\frac{d_{T,i}^2}{2}\frac{\partial}{\partial x}\cos 2\theta_i+\cos 2\theta_i\frac{\partial}{\partial x}\frac{d_{T,i}^2}{2}\right)\\
=& \Big(x-\bar{x}_i\Big)+\sin 2\theta_i\Big(y-\bar{y}_i\Big)+\cos 2\theta_i\Big(x-\bar{x}_i\Big)\\
=& \Big(x-\bar{x}_i\Big)\left(1+\cos 2\theta_i+\sin 2\theta_i\frac{\Big(y-\bar{y}_i\Big)}{\Big(x-\bar{x}_i\Big)}\right)\\
=& \Big(x-\bar{x}_i\Big)\left(1+\cos 2\theta_i+\sin 2\theta_i\tan\theta_i\right)\\
=& \Big(x-\bar{x}_i\Big)\left(1+\Big(\cos^2\theta_i-\sin^2\theta_i\Big)+2\sin\theta_i\cos\theta_i\frac{\sin\theta_i}{\cos\theta_i}\right)\\
=& \Big(x-\bar{x}_i\Big)\Big(\cos^2\theta_i+\cos^2\theta_i+2\sin^2\theta_i\Big)\\
=& 2\Big(x-\bar{x}_i\Big).
\end{aligned}$$

$$\boxed{\frac{\partial}{\partial x}\left(d_{T,i}\cos\theta_i\right)^2 = 2\Big(x-\bar{x}_i\Big)}$$

5. $\dfrac{\partial}{\partial x}\left(d_{T,i}^2 \cos\theta_i \sin\theta_i\right)$

$$
\begin{aligned}
&= d_{T,i}^2 \cos\theta_i \frac{\partial}{\partial x}\sin\theta_i + \sin\theta_i \frac{\partial}{\partial x} d_{T,i}^2 \cos\theta_i \\
&= -\, d_{T,i}^2 \cos^2\theta_i \left(\frac{y-\bar{y}_i}{d_{T,i}^2}\right) + \sin\theta_i \left(d_{T,i}^2 \frac{\partial}{\partial x}\cos\theta_i + \cos\theta_i \frac{\partial}{\partial x} d_{T,i}^2\right) \\
&= -\cos^2\theta_i\,(y-\bar{y}_i) + \sin\theta_i \left(d_{T,i}^2 \sin\theta_i \left(\frac{y-\bar{y}_i}{d_{T,i}^2}\right) + 2\cos\theta_i\,(x-\bar{x}_i)\right) \\
&= -\cos^2\theta_i\,(y-\bar{y}_i) + \sin^2\theta_i\,(y-\bar{y}_i) + 2\cos\theta_i \sin\theta_i\,(x-\bar{x}_i) \\
&= (y-\bar{y}_i)\left(-\cos^2\theta_i + \sin^2\theta_i + 2\cos\theta_i \sin\theta_i \cot\theta_i\right) \\
&= (y-\bar{y}_i)\left(-\cos^2\theta_i + \sin^2\theta_i + 2\cos\theta_i \sin\theta_i \frac{\cos\theta_i}{\sin\theta_i}\right) \\
&= (y-\bar{y}_i)\left(-\cos^2\theta_i + \sin^2\theta_i + 2\cos^2\theta_i\right) \\
&= (y-\bar{y}_i)\left(\sin^2\theta_i + \cos^2\theta_i\right) \\
&= (y-\bar{y}_i)
\end{aligned}
$$

$$\boxed{\frac{\partial}{\partial x}\left(d_{T,i}^2 \cos\theta_i \sin\theta_i\right) = (y-\bar{y}_i)}$$

6. $\dfrac{\partial}{\partial x}\left(\cos\theta_i \sin\theta_i\right)$

$$
\begin{aligned}
&= \cos\theta_i \frac{\partial}{\partial x}\sin\theta_i + \sin\theta_i \frac{\partial}{\partial x}\cos\theta_i \\
&= \cos^2\theta_i \frac{\partial}{\partial x}\theta_i - \sin^2\theta_i \frac{\partial}{\partial x}\theta_i \\
&= -\cos^2\theta_i \frac{\left(y-\bar{y}_i\right)}{d_{T,i}^2} + \sin^2\theta_i \frac{\left(y-\bar{y}_i\right)}{d_{T,i}^2}
\end{aligned}
$$

Taking derivative of (2.51), (2.52) and (2.53) w.r.t y i.e.

$$\frac{\partial \mathbf{C}_{\mathrm{AT}}^{x}}{\partial y} = \left[\frac{\partial}{\partial y}\left(\frac{d_{T,i}^2}{2}\right) + \frac{\partial}{\partial y}\left(\frac{\sigma_{n_i}^2}{2}\right)\right] \exp\left(\sigma_{m_i}^2\right) + \left[\frac{\partial}{\partial y}\left(\frac{d_{T,i}^2}{2}\cos 2\theta_i\right) + \frac{\partial}{\partial y}\left(\frac{\sigma_{n_i}^2}{2}\cos 2\theta_i\right)\right] \times \exp\left(-\sigma_{m_i}^2\right) - \frac{\partial}{\partial y}\left[\left(d_{T,i}\cos\theta_i\right)^2\right] \tag{7.23}$$

$$\frac{\partial \mathbf{C}_{\mathrm{AT}}^{y}}{\partial y} = \left[\frac{\partial}{\partial y}\left(\frac{d_{T,i}^2}{2}\right) + \frac{\partial}{\partial y}\left(\frac{\sigma_{n_i}^2}{2}\right)\right] \exp\left(\sigma_{m_i}^2\right) - \left[\frac{\partial}{\partial y}\left(\frac{d_{T,i}^2}{2}\cos 2\theta_i\right) + \frac{\partial}{\partial y}\left(\frac{\sigma_{n_i}^2}{2}\cos 2\theta_i\right)\right] \times \exp\left(-\sigma_{m_i}^2\right) - \frac{\partial}{\partial y}\left(d_{T,i}\sin\theta_i\right)^2 \tag{7.24}$$

$$\frac{\partial \mathbf{C}_{\mathrm{AT}}^{xy}}{\partial y} = \frac{\partial}{\partial y}\left(d_{T,i}^2\cos\theta_i\sin\theta_i\right)\left[\exp\left(-\sigma_{m_i}^2\right) - 1\right] + \frac{\partial}{\partial y}\left(\cos\theta_i\sin\theta_i\right)\left[\sigma_{n_i}^2\exp\left(-\sigma_{m_i}^2\right)\right]. \tag{7.25}$$

The derivates in (7.18), (7.24) and (7.25) are given below

7. $$\begin{aligned}\frac{\partial}{\partial y}\left(\frac{d_{T,i}^2}{2}\right) &= \frac{1}{2}\frac{\partial\left(d_{T,i}^2\right)}{\partial y} \\ &= \frac{1}{2}\left(\cancelto{0}{\frac{\partial}{\partial y}\left(x-\bar{x}_i\right)^2} + \frac{\partial}{\partial y}\left(y-\bar{y}_i\right)^2\right) \\ &= \frac{1}{2}\left(2\left(y-\bar{y}_i\right)\frac{\partial}{\partial y}\left(y-\bar{y}_i\right)\right) \\ &= \left(y-\bar{y}_i\right)\end{aligned}$$

$$\frac{\partial}{\partial y}\left(\frac{d_{T,i}^2}{2}\right) = (y - \bar{y}_i)$$

8. $$\begin{aligned}
\frac{\partial}{\partial y}\left(\frac{d_{T,i}^2}{2}\cos 2\theta_i\right) =& \frac{d_{T,i}^2}{2}\frac{\partial}{\partial y}\cos 2\theta_i + \cos 2\theta_i \frac{\partial}{\partial y}\frac{d_{T,i}^2}{2} \\
=& -\frac{d_{T,i}^2}{2}\sin 2\theta_i \frac{\partial}{\partial y}(2\theta_i) + \cos 2\theta_i\left(y - \bar{y}_i\right) \\
=& -\frac{d_{T,i}^2}{2}\sin 2\theta_i 2\frac{\partial}{\partial y}\arctan\left(\frac{y - \bar{y}_i}{x - \bar{x}_i}\right) + \cos 2\theta_i\left(y - \bar{y}_i\right) \\
=& -d_{T,i}^2 \sin 2\theta_i \left(\frac{1}{1 + \left(\frac{y-\bar{y}_i}{x-\bar{x}_i}\right)^2}\right)\frac{\partial}{\partial y}\left(\frac{y - \bar{y}_i}{x - \bar{x}_i}\right) + \cos 2\theta_i\left(y - \bar{y}_i\right) \\
=& -d_{T,i}^2 \sin 2\theta_i \frac{(x - \bar{x}_i)^2}{d_{T,i}^2}\left(\frac{1}{(x - \bar{x}_i)}\right) + \cos 2\theta_i\left(y - \bar{y}_i\right) \\
=& -(x - \bar{x}_i)\sin 2\theta_i + \cos 2\theta_i\left(y - \bar{y}_i\right)
\end{aligned}$$

$$\frac{\partial}{\partial y}\left(\frac{d_{T,i}^2}{2}\cos 2\theta_i\right) = \cos 2\theta_i\left(y - \bar{y}_i\right) - (x - \bar{x}_i)\sin 2\theta_i$$

9. $$\begin{aligned}\frac{\partial}{\partial y}\left(\frac{\sigma_{n_i}^2}{2}\cos 2\theta_i\right) &= \frac{\sigma_{n_i}^2}{2}\frac{\partial}{\partial y}\cos 2\theta_i \\ &= -\frac{\sigma_{n_i}^2}{2}\sin 2\theta_i \frac{\partial}{\partial y}\left(2\theta_i\right) \\ &= -\sigma_{n_i}^2 \sin 2\theta_i \frac{\partial}{\partial y}\arctan\left(\frac{y-\bar{y}_i}{x-\bar{x}_i}\right) \\ &= -\sigma_{n_i}^2 \sin 2\theta_i \left(\frac{1}{1+\left(\frac{y-\bar{y}_i}{x-\bar{x}_i}\right)^2}\right)\frac{\partial}{\partial y}\left(\frac{y-\bar{y}_i}{x-\bar{x}_i}\right) \\ &= -\sigma_{n_i}^2 \sin 2\theta_i \left(\frac{(x-\bar{x}_i)^2}{(x-\bar{x}_i)^2+(y-\bar{y}_i)^2}\right)\left(\frac{1}{(x-\bar{x}_i)}\right) \\ &= \sigma_{n_i}^2 \sin\Big(2\theta_i\Big)\frac{(x-\bar{x}_i)}{d_{T,i}^2}.\end{aligned}$$

$$\frac{\partial}{\partial y}\left(\frac{\sigma_{n_i}^2}{2}\cos 2\theta_i\right) = \sigma_{n_i}^2 \sin\Big(2\theta_i\Big)\frac{(x-\bar{x}_i)}{d_{T,i}^2}$$

10. $$\begin{aligned}\frac{\partial}{\partial y}\left(d_{T,i}\cos\theta_i\right)^2 &= \frac{\partial}{\partial y}\left(d_{T,i}\left(\frac{1}{2}+\frac{1}{2}\cos 2\theta_i\right)\right) \\ &= \frac{\partial}{\partial y}\left(\frac{d_{T,i}^2}{2}\right)+\frac{\partial}{\partial y}\left(\frac{d_{T,i}^2}{2}\cos 2\theta_i\right) \\ &= \frac{\partial}{\partial y}\left(\frac{d_{T,i}^2}{2}\right)+\left(\frac{d_{T,i}^2}{2}\frac{\partial}{\partial y}\cos 2\theta_i+\cos 2\theta_i\frac{\partial}{\partial y}\frac{d_{T,i}^2}{2}\right) \\ &= \Big(y-\bar{y}_i\Big)-\sin 2\theta_i\Big(x-\bar{x}_i\Big)+\cos 2\theta_i\Big(y-\bar{y}_i\Big) \\ &= \Big(y-\bar{y}_i\Big)\left(1-\sin 2\theta_i\frac{\Big(x-\bar{x}_i\Big)}{\Big(y-\bar{y}_i\Big)}+\cos 2\theta_i\right) \\ &= \Big(y-\bar{y}_i\Big)\left(1-\sin 2\theta_i\cot\theta_i+\cos 2\theta_i\right)\end{aligned}$$

Using double angle identity i.e. $\sin 2\theta_i = \sin\theta_i\cos\theta_i$ and $\cos 2\theta_i = \cos^2\theta_i - \sin^2\theta_i$

we get

$$\begin{aligned}\frac{\partial}{\partial y}\left(d_{T,i}\cos\theta_i\right)^2 =&\Big(y-\bar{y}_i\Big)\left(1-2\sin\theta_i\cos\theta_i\frac{\cos\theta_i}{\sin\theta_i}+\cos^2\theta_i-\sin^2\theta_i\right)\\ =&\Big(y-\bar{y}_i\Big)\left(1-\sin^2\theta_i+\cos^2\theta_i-2\cos^2\theta_i\right)\\ =&\Big(y-\bar{y}_i\Big)\left(2\cos^2\theta_i-2\cos^2\theta_i\right)\\ =&0.\end{aligned}$$

$$\boxed{\frac{\partial}{\partial y}\left(d_{T,i}\cos\theta_i\right)^2=0}$$

11. $$\begin{aligned}\frac{\partial}{\partial y}\Big(d_{T,i}^2\cos\theta_i\sin\theta_i\Big) =&d_{T,i}^2\cos\theta_i\frac{\partial}{\partial y}\sin\theta_i+\sin\theta_i\frac{\partial}{\partial y}d_{T,i}^2\cos\theta_i\\ =&d_{T,i}^2\cos\theta_i\left(\cos\theta_i\frac{\partial}{\partial y}\theta_i\right)+\sin\theta_i\left(d_{T,i}^2\frac{\partial}{\partial y}\cos\theta_i+\cos\theta_i\frac{\partial}{\partial y}d_{T,i}^2\right)\\ =&d_{T,i}^2\cos^2\theta_i\frac{\partial}{\partial y}\arctan\left(\frac{y-\bar{y}_i}{x-\bar{x}_i}\right)+\sin\theta_i\Big(-d_{T,i}^2\sin\theta_i\frac{\partial}{\partial y}\theta_i\\ &+2\cos\theta_i\left(y-\bar{y}_i\right)\Big)\\ =&d_{T,i}^2\cos^2\theta_i\left(\frac{1}{1+\left(\frac{y-\bar{y}_i}{x-\bar{x}_i}\right)^2}\right)\frac{\partial}{\partial y}\left(\frac{y-\bar{y}_i}{x-\bar{x}_i}\right)-d_{T,i}^2\sin^2\theta_i\\ &\times\left(\frac{1}{1+\left(\frac{y-\bar{y}_i}{x-\bar{x}_i}\right)^2}\right)\frac{\partial}{\partial y}\left(\frac{y-\bar{y}_i}{x-\bar{x}_i}\right)+2\cos\theta_i\left(y-\bar{y}_i\right)\end{aligned}$$

$$
\begin{aligned}
=& d_{T,i}^2 \cos^2\theta_i \left(\frac{(x-\bar{x}_i)^2}{d_{T,i}^2}\right)\left(\frac{1}{x-\bar{x}_i}\right) - d_{T,i}^2 \sin^2\theta_i \left(\frac{(x-\bar{x}_i)^2}{d_{T,i}^2}\right) \\
& \times \left(\frac{1}{x-\bar{x}_i}\right) + 2\cos\theta_i \,(y-\bar{y}_i) \\
=& \,(x-\bar{x}_i)\cos^2\theta_i - (x-\bar{x}_i)\sin^2\theta_i + 2\cos\theta_i\,(y-\bar{y}_i) \\
=& \,(x-\bar{x}_i)\left(\cos^2\theta_i - \sin^2\theta_i + 2\cos\theta_i \frac{(y-\bar{y}_i)}{(x-\bar{x}_i)}\right) \\
=& \,(x-\bar{x}_i)\left(\cos^2\theta_i - \sin^2\theta_i + 2\cos\theta_i \tan\theta_i\right) \\
=& \,(x-\bar{x}_i)\left(\cos^2\theta_i - \sin^2\theta_i + 2\cos\theta_i \frac{\sin\theta_i}{\cos\theta_i}\right) \\
=& \,(x-\bar{x}_i)\left(\cos^2\theta_i - \sin^2\theta_i + 2\sin\theta_i\right)
\end{aligned}
$$

Using double angle identity i.e. $\cos^2\theta_i - \sin^2\theta_i = 1 - 2\sin\theta_i$ we get

$$
\begin{aligned}
\frac{\partial}{\partial y}\left(d_{T,i}^2 \cos\theta_i \sin\theta_i\right) &= (x-\bar{x}_i)\,(1 - 2\sin\theta_i + 2\sin\theta_i) \\
&= (x-\bar{x}_i)
\end{aligned}
$$

$$
\boxed{\frac{\partial}{\partial y}\left(d_{T,i}^2 \cos\theta_i \sin\theta_i\right) = (x-\bar{x}_i)}
$$

12. $$\begin{aligned}\frac{\partial}{\partial y}\Big(\cos\theta_i \sin\theta_i\Big) &= \cos\theta_i \frac{\partial}{\partial y}\sin\theta_i + \sin\theta_i \frac{\partial}{\partial y}\cos\theta_i \\ &= \cos\theta_i \left(\cos\theta_i \frac{\partial}{\partial y}\theta_i\right) - \sin\theta_i \left((\sin\theta_i)\,\frac{\partial}{\partial y}\theta_i\right) \\ &= \cos^2\theta_i \left(\frac{x-\bar{x}_i}{d_{T,i}^2}\right) - \sin^2\theta_i \left(\frac{x-\bar{x}_i}{d_{T,i}^2}\right)\end{aligned}$$

$$\frac{\partial}{\partial y}\Big(\cos\theta_i \sin\theta_i\Big) = \cos^2\theta_i \left(\frac{x-\bar{x}_i}{d_{T,i}^2}\right) - \sin^2\theta_i \left(\frac{x-\bar{x}_i}{d_{T,i}^2}\right)$$

Appendix III: Derivation Of Covariance Matrix For AoA-RSS Signal

This appendix presents the covariance matrix derivation for AoA-RSS signal model

Derivation of Equation (3.16). From (3.15), we have $\mathbf{C}^{x}_{\mathrm{AR}} = E\left[(\hat{\mathbf{r}}_x - \mathbf{r}_x)(\hat{\mathbf{r}}_x - \mathbf{r}_x)^T\right]$, putting the value of $\hat{\mathbf{r}}_x$ and $\mathbf{r}_x$ for $i = j$, we get

$$\begin{aligned}
\mathbf{C}^{x}_{\mathrm{AR}_{ii}} =& E_{\check{w}_i, m_i}\left(\left(d_{R,i}\exp\left(\frac{\check{w}_i}{\gamma\alpha}\right)\cos\Big(\theta_i + m_i\Big)\delta_{R,i} - d_{R,i}\cos\theta_i\right)^2\right) \\
=& E_{\check{w}_i, m_i}\Bigg[\left(\left(d_{R,i}\exp\left(\frac{\check{w}_i}{\gamma\alpha}\right)\right)^2\cos^2\Big(\theta_i + m_i\Big)\right)\delta^2_{R,i} + \Big(d_{R,i}\cos\theta_i\Big)^2 - 2\delta_{R,i}\Big(d_{R,i}\cos\theta_i\Big) \\
& \left(d_{R,i}\exp\left(\frac{\check{w}_i}{\gamma\alpha}\right)\right)\cos\Big(\theta_i + m_i\Big)\Bigg] \qquad (7.26) \\
=& E_{\check{w}_i, m_i}\Bigg[d^2_{R,i}\exp\left(\frac{2\check{w}_i}{\gamma\alpha}\right)\Big(0.5 + 0.5\Big(\cos 2\theta_i\cos 2m_i \; - \sin 2\theta_i \sin 2m_i\Big)\Big)\delta^2_{R,i} \\
& + \Big(d_{R,i}\cos\theta_i\Big)^2 - 2\delta_{R,i}\left(d^2_{R,i}\exp\left(\frac{\check{w}_i}{\gamma\alpha}\right)\right)\Big(\cos^2\theta_i\cos m_i - \cos\theta_i\sin\theta_i\sin m_i\Big)\Bigg] \\
& \qquad (7.27)
\end{aligned}$$

Equ. (7.27) is obtained from (7.26) by using the identity $\cos^2(t) = 0.5 + 0.5\cos(2t)$. Also using the expectation $E_{m_i}[\sin(m_i)] = 0$ and $E_{m_i}[\sin(2m_i)] = 0$, (7.28) is obtained.

$$\mathbf{C}^{x}_{\mathrm{AR}_{ii}} = \left(\frac{d^2_{R,i}}{2} E_{\check{w}_i} \left[\exp\Big(\frac{2\check{w}_i}{\gamma\alpha} \Big) \right] + \frac{d^2_{R,i}}{2} E_{\check{w}_i} \left[\exp\Big(\frac{2\check{w}_i}{\gamma\alpha} \Big) \right] \cos 2\theta_i \times E_{m_i} \Big[\cos 2 m_i \Big] \right) \delta^2_{R,i} + \Big(d_{R,i} \cos\theta_i \Big)^2 - 2\delta_{R,i} \left(\Big(d_{R,i} \cos\theta_i \Big)^2 E_{\check{w}_i} \left[\exp\Big(\frac{\check{w}_i}{\gamma\alpha} \Big) \right] E_{m_i} \Big[\cos m_i \Big] \right) \tag{7.28}$$

Taking the expectation in (7.28), which are given in table. 2.1, we conclude the proof by obtaining **(3.16)**.

For the non diagonal terms of $\mathbf{C}^{x}_{\mathrm{AR}} = E\left[(\hat{\mathbf{r}}_x - \mathbf{r}_x) (\hat{\mathbf{r}}_x - \mathbf{r}_x)^T \right]$, i.e. $i \neq j$ we have

$$\mathbf{C}^{x}_{\mathrm{AR}_{ij}} = E_{\check{w}_{ij}, m_{ij}} \left[\left(d_{R,i} \exp\Big(\frac{\check{w}_i}{\gamma\alpha} \Big) \cos\Big(\theta_i + m_i \Big) \delta_{R,i} - d_{R,i} \cos\theta_i \right) \left(d_{R,j} \exp\Big(\frac{\check{w}_j}{\gamma\alpha} \Big) \cos\Big(\theta_j + m_j \Big) \delta_{R,j} - d_{R,j} \cos\theta_j \right) \right]$$

$$\mathbf{C}^{x}_{\mathrm{AR}_{ij}} = E_{\check{w}_{ij}, m_{ij}} \Bigg[\left(\left(d_{R,i} d_{R,j} \exp\Big(\frac{\check{w}_i}{\gamma\alpha} \Big) \exp\Big(\frac{\check{w}_j}{\gamma\alpha} \Big) \right) \Big(\cos\theta_i \cos m_i + \sin\theta_i \sin m_i \Big) \Big(\cos\theta_j \cos m_j + \sin\theta_j \sin m_j \Big) \delta_{ij} \right) \left(\left(d_{R,i} d_{R,j} \exp\Big(\frac{\check{w}_i}{\gamma\alpha} \Big) \right) \Big(\cos\theta_i \cos\theta_j \cos m_i + \sin\theta_i \cos\theta_j \sin m_i \Big) \delta_{R,i} \right) - \left(\left(d_{R,i} d_{R,j} \exp\Big(\frac{\check{w}_j}{\gamma\alpha} \Big) \right) \Big(\cos\theta_i \cos\theta_j \cos m_j + \sin\theta_i \cos\theta_j \sin m_j \Big) \delta_{R,j} \right) + d_{R,i} d_{R,j} \cos\theta_i \cos\theta_j \Bigg]$$

where $\delta_{R,ij} = \delta_{R,i} \delta_{R,j}$. taking expectation

$$\begin{aligned}\mathbf{C}^{x}_{\mathrm{AR}_{ij}} =& d_{R,i}d_{R,j}\cos\theta_i\cos\theta_j - d_{R,i}d_{R,j}\cos\theta_i\cos\theta_j - d_{R,i}d_{R,j}\cos\theta_i\cos\theta_j \\ &+ d_{R,i}d_{R,j}\cos\theta_i\cos\theta_j \\ =& 0\end{aligned}$$

The derivation of (3.17) is similar to (3.16), other than the fact that x coordinate is replaced with y coordinate i.e. cos function is replaced with sin function.

Derivation of Equation (3.18). From (3.15), we have $\mathbf{C}^{x}_{\mathrm{AR}} = E\left[\left(\hat{\mathbf{r}}_x - \mathbf{r}_x\right)\left(\hat{\mathbf{r}}_y - \mathbf{r}_y\right)^T\right]$, putting the value of $\hat{\mathbf{r}}_x$, $\mathbf{r}_x$, $\hat{\mathbf{r}}_y$ and $\mathbf{r}_y$ for $i = j$, we get

$$\begin{aligned}\mathbf{C}^{xy}_{\mathrm{AR}_{ij}} =& E_{\check{w}_i,m_i}\Bigg[\left(d_{R,i}\exp\left(\frac{\check{w}_i}{\gamma\alpha}\right)\cos\Big(\theta_i + m_i\Big)\delta_{R,i} - d_{R,i}\cos\theta_i\right) \\ &\left(d_{R,i}\exp\left(\frac{\check{w}_i}{\gamma\alpha}\right)\sin\Big(\theta_i + m_i\Big)\delta_{R,i} - d_{R,i}\sin\theta_i\right)\Bigg] \\ =& E_{\check{w}_i,m_i}\Bigg[\left(d_{R,i}\exp\left(\frac{\check{w}_i}{\gamma\alpha}\right)\right)^2\cos\Big(\theta_i + m_i\Big)\sin\Big(\theta_i + m_i\Big)\delta^2_{R,i} - d_{R,i}\left(d_{R,i}\exp\left(\frac{\check{w}_i}{\gamma\alpha}\right)\right) \\ &\cos\Big(\theta_i + m_i\Big)\sin\theta_i\delta_{R,i} - d_{R,i}\left(d_{R,i}\exp\left(\frac{\check{w}_i}{\gamma\alpha}\right)\right)\sin\Big(\theta_i + m_i\Big)\cos\theta_i\delta_{R,i} \\ &+ d^2_{R,i}\cos\theta_i\sin\theta_i\Bigg] \qquad (7.29)\end{aligned}$$

Expanding (7.29), and then using double angle identity $\cos^2 t - \sin^2 t = \cos(2t)$, and also $E[\sin(m_i)] = 0$, we obtain

$$\begin{aligned}\mathbf{C}^{xy}_{\mathrm{AR}_{ij}} =& E_{\check{w}_i,m_i}\Bigg[\bigg(d^2_{R,i}\exp\Big(\frac{2\check{w}_i}{\gamma\alpha}\Big)\cos\theta_i\sin\theta_i\cos 2m_i\bigg)\delta^2_{R,i} - \bigg(d^2_{R,i}\exp\Big(\frac{\check{w}_i}{\gamma\alpha}\Big)\\ &\cos\theta_i\cos m_i\sin\theta_i\bigg)\delta_{R,i} - \bigg(d^2_{R,i}\exp\Big(\frac{\check{w}_i}{\gamma\alpha}\Big)\sin\theta_i\cos m_i\cos\theta_i\bigg)\delta_{R,i}\\ &+ d^2_{R,i}\cos\theta_i\sin\theta_i\Bigg] \end{aligned} \tag{7.30}$$

Finally, using expectations in (7.30), we conclude the proof by obtaining (3.18) from (7.30).

For the non diagonal terms of $\mathbf{C}^{xy}_{\mathrm{AR}} = E\left[(\hat{\mathbf{r}}_x - \mathbf{r}_x)(\hat{\mathbf{r}}_y - \mathbf{r}_y)^T\right]$, i.e. $i \neq j$ we have

$$\begin{aligned}\mathbf{C}^{xy}_{\mathrm{AR}_{ij}} =& E_{\check{w}_{ij},m_{ij}}\Bigg[\bigg(d_{R,i}\exp\Big(\frac{\check{w}_i}{\gamma\alpha}\Big)\cos\Big(\theta_i + m_i\Big)\delta_{R,i} - d_{R,i}\cos\theta_i\bigg)\\ &\bigg(d_{R,j}\exp\Big(\frac{\check{w}_j}{\gamma\alpha}\Big)\sin\Big(\theta_j + m_j\Big)\delta_{R,j} - d_{R,j}\sin\theta_j\bigg)\Bigg]\\ =& E_{\check{w}_{ij},m_{ij}}\Bigg[\Bigg(\bigg(d_{R,i}d_{R,j}\exp\Big(\frac{\check{w}_i}{\gamma\alpha}\Big)\exp\Big(\frac{\check{w}_j}{\gamma\alpha}\Big)\bigg)\Big(\cos\theta_i\cos m_i - \sin\theta_i\sin m_i\Big)\\ &\Big(\sin\theta_j\cos m_j + \cos\theta_j\sin m_j\Big)\delta_{ij}\Bigg) - \Bigg(\bigg(d_{R,i}d_{R,j}\exp\Big(\frac{\check{w}_i}{\gamma\alpha}\Big)\bigg)\Big(\cos\theta_i\sin\theta_j\cos m_i\\ &+ \sin\theta_i\sin\theta_j\sin m_i\Big)\delta_{R,i}\Bigg) - \Bigg(\bigg(d_{R,i}d_{R,j}\exp\Big(\frac{\check{w}_j}{\gamma\alpha}\Big)\bigg)\Big(\cos\theta_i\sin\theta_j\cos m_j\\ &+ \cos\theta_i\cos\theta_j\sin m_j\Big)\delta_{R,j}\Bigg) + d_{R,i}d_{R,j}\cos\theta_i\sin\theta_j\Bigg]\end{aligned} \tag{7.31}$$

Taking expectations in (7.31), we obtain

$$\begin{aligned}\mathbf{C}^{xy}_{\mathrm{AR}_{ij}} &= d_{R,i}d_{R,j}\cos\theta_i\sin\theta_j - d_{R,i}d_{R,j}\cos\theta_i\sin\theta_j - d_{R,i}d_{R,j}\cos\theta_i\sin\theta_j \\ &\quad + d_{R,i}d_{R,j}\cos\theta_i\sin\theta_j \\ &=0\end{aligned}$$

Appendix IV: Derivation of covariance matrix for AoA-RSS Signal Model with Incorrect PLE Values.

This appendix presents the derivation of noise covariance matrix for AoA-RSS signal model with incorrect PLE vector.

Derivation of Equation (5.26). From (5.23), we have $\mathbf{C}_{\alpha}\left(x\right) = E_{\mathbf{w},\mathbf{m}}\Bigg[\Big(\hat{\mathbf{b}}_{x,\alpha} - \mathbf{b}_{x,\alpha}\Big)\Big(\hat{\mathbf{b}}_{x,\alpha} - \mathbf{b}_{x,\alpha}\Big)^{T}\Bigg] \in \mathbb{R}^{N\times N}$, putting the value of $\hat{\mathbf{b}}_{x,\alpha}$ and $\mathbf{b}_{x,\alpha}$ for $i = j$, we get

$$\begin{aligned}
\mathbf{C}_{\alpha}\left(x\right)_{ii} =& E_{\check{w}_i,m_i}\left[\left(d_i^{\kappa_i}\exp\left(\frac{\check{w}_i}{\gamma\check{\alpha}_i}\right)\cos\left(\theta_i + m_i\right)\check{\delta}_i - d_i\cos\theta_i\right)^2\right] \\
=& E_{\check{w}_i,m_i}\Bigg[d_i^{2\kappa_i}\exp\Big(\frac{2\check{w}_i}{\gamma\check{\alpha}_i}\Big)\cos^2(\theta_i + m_i)\,\check{\delta}_i^2 + \Big(d_i\cos\theta_i\Big)^2 \\
& - 2\check{\delta}_i\Big(d_i\cos\theta_i\Big)\Big(d_i^{\kappa_i}\exp\Big(\frac{\check{w}_i}{\gamma\check{\alpha}_i}\Big)\Big)\cos\left(\theta_i + m_i\right)\Bigg] \qquad (7.32) \\
=& E_{\check{w}_i,m_i}\Bigg[d_i^{2\kappa_i}\exp\Big(\frac{2\check{w}_i}{\gamma\check{\alpha}_i}\Big)\Big(\frac{1}{2} + \frac{1}{2}\cos\left(2\theta_i + 2m_i\right)\Big)\check{\delta}_i^2 + \Big(d_i\cos\theta_i\Big)^2 \\
& - 2\check{\delta}_i d_i d_i^{\kappa_i}\exp\Big(\frac{\check{w}_i}{\gamma\check{\alpha}_i}\Big)\cos\left(\theta_i + m_i\right)\cos\theta_i \qquad (7.33)
\end{aligned}$$

Equation (7.33) is obtained from (7.32) by using trigonometric half angle identity, $\cos^2\left(t\right) = 0.5 + 0.5\cos\left(2t\right)$. Also using trigonometric sum-difference formula, $\cos\left(\mathrm{A} + \mathrm{B}\right) = \cos\mathrm{A}\cos\mathrm{B} + \sin\mathrm{A}\sin\mathrm{B}$, (7.34) is obtained

$$\begin{aligned}
\mathbf{C}_{\alpha}\left(x\right)_{ii} =& E_{\check{w}_i,m_i}\Bigg[d_i^{2\kappa_i}\exp\Big(\frac{2\check{w}_i}{\gamma\check{\alpha}_i}\Big)\Big(\frac{1}{2} + \frac{1}{2}\Big(\cos 2\theta_i\cos 2m_i + \sin 2\theta_i\sin 2m_i\Big)\Big)\check{\delta}_i^2 \\
& + \Big(d_i\cos\theta_i\Big)^2 - 2\check{\delta}_i d_i d_i^{\kappa_i}\exp\Big(\frac{\check{w}_i}{\gamma\check{\alpha}_i}\Big)\Big(\cos^2\theta_i\cos m_i + \sin\theta_i\sin m_i\Big) \qquad (7.34)
\end{aligned}$$

Finally taking the expectations in (7.34) which are given in table. 2.1 and derived

in appendix I, we conclude the proof by obtaining **(5.26)**.

For non diagonal terms i.e. $i \neq j$ we have from (5.23)

$$\begin{aligned}\mathbf{C}_{\alpha}(x)_{ij} =& E_{\check{w}_{ii},m_i}\Bigg[\Bigg(d_i^{\kappa_i}\exp\Big(\frac{\check{w}_i}{\gamma\check{\alpha}_i}\Big)\cos(\theta_i+m_i)\,\check{\delta}_i - d_i\cos\theta_i\Big)\Big)\\ &\Big(d_j^{\kappa_j}\exp\Big(\frac{\check{w}_j}{\gamma\check{\alpha}_j}\Big)\cos(\theta_j+m_j)\,\check{\delta}_j - d_j\cos\theta_j\Big)\Big)\Bigg]\end{aligned}$$

$$\begin{aligned}\mathbf{C}_{\alpha}(x)_{ij} =& E_{\check{w}_i,m_i}\Bigg[d_i^{\kappa_i}\exp\Big(\frac{\check{w}_i}{\gamma\check{\alpha}_i}\Big)d_j^{\kappa_j}\exp\Big(\frac{\check{w}_j}{\gamma\check{\alpha}_j}\Big)\cos(\theta_i+m_i)\,\check{\delta}_i\cos(\theta_j+m_j)\,\check{\delta}_j\\ &- d_i^{\kappa_i}\exp\Big(\frac{\check{w}_i}{\gamma\check{\alpha}_i}\Big)d_j\cos\theta_j\cos(\theta_i+m_i)\,\check{\delta}_i - d_j^{\kappa_j}\exp\Big(\frac{\check{w}_j}{\gamma\check{\alpha}_j}\Big)\\ &\cos(\theta_j+m_j)\,\check{\delta}_j d_i\cos\theta_i + d_i\cos\theta_i d_j\cos\theta_j\Bigg] \qquad (7.35)\end{aligned}$$

Using sum-difference formula (7.35) can be expanded as

$$\begin{aligned}\mathbf{C}_{\alpha}(x)_{ij} =& d_i^{\kappa_i}d_j^{\kappa_j}E_{\check{w}_i}\Big[\exp\Big(\frac{\check{w}_i}{\gamma\check{\alpha}_i}\Big)\Big]E_{\check{w}_j}\Big[\exp\Big(\frac{\check{w}_j}{\gamma\check{\alpha}_j}\Big)\Big]\Big(\cos\theta_i E_{m_i}\Big[\cos m_i\Big]\cos\theta_j\cos m_j\\ &+\cos\theta_i E_{m_j}\Big[\cos m_i\Big]\sin\theta_j E_{m_j}\Big[\sin m_j\Big] + \sin\theta_i E_{m_i}\Big[\sin m_i\Big]\cos\theta_j\\ &E_{m_j}\Big[\cos m_j\Big] + \sin\theta_i E_{m_i}\Big[\sin m_i\Big]\sin\theta_j E_{m_j}\Big[\sin m_j\Big]\Big)\check{\delta}_i\check{\delta}_j - d_i^{\kappa_i}d_j\\ &E_{\check{w}_i}\Big[\exp\Big(\frac{\check{w}_i}{\gamma\check{\alpha}_i}\Big)\Big]\cos\theta_i E_{m_i}\Big[\cos m_i\Big]\cos\theta_j\check{\delta}_i - d_j^{\kappa_j}d_i E_{\check{w}_j}\Big[\exp\Big(\frac{\check{w}_j}{\gamma\check{\alpha}_j}\Big)\Big]\\ &\cos\theta_j E_{m_j}\Big[\cos m_j\Big]\cos\theta_i\check{\delta}_j + d_i d_j\cos\theta_i\cos\theta_j. \qquad (7.36)\end{aligned}$$

Taking expectation in (7.36), we conclude the proof by obtaining (5.29). The derivation of (5.27) and (5.28) is similar except that $\hat{\mathbf{b}}_{x,\alpha}$ is replaced with $\hat{\mathbf{b}}_{y,\alpha}$.

Bibliography

[1] I. Rasool, "RSSI and TOF based localization improvement in a wireless sensor network (WSN)," Master's thesis, University of Leeds, December 2012.

[2] W. R. F. Myron Kayton, *Avionics navigation systems 2nd edition.* Wiley-IEEE, 1997.

[3] I. G. group, online: http://www.insidegnss.com/glonass.

[4] K. O'Neil, "Galileo - european satellite navigation system," Advanced Aviation Technology Ltd. online: http://www.aatl.net/publications/galileo.htm.

[5] I. Akyildiz, W. Su, Y. Sankarasubramaniam, and E. Cayirci, "A survey on sensor networks," *IEEE Communications Magazine*, vol. 40, no. 8, pp. 102–114, 2002.

[6] D. Ye, D. Gong, and W. Wang, "Application of wireless sensor networks in environmental monitoring," in *2nd International Conference onPower Electronics and Intelligent Transportation System (PEITS)*, vol. 1, 2009, pp. 205–208.

[7] S. Lan, M. Qilong, and J. Du, "Architecture of wireless sensor networks for environmental monitoring," in *nternational Workshop on Education Techno-*

logy and Training and International Workshop on Geoscience and Remote Sensing. ETT and GRS, vol. 1, 2008, pp. 579–582.

[8] D. Dardari, A. Conti, U. Ferner, A. Giorgetti, and M. Win, "Ranging with ultrawide bandwidth signals in multipath environments," *Proceedings of the IEEE*, vol. 97, no. 2, pp. 404–426, 2009.

[9] Y. Zhang, A. Brown, W. Malik, and D. Edwards, "High resolution 3-D angle of arrival determination for indoor UWB multipath propagation," *IEEE Transactions on Wireless Communications,*, vol. 7, no. 8, pp. 3047–3055, August 2008.

[10] M. Khan, N. Salman, and A. H. Kemp, "Enhanced hybrid positioning in wireless networks I: AoA-ToA," in *IEEE International Conference on Telecommunications and Multimedia (TEMU)*, pp. 86–91, July 2014.

[11] N. Salman, M. W. Khan, and A. H. Kemp, "Enhanced hybrid positioning in wireless networks II: AoA-RSS," in *IEEE International Conference on Telecommunications and Multimedia (TEMU)*, pp. 92–97, July 2014.

[12] J. Ko, T. Gao, R. Rothman, and A. Terzis, "Wireless sensing systems in clinical environments: Improving the efficiency of the patient monitoring process," *IEEE Engineering in Medicine and Biology Magazine*, vol. 29, no. 2, pp. 103–109, March 2010.

[13] F. Michahelles, P. Matter, A. Schmidt, and B. Schiele, "Applying wearable sensors to avalanche rescue," *Computers & Graphics*, vol. 27, 2003.

[14] P. Juang, H. Oki, Y. Wang, M. Martonosi, L. S. Peh, and D. Rubenstein, "Energy-efficient computing for wildlife tracking: Design tradeoffs and early experiences with zebranet," *SIGARCH Comput. Archit. News*, vol. 30, no. 5, pp. 96–107, Oct. 2002.

[15] T. Damarla, L. Kaplan, and G. Whipps, "Sniper localization using acoustic asynchronous sensors," *IEEE Sensors Journal*, vol. 10, no. 9, pp. 1469–1478, 2010.

[16] R. Ca rdenas Tamayo, M. Lugo Ibarra, and J. Garcia Macias, "Better crop management with decision support systems based on wireless sensor networks," in *7th International Conference on Electrical Engineering Computing Science and Automatic Control (CCE)*, 2010, pp. 412–417.

[17] Z. Butler, P. Corke, R. Peterson, and D. Rus, "Virtual fences for controlling cows," in *Proc. IEEE International Conference on Robotics and Automation (ICRA)*, vol. 5, 2004, pp. 4429–4436 Vol.5.

[18] S. Pandey, "A survey of lcalization techniques for wireless networks," *journal of chinese institute of engineers*, vol. 29, pp. 1125–1148, 2006.

[19] s. g. Zafer S.G and ismail guvenc, Eds., *Ultra-wide band positioning systems, theoretical limits, ranging algorithms and protocols.* Cambridge University Press, 2011.

[20] K. Whitehouse, C. Karlof, and D. Culler, "A practical evaluation of radio signal strength for ranging-based localization," *SIGMOBILE Mob. Comput. Commun. Rev.*, vol. 11, no. 1, pp. 41–52, Jan. 2007. [Online]. Available: http://doi.acm.org/10.1145/1234822.1234829

[21] V. Moghtadaiee, A. Dempster, and S. Lim, "Indoor localization using FM radio signals: A fingerprinting approach," in *International Conference on Indoor Positioning and Indoor Navigation (IPIN)*, Sept 2011, pp. 1–7.

[22] A. Runge, M. Baunach, and R. Kolla, "Precise self-calibration of ultrasound based indoor localization systems," in *International Conference on Indoor Positioning and Indoor Navigation (IPIN),*, Sept 2011, pp. 1–8.

[23] D. Hauschildt and N. Kirchhof, "Improving indoor position estimation by combining active tdoa ultrasound and passive thermal infrared localization," in *8th Workshop on Positioning Navigation and Communication (WPNC)*, April 2011, pp. 94–99.

[24] E. Brassart, C. Pegard, and M. Mouaddib, "Localization using infrared beacons," *Robotica*, vol. 18, no. 2, pp. 153–161, Mar. 2000. [Online]. Available: http://dx.doi.org/10.1017/S0263574799001927

[25] S. Lee and J.-B. Song, "Mobile robot localization using infrared light reflecting landmarks," in *International Conference on Control, Automation and Systems,)ICCAS)*, Oct 2007, pp. 674–677.

[26] D. Humphrey and M. Hedley, "Super-resolution time of arrival for indoor localization," in *IEEE International Conference on Communications, (ICC 08)*, 2008, pp. 3286–3290.

[27] A. Rabbachin, I. Oppermann, and B. Denis, "ML time-of-arrival estimation based on low complexity UWB energy detection," in *IEEE International Conference on Ultra-Wideband*, 2006, pp. 599–604.

[28] T. Sathyan, D. Humphrey, and M. Hedley, "WASP: A system and algorithms for accurate radio localization using low-cost hardware," *IEEE Transactions on Systems, Man, and Cybernetics, Part C: Applications and Reviews*, vol. 41, no. 2, pp. 211–222, March 2011.

[29] IEEE, "IEEE std 802.15.4-2007 (amendment to IEEE std 802.15.-2006)."

[30] X. Li, "Performance study of RSS-based location estimation techniques for wireless sensor networks," in *IEEE Military Communications Conference, (MILCOM)*, 2005, pp. 1064–1068 Vol. 2.

[31] Z. Jie, L. HongLi, and Tanjian, "Research on ranging accuracy based on

RSSI of wireless sensor network," in *Information Science and Engineering (ICISE), 2010 2nd International Conference on*, 2010, pp. 2338–2341.

[32] M. M. Simon O. Haykin, *Modern Wireless Communications*. Prentice Hall, 2004.

[33] Jennic, "www.jennic.com/products/modules."

[34] G. Mao, Fidan, and B. D. Anderson, "Wireless sensor network localization techniques," *Computer Networks*, vol. 51, no. 10, pp. 2529 – 2553, 2007. [Online]. Available: http://www.sciencedirect.com/science/article/pii/S1389128606003227

[35] D. Niculescu and B. Nath, "Ad hoc positioning system (APS) using AOA," in *Twenty-Second Annual Joint Conference of the IEEE Computer and Communications. IEEE Societies*, vol. 3, 2003, pp. 1734–1743 vol.3.

[36] P. Kulakowski, J. Vales-Alonso, E. Egea-López, W. Ludwin, and J. García-Haro, "Angle-of-arrival localization based on antenna arrays for wireless sensor networks," *Computers & Electrical Engineering*, vol. 36, no. 6, pp. 1181 – 1186, 2010.

[37] ——, "Angle-of-arrival localization based on antenna arrays for wireless sensor networks." *Computers & Electrical Engineering*, vol. 36, no. 6, pp. 1181–1186, 2010. [Online]. Available: http://dblp.uni-trier.de/db/journals/cee/cee36.htmlKulakowskiVELG10

[38] R. Schmidt, "Multiple emitter location and signal parameter estimation," *IEEE Transactions on Antennas and Propagation*, vol. 34, no. 3, pp. 276–280, 1986.

[39] R. Roy and T. Kailath, "Esprit-estimation of signal parameters via rotational invariance techniques," *Acoustics, Speech and Signal Processing, IEEE Transactions on*, vol. 37, no. 7, pp. 984–995, 1989.

[40] N. Patwari, J. Ash, S. Kyperountas, A. Hero, R. Moses, and N. Correal, "Locating the nodes: cooperative localization in wireless sensor networks," *IEEE Signal Processing Magazine*, vol. 22, no. 4, pp. 54–69, 2005.

[41] K. Yu, "3-D localization error analysis in wireless networks," *IEEE Transactions on Wireless Communications*, vol. 6, no. 10, pp. 3472–3481, 2007.

[42] de S.Muswieck Bruno, J. L. Russi, and M. V. Heckler, "Hybrid method uses RSS and AoA to establish a low-cost localization system," in *Embedded Systems (SASE/CASE), 2013 Fourth Argentine Symposium and Conference on*, 2013, pp. 1–6.

[43] N. A. M. Maung and M. Kawai, "An improved hybrid localization scheme for wireless ad hoc and sensor networks," in *IEEE 24th International Symposium on Personal Indoor and Mobile Radio Communications (PIMRC)*, pp. 3181–3185, Sept 2013.

[44] J. A. Costa, N. Patwari, and A. O. Hero, III, "Distributed weighted-multidimensional scaling for node localization in sensor networks," *ACM Trans. Sen. Netw.*, vol. 2, no. 1, pp. 39–64, Feb. 2006. [Online]. Available: http://doi.acm.org/10.1145/1138127.1138129

[45] M. Khan, N. Salman, and A. H. Kemp, "Cooperative positioning using angle of arrival and time of arrival," in *Sensor Signal Processing for Defence (SSPD)*, pp. 1–5, Sept 2014.

[46] N. Vo, S. Lee, and S. Challa, "Weighted nonmetric MDS for sensor localization," in *Proc. International Conference on Advanced Technologies for Communications (ATC)*, 2008, pp. 391–394.

[47] N. Salman, H. Maheshwari, A. Kemp, and M. Ghogho, "Effects of anchor placement on mean-crb for localization," in *Ad Hoc Networking Workshop*

(Med-Hoc-Net), 2011 The 10th IFIP Annual Mediterranean, 2011, pp. 115–118.

[48] C.-H. Wu, W. Sheng, and Y. Zhang, "Mobile sensor networks self localization based on multi-dimensional scaling," in *Proc. IEEE International Conference on Robotics and Automation*, 2007, pp. 4038–4043.

[49] D. Niculescu and B. Nath, "Ad hoc positioning system (APS) using AOA," in *INFOCOM 2003. Twenty-Second Annual Joint Conference of the IEEE Computer and Communications. IEEE Societies*, vol. 3, 2003, pp. 1734–1743 vol.3.

[50] I. Rasool, N. Salman, and A. Kemp, "GOF analysis for gaussianity assumption of range errors in WSN," in *in Proc. 7th International Symposium on Wireless Communication Systems (ISWCS)*, 2010, pp. 154–158.

[51] L. Gui, A. Wei, and T. Val, "A range-free localization protocol for wireless sensor networks," in *Proc. International Symposium on Wireless Communication Systems (ISWCS)*, 2012, pp. 496–500.

[52] W. Chebbi, M. Benjemaa, L. Kamoun, M. Jabloun, and A. Sahli, "Development of a WSN integrated weather station node for an irrigation alert program under tunisian conditions," in *8th International Multi-Conference on Systems, Signals and Devices (SSD)*, 2011, pp. 1–6.

[53] S.-Y. Chen, W.-T. Lee, H.-C. Chao, Y.-M. Huang, and C.-F. Lai, "Adaptive reconstruction of human motion on wireless body sensor networks," in *Proc. International Conference on Wireless Communications and Signal Processing (WCSP)*, 2011, pp. 1–5.

[54] B. Warneke, M. Last, B. Liebowitz, and K. Pister, "Smart dust: communicating with a cubic-millimeter computer," *Computer*, vol. 34, no. 1, pp. 44–51, 2001.

[55] S. Venkatesh and R. Buehrer, "A linear programming approach to NLOS error mitigation in sensor networks," in *The Fifth International Conference on Information Processing in Sensor Networks, IPSN*, 2006, pp. 301–308.

[56] J. Caffery, "A new approach to the geometry of TOA location," in *52nd IEEE Vehicular Technology Conference (IEEE-VTS Fall VTC 2000)*, 2000, pp. 1943–1949 vol.4.

[57] I. Guvenc, S. Gezici, F. Watanabe, and H. Inamura, "Enhancements to linear least squares localization through reference selection and ML estimation," in *Proc. IEEE Wireless Communications and Networking Conference*, pp. 284–289, March 2008.

[58] N. Patwari, A. Hero, M. Perkins, N. Correal, and R. O'Dea, "Relative location estimation in wireless sensor networks," *IEEE Transactions on Signal Processing*, vol. 51, no. 8, pp. 2137–2148, 2003.

[59] K. Pahlavan and A. Levesque, *Wireless Information Networks*. New York: John Wiley & Sons, Inc, 1995.

[60] N. Salman, M. Ghogho, and A. H. Kemp, "Optimized low complexity sensor node positioning in wireless sensor networks," *IEEE Sensors Journal*, vol. 14, no. 1, pp. 39–46, 2014.

[61] S. M. Kay, *Fundamentals of Statistical Signal Processing: Estimation Theory*. Upper Saddle River, NJ: Prentice Hall, Inc., 1993.

[62] S. Gezici, I. Guvenc, and Z. Sahinoglu, "On the performance of linear least-squares estimation in wireless positioning systems," in *Proc. IEEE International Conference on Communications*, pp. 4203–4208, May 2008.

[63] I. Guvenc, C.-C. Chong, and F. Watanabe, "Analysis of a linear least-squares localization technique in LOS and NLOS environments," in *Proc. 65th IEEE Vehicular Technology Conference*, pp. 1886–1890, April 2007.

[64] R. Ouyang, A.-S. Wong, and C.-T. Lea, "Received signal strength-based wireless localization via semidefinite programming: Noncooperative and cooperative schemes," *IEEE Transactions on Vehicular Technology*, vol. 59, no. 3, pp. 1307–1318, 2010.

[65] N. Alsindi, K. Pahlavan, and B. Alavi, "An error propagation aware algorithm for precise cooperative indoor localization," in *Military Communications Conference, 2006. MILCOM 2006. IEEE*, 2006, pp. 1–7.

[66] X. Li, "RSS-based location estimation with unknown pathloss model," *IEEE Transactions on Wireless Communications*, vol. 5, no. 12, pp. 3626–3633, 2006.

[67] N. Salman, A. H. Kemp, and M. Ghogho, "Low complexity joint estimation of location and path-loss exponent," *IEEE Wireless Communications Letters,*, vol. 1, no. 4, pp. 364–367, 2012.

[68] V. Torczon, "On the convergence of pattern search algorithms," *SIAM J. on Optimization*, vol. 7, no. 1, pp. 1–25, Jan. 1997.

[69] C. Audet and J. E. Dennis, "Analysis of generalized pattern searches," *SIAM J. on Optimization*, vol. 13, pp. 889–903, 2000.

[70] T. Bailey, M. Bryson, H. Mu, J. Vial, L. McCalman, and H. Durrant-Whyte, "Decentralised cooperative localisation for heterogeneous teams of mobile robots," in *Proc. IEEE International Conference onRobotics and Automation (ICRA)*, May 2011, pp. 2859–2865.

[71] D. Dardari, C.-C. Chong, D. Jourdan, and L. Mucchi, "Cooperative localization in wireless ad hoc and sensor networks," *EURASIP Journal on Advances in Signal Processing*, no. 1, p. 353289, 2008. [Online]. Available: http://asp.eurasipjournals.com/content/2008/1/353289

[72] S. heui Jeong and C.-H. Oh, "RSS-based cooperative localization algorithm using virtual reference node in wireless sensor networks," in *11th International Conference on Advanced Communication Technology, (ICACT)*, vol. 01, Feb 2009, pp. 895–900.

[73] S. Yousefi, X. Chang, and B. Champagne, "Distributed cooperative localization in wireless sensor networks without NLOS identification," *in Proc. 11th IEEE Workshop on Positioning, Navigation, and Communication, Mar. 2014*, vol. abs/1403.0503, 2014.

[74] B. Ananthasubramaniam and U. Madhow, "Cooperative localization using angle of arrival measurements in non-line-of-sight environments," in *Proceedings of the First ACM International Workshop on Mobile Entity Localization and Tracking in GPS-less Environments*, ser. MELT 08. New York, NY, USA: ACM, 2008, pp. 117–122.

[75] L. Gazzah, L. Najjar, and H. Besbes, "Hybrid RSSD/AOA cooperative localization for 4G wireless networks with uncooperative emitters," in *Proc. International Wireless Communications and Mobile Computing Conference (IWCMC)*, Aug 2015, pp. 874–879.

[76] G. Ding, Z. Tan, L. Zhang, Z. Zhang, and J. Zhang, "Hybrid TOA/AOA cooperative localization in non-line-of-sight environments," in *IEEE 75th Vehicular Technology Conference (VTC Spring)*, May 2012, pp. 1–5.

[77] M. Khan, N. Salman, and A. Kemp, "Cooperative positioning using angle of arrival and time of arrival," in *Proc. Sensor Signal Processing for Defence (SSPD)*, Sept 2014, pp. 1–5.

[78] N. Salman, M. Ghogho, and A. Kemp, "Optimized low complexity sensor node positioning in wireless sensor networks," *Sensors Journal, IEEE*, vol. 14, no. 1, pp. 39–46, 2014.

[79] I. Guvenc, S. Gezici, and Z. Sahinoglu, "Fundamental limits and improved algorithms for linear least-squares wireless position estimation." *Wireless Communications and Mobile Computing*, vol. 12, no. 12, pp. 1037–1052, 2012.

[80] R. Faragher, "Understanding the basis of the kalman filter via a simple and intuitive derivation," *IEEE Signal Processing Magazine*, vol. 29, no. 5, pp. 128–132, Sept 2012.

[81] R. E. Kalman, "A new approach to linear filtering and prediction problems," *Transactions of the ASME–Journal of Basic Engineering*, vol. 82, no. Series D, pp. 35–45, 1960.

[82] T. Pera la and R. Piche, "Robust extended kalman filtering in hybrid positioning applications," in *4th Workshop on Positioning, Navigation and Communication, WPNC '07*, March 2007, pp. 55–63.

[83] H. Long, Z. Qu, X. Fan, and S. Liu, "Distributed extended kalman filter based on consensus filter for wireless sensor network," in *10th World Congress on Intelligent Control and Automation (WCICA)*, July 2012, pp. 4315–4319.

[84] N. Salman, N. Alsindi, L. Mihaylova, and A. H. Kemp, "Super resolution WiFi indoor localization and tracking," in *Sensor Data Fusion: Trends, Solutions, Applications (SDF)*, pp. 1–5, Oct 2014.

[85] L. Mihaylova and A. Carmi, "Particle algorithms for filtering in high dimensional state spaces: A case study in group object tracking," in *IEEE International Conference on Acoustics, Speech and Signal Processing (ICASSP) 2011,*, May 2011, pp. 5932–5935.

[86] P. Juang, H. Oki, Y. Wang, M. Martonosi, L. S. Peh, and D. Rubenstein, "Energy-efficient computing for wildlife tracking: design tradeoffs and early experiences with zebranet," *SIGOPS Oper. Syst.*

Rev., vol. 36, no. 5, pp. 96–107, Oct. 2002. [Online]. Available: http://doi.acm.org/10.1145/635508.605408

[87] M. Mazo, A. Speranzon, K. Johansson, and X. Hu, "Multi-robot tracking of a moving object using directional sensors," in *Proc. IEEE International Conference on Robotics and Automation, 2004(ICRA)*, vol. 2, April 2004, pp. 1103–1108 Vol.2.

[88] L. Mihaylova, D. Angelova, S. Honary, D. Bull, C. Canagarajah, and B. Ristic, "Mobility tracking in cellular networks using particle filtering," *IEEE Transactions on Wireless Communications*, vol. 6, no. 10, pp. 3589–3599, October 2007.

[89] T. Camp, J. Boleng, and V. Davies, "A survey of mobility models for ad hoc network research." *Wireless Communications and Mobile Computing*, vol. 2, no. 5, pp. 483–502, 2002.

[90] N. Salman, N. Alsindi, L. Mihaylova, and A. Kemp, "Super resolution WiFi indoor localization and tracking," in *Sensor Data Fusion: Trends, Solutions, Applications (SDF)*, Oct 2014, pp. 1–5.

[91] M. Khan, A. Kemp, N. Salman, and L. Mihaylova, "Tracking of wireless mobile nodes in the presence of unknown path-loss characteristics," in *18th International Conference on Information Fusion (Fusion)*, July 2015, pp. 104–111.

[92] B. M. Yu, K. V. Shenoy, and M. Sahani, "Derivation of Kalman Filtering and Smoothing Equations," Oct. 2004.

[93] ——, "Derivation of Extented Kalman Filtering and Smoothing Equations," Oct. 2004.

[94] H. Liu and F. Sun, "Proc. particle filter with improved proposal distribution for vehicle tracking," in *Advances in Neural Networks (ISNN)*, ser. Lecture

Notes in Computer Science. Springer Berlin Heidelberg, 2008, vol. 5263, pp. 422–431.

[95] T. Jia and R. Buehrer, "A new cramer-rao lower bound for TOA-based localization," in *Proc. IEEE Military Communications Conference (MILCOM)*, 2008, pp. 1–5.